PACIFIC EARTHQUAKE ENGINEERING
RESEARCH CENTER

Seismic Design and Performance of Bridges with Columns on Rocking Foundations

Grigorios Antonellis
Marios Panagiotou

Department of Civil and Environmental Engineering
University of California, Berkeley

PEER 2013/21
SEPTEMBER 2013

Seismic Design and Performance of Bridges with Columns on Rocking Foundations

Grigorios Antonellis

Marios Panagiotou

Department of Civil and Environmental Engineering
University of California, Berkeley

PEER Report 2013/21
Pacific Earthquake Engineering Research Center
Headquarters at the University of California, Berkeley

September 2013

ABSTRACT

Traditional seismic design of bridges includes ductile details that allow bridges to develop substantial inelastic deformations when subjected to severe earthquakes. While bridges designed in this manner may be safe from collapse following an earthquake, they are susceptible to considerable damage and permanent lateral displacements that can impair traffic flow and necessitate costly and time-consuming inspections and repairs (perhaps even demolition). Nowadays, as an alternative design strategy, bridges with columns supported on rocking foundations are designed to undergo large deformations but sustain far less damage and can re-center after large earthquakes.

The numerical study presented herein investigates the seismic response of two bridges subjected to two sets of forty ground motions each, one consisting of pulse-type near-fault ground motions and another containing a mix of near- and far-fault ground motions. Three design strategies were considered for each of the two bridges. The first design is based on current common practice, which expects flexural plastic hinging in the columns. The other two designs use rocking shallow and pile foundations, respectively. The columns in the bridge with the rocking foundation are designed to remain elastic while also accounting for the effect of framing between the columns, the deck, and the abutments. The bridges with rocking foundations consider several different cases in terms of size of columns, bearings, and expansion joints at the abutments.

Each bridge model is subjected to the two sets of ground motions using two horizontal components for each ground motion. The numerical results show that lateral drift similar to that experienced by fixed-base bridges is possible in the bridges with rocking pile foundations, with essentially an elastic response in the columns. A comparison of the seismic performance of the bridges in terms of post-earthquake repair cost is conducted using an existing performance evaluation framework based on the Pacific Earthquake Engineering Research Center's performance-based earthquake engineering method. Existing damage models for the columns, bearings, and shear keys are used, while a new damage model of rocking shallow foundations is developed. The structural components are classified in different performance groups, with discrete damage states and repair methods. Based on an existing methodology developed by other researchers, repair costs are calculated based on the repair quantities and the materials used in the repair methods of every performance group. The post-earthquake repair cost of the rocking bridges is negligible for the range of intensity measures considered in this study.

ACKNOWLEDGMENTS

This work was supported primarily by the State of California through the Transportation System Research Program of the Pacific Earthquake Engineering Research Center (PEER). Any opinions, findings, and conclusions or recommendations expressed in this material are those of the authors and do not necessarily reflect those of PEER or any other sponsors

CONTENTS

LIST OF FIGURES

LIST OF TABLES

1 Introduction

Traditional design of fixed-base bridges includes ductile details that permit bridges to develop substantial inelastic deformations when subjected to severe earthquakes. While bridges designed in this manner may be safe from collapse, they are susceptible to considerable damage and permanent lateral displacements that can impair traffic flow and necessitate costly, time-consuming, dangerous, and disruptive inspections and repairs (and perhaps even demolition). As an alternative design, bridges with columns supported on foundations allowed to uplift can undergo large deformations but suffer far less damage, with the added bonus of re-centering following large earthquakes. Compared to fixed-base bridges, bridges supported on rocking foundations may have additional economic benefit because fixed-base bridges require larger spread foundations as well as larger and/or more piles.

The rocking behavior of structures has been investigated numerically and experimentally since the nineteenth century [Milne and Omori 1893] and early in the twentieth century by Kirkpatrick [1927]. For forty years rocking of structures has been considered an effective mechanism of resisting lateral forces and developing deformations expected during earthquake excitation. Early numerical studies include Muto et al. [1960], who studied numerically the overturning vibration of slender structures, and Housner [1963], who studied numerically the rocking behavior of rigid blocks supported on a rigid base subjected to sinusoidal excitation. Beck and Skinner [1974] studied the rocking response of a step bridge pier, a system later used in the design of the South Rangitikei Railway Bridge, New Zealand, constructed in 1981. The rocking behavior of rigid blocks on a rigid base has been studied considering harmonic [Spanos and Koh 1984; Tso and Wong 1989], broadband [Ishiyama 1983], and pulse-type ground excitations [Makris and Roussos 2000; Makris and Zhang 2001; Makris and Konstantinidis 2003]. Other studies have considered the rocking response of rigid blocks on elastic [Psycharis and Jennings 1983] and inelastic bases [Apostolou et al. 2007].The rocking response of flexible structures supported on rigid [Meek 1978; Chopra and Yim 1985], flexible [Chopra and Yim 1985], and inelastic bases [Apostolou et al. 2007] has also been studied. Finally, Cremer et al. [2001; 2002] studied numerically the nonlinear two-dimensional (2D) response of rocking shallow foundations. Foundation rocking has been identified numerically as a mechanism that may explain why some engineered structures did not sustain as severe damage during earthquakes [Rutenberg et al. 1982]. In contrast, overturning of equipment or structures due to rocking during earthquakes has also been reported [Anooshehpoor et al. 1999; Shi et al. 1996].

Shaking table tests of buildings using rocking foundations supported on a rigid base [Kelly and Tsztoo 1977; Clough and Huckelbridge 1977] and simple single-mass structures supported on a rigid or flexible base [Priestley et al. 1978] were first conducted in the 1970s. Shake table tests with either of single bridge columns or two-column subassemblies supported on rocking foundations [Saidi et al. 2002; Chen et al. 2006; Sakellaraki and Kawashima 2006; Espinoza and Mahin 2008] were conducted thereafter. Large-scale experimental studies involving geotechnical aspects of rocking of shallow foundations include research done by Bartlett [1976], Wiessing [1979], Georgiadis and Butterfield [1988], Pecker and Pender [2000], Faccioli et al. [2001], and Paolucci et al. [2007].

Numerous centrifuge tests of simple piers supported on rocking shallow foundations [Harden et al. 2005; Kutter et al. 2006; Gajan et al. 2008; Ugalde et al. 2010] and rocking pile-foundations [Deng and Kutter 2011] as well as of simple bridge models [Deng et al. 2011] with columns supported on rocking foundations have been conducted. The latter study considered model columns with different heights, footing widths, and skews relative to the axis of shaking.

Rocking foundations have been utilized in the design of major bridges like the Rion Antirion Bridge, Greece [Pecker 2006], and the retrofit of bridges, including the Golden Gate Bridge, San Francisco, California, [Ingham et al. 1995], the Carquinez Bridge, Vallejo, California [Jones et al. 1997] and the Lions Gate Bridge, Vancouver, British Columbia [Dowdell and Hamersley 2000]. They have also been proposed for a retrofit scheme [Astaneh-Asl et al. 1993].

1.1 REPORT OUTLINE

This report contains six chapters, including the Introduction. Chapter 2 describes the benchmark bridges considered in this study, their design, and the seismic hazard and the ground motions used. Linear and nonlinear single-degree-of-freedom (SDOF) response spectra are also presented. Next, the objectives and the design procedure are presented for both the fixed-base bridges and the bridges with rocking foundations. Chapter 3 presents the three-dimensional (3D) numerical model of the bridge. Chapter 4 presents the results from modal and nonlinear response history analysis (NRHA) of the bridges. These results are presented in terms of relative deformations of the top of the bridge columns with respect to the ground, displacements of the bearings of the abutments, settlement of the shallow foundations, and steel tensile strains in the columns, including axial load variation in the columns due to vertical inertial and kinematic interaction effects between the columns, the deck, and the abutments.

Chapter 5 performs a probabilistic seismic performance evaluation of the bridges using the methodology and framework developed by Mackie et al. [2008] for the Pacific Earthquake Engineering Research Center (PEER) with the results presented in terms of repair cost versus intensity measure of the ground motion. The disaggregation of the cost into different repair cost quantities is also discussed. Finally, Chapter 6 presents the conclusions of this study.

2 Benchmark Bridges and Ground Motions

2.1 GROUND MOTION REPRESENTATION

Two different sets of ground motions [Baker et al. 2011] were used for the NRHA of the bridges, see Chapter 4. The first set (see Table 2.1) consisted of 40 ground near-fault motions that included strong acceleration, velocity, and displacement pulses as a result of directivity [Baker et al. 2011]. For each of the near-fault motions, the fault-normal and fault-parallel horizontal components were used in the NRHA. The second set (broadband set of ground motions, see

Table 2.2) consisted of 40 unscaled ground motions selected so that their mean response spectrum matched the median spectrum, in the period range of 0−5 sec computed from Boore and Atkinson [2008], of a magnitude 7 strike-slip earthquake at a distance of 10 km from the fault for a site with V_{s30} equal to 250 m/sec [Baker et al. 2011].

The mean linear acceleration spectra of the sets of ground motions are shown in Figure 2.1. The mean spectrum of the broadband set of ground motions is similar to the corresponding spectrum of the fault-normal, near-fault motions in the period range of 2 to 3 sec, while stronger for periods larger than 3.2 sec. Figure 2.1 also depicts the single-degree-of-freedom (SDOF) oscillator nonlinear displacement spectra for two different force-displacement (F-D) relationships: bilinear plastic and bilinear elastic. These two force displacements are shown in Figure 2.2. These F-D relationships were considered because they approximate reasonably well the force-displacement relationship of bridges with fixed-base columns and with columns supported on rocking pile foundations that are used in this study.

Figure 2.3 plots the linear acceleration and displacement response spectra of the individual ground motions of the two sets including their mean spectra. Figures 2.4 to 2.6 plot the nonlinear displacement spectra of the near-fault, fault-normal component, near-fault, fault-parallel component, and broadband sets of ground motions, respectively. The comparison of the mean linear and nonlinear displacement spectra is shown in Figure 2.7, and the following conclusions can be drawn:

1. The spectral displacements for the bilinear elastic response (for bridges with rocking pile-foundations) are 1.3 to 2 times larger than the corresponding displacements for bilinear plastic response (for fixed-base bridges) for the period range of interest (T = 1−3 sec).

2. Linear and nonlinear spectral displacements (both for bilinear plastic and bilinear elastic response) increase almost linearly with an increase of period for periods up to 3 sec.

3. An increase of R from 2 to 4 results in 20–60% increase of the spectral displacements in the period range $T = 1–3$ sec.

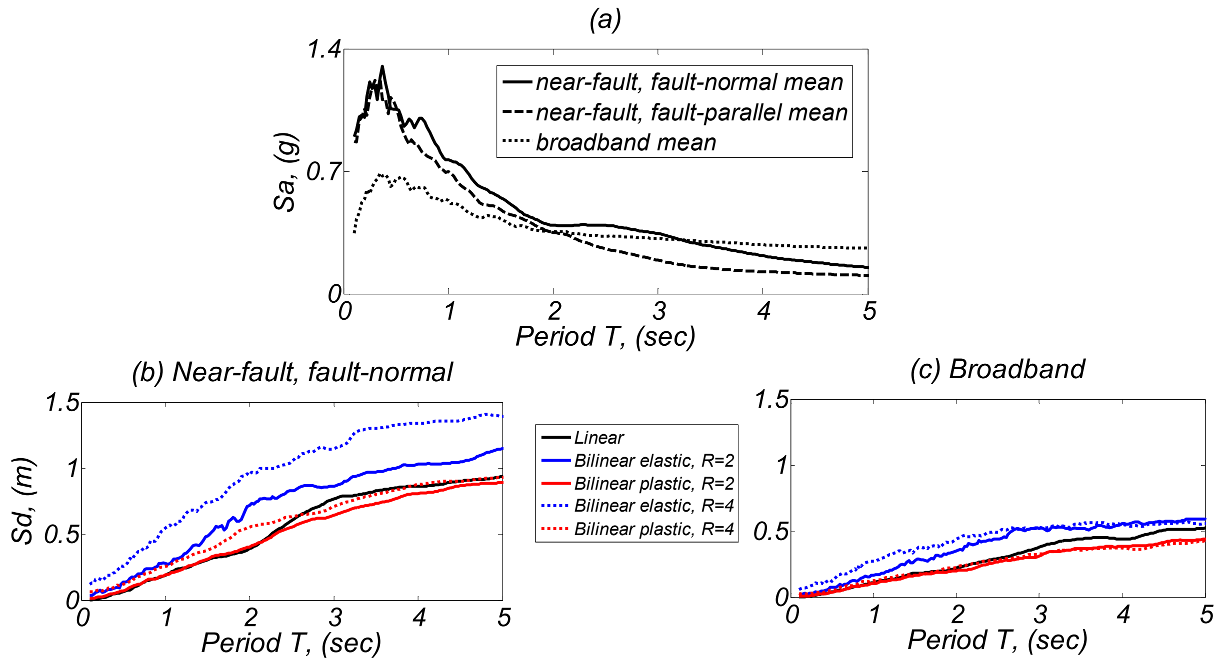

Figure 2.1 **(a) Mean linear acceleration spectra of the 40 near-fault, fault-normal ground motions, the 40 near-fault, fault-parallel ground motions, and 40 ground motions of the broadband set at 2% damping. Linear, bilinear elastic, and bilinear plastic displacement spectra for the (b) near-fault set (fault-normal component) and (c) the broadband set of ground motions.**

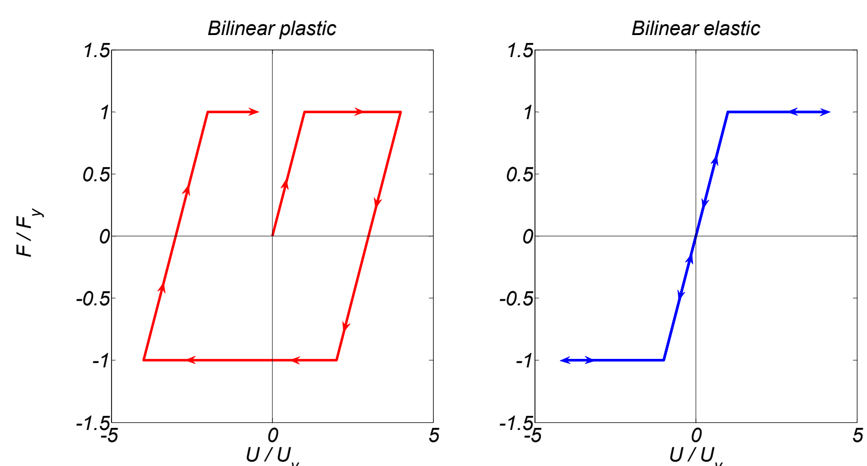

Figure 2.2 **Nonlinear force-displacement relation of the SDOF systems considered.**

Table 2.1 Near-fault set of ground motions.

Number	NGA Record	Earthquake Name	Year	Magnitude	Station Name
1	170	Imperial Valley	1979	6.5	EC County Center FF
2	171	Imperial Valley	1979	6.5	EC Meloland Overpass FF
3	179	Imperial Valley	1979	6.5	El Centro Array #4
4	180	Imperial Valley	1979	6.5	El Centro Array #5
5	181	Imperial Valley	1979	6.5	El Centro Array #6
6	182	Imperial Valley	1979	6.5	El Centro Array #7
7	183	Imperial Valley	1979	6.5	El Centro Array #8
8	184	Imperial Valley	1979	6.5	El Centro Differential Array
9	451	Morgan Hill	1984	6.2	Coyote Lake Dam (SW Abut)
10	77	Loma Prieta	1989	6.9	Gilroy - Gavilan Coll.
11	779	Loma Prieta	1989	6.9	LGPC
12	879	Landers	1992	7.3	Lucerne
13	900	Landers	1992	7.3	Yermo Fire Station
14	982	Northridge	1994	6.7	Jensen Filter Plant
15	983	Northridge	1994	6.7	Jensen Filter Plant Generator
16	1044	Northridge	1994	6.7	Newhall - Fire Sta.
17	1045	Northridge	1994	6.7	Newhall - W Pico Canyon Rd.
18	1063	Northridge	1994	6.7	Rinaldi Receiving Sta.
19	1084	Northridge	1994	6.7	Sylmar - Converter Sta.
20	1085	Northridge	1994	6.7	Sylmar - Converter Sta East
21	1086	Northridge	1994	6.7	Sylmar - Olive View Med FF
22	1050	Kobe, Japan	1995	6.7	KJMA
23	1119	Kobe, Japan	1995	6.7	Takarazuka
24	1161	Kocaeli, Turkey	1999	7.5	Gebze
25	3548	Chi-Chi, Taiwan	1999	7.6	CHY028
26	1244	Chi-Chi, Taiwan	1999	7.6	CHY101
27	1489	Chi-Chi, Taiwan	1999	7.6	TCU049
28	1492	Chi-Chi, Taiwan	1999	7.6	TCU052
29	1493	Chi-Chi, Taiwan	1999	7.6	TCU053
30	1494	Chi-Chi, Taiwan	1999	7.6	TCU054
31	1505	Chi-Chi, Taiwan	1999	7.6	TCU068
32	1510	Chi-Chi, Taiwan	1999	7.6	TCU075
33	1511	Chi-Chi, Taiwan	1999	7.6	TCU076
34	1515	Chi-Chi, Taiwan	1999	7.6	TCU082
35	1519	Chi-Chi, Taiwan	1999	7.6	TCU087
36	1528	Chi-Chi, Taiwan	1999	7.6	TCU101
37	1529	Chi-Chi, Taiwan	1999	7.6	TCU102
38	1530	Chi-Chi, Taiwan	1999	7.6	TCU103
39	1546	Chi-Chi, Taiwan	1999	7.6	TCU122
40	1595	Chi-Chi, Taiwan	1999	7.6	WGK

Table 2.2 Broadband set of ground motions.

Number	NGA Record	Earthquake Name	Year	Magnitude	Station Name
1	231	Mammoth Lakes	1980	6.0	Long Valley Dam (Upr L Abut)
2	1203	Chi-Chi, Taiwan	1999	7.6	CHY036
3	829	Cape Mendocino	1992	7.0	Rio Dell Overpass – FF
4	169	Imperial Valley	1979	6.5	Delta
5	1176	Kocaeli, Turkey	1999	7.5	Yarimca
6	163	Imperial Valley	1979	6.5	Calipatria Fire Station
7	1201	Chi-Chi, Taiwan	1999	7.6	CHY034
8	1402	Chi-Chi, Taiwan	1999	7.6	NST
9	1158	Kocaeli, Turkey	1999	7.5	Duzce
10	281	Trinidad	1980	7.2	Rio Dell Overpass, E Ground
11	730	Spitak, Armenia	1988	6.8	Gukasian
12	768	Loma Prieta	1989	6.9	Gilroy Array #4
13	1499	Chi-Chi, Taiwan	1999	7.6	TCU060
14	266	Victoria, Mexico	1980	6.3	Chihuahua
15	761	Loma Prieta	1989	6.9	Fremont - Emerson Court
16	558	Chalfant Valley	1986	6.2	Zack Brothers Ranch
17	1543	Chi-Chi, Taiwan	1999	7.6	TCU118
18	2114	Denali, Alaska	2002	7.9	TAPS Pump Station #10
19	179	Imperial Valley	1979	6.5	El Centro Array #4
20	931	Big Bear	1992	6.5	San Bernardino - E & Hospitality
21	900	Landers	1992	7.2	Yermo Fire Station
22	1084	Northridge	1994	6.7	Sylmar - Converter Sta
23	68	San Fernando	1971	6.6	LA - Hollywood Stor FF
24	527	N. Palm Springs	1986	6.0	Morongo Valley
25	776	Loma Prieta	1989	6.9	Hollister - South & Pine
26	1495	Chi-Chi, Taiwan	1999	7.6	TCU055
27	1194	Chi-Chi, Taiwan	1999	7.6	CHY025
28	161	Imperial Valley	1979	6.5	Brawley Airport
29	1236	Chi-Chi, Taiwan	1999	7.6	CHY088
30	1605	Duzce, Turkey	1999	7.1	Duzce
31	1500	Chi-Chi, Taiwan	1999	7.6	TCU061
32	802	Loma Prieta	1989	6.9	Saratoga - Aloha Ave
33	6	Imperial Valley	1940	7.0	El Centro Array #9
34	2656	Chi-Chi, Taiwan	1999	6.	TCU123
35	982	Northridge	1994	6.7	Jensen Filter Plant
36	2509	Chi-Chi, Taiwan	1999	6.2	CHY104
37	800	Loma Prieta	1989	6.9	Salinas - John & Work
38	754	Loma Prieta	1989	6.9	Coyote Lake Dam (Downst)
39	1183	Chi-Chi, Taiwan	1999	7.6	CHY008
40	3512	Chi-Chi, Taiwan	1999	6.3	TCU141

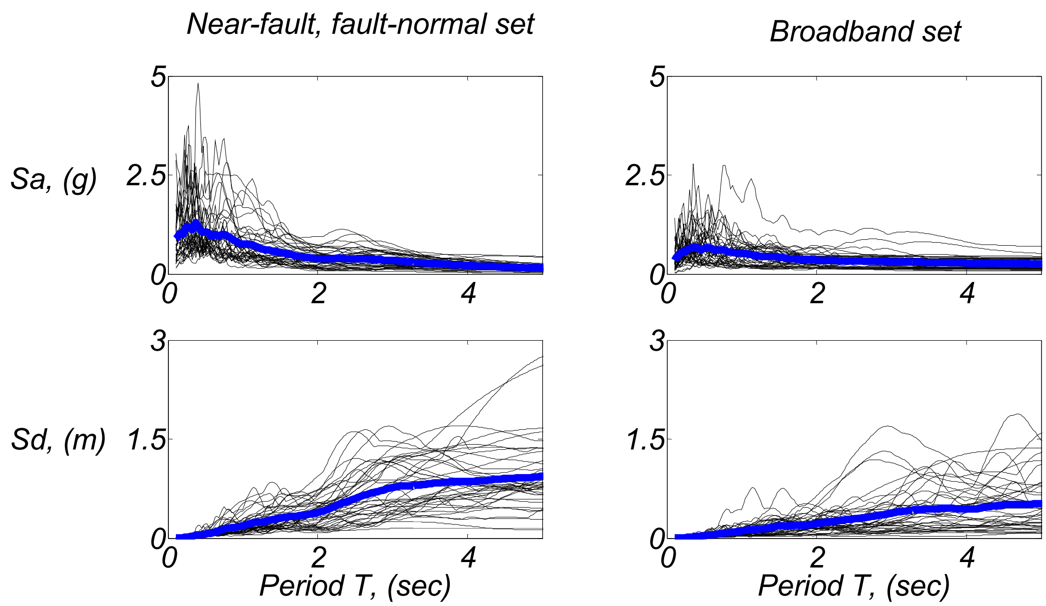

Figure 2.3 **Linear acceleration and linear displacement spectra for the two sets of ground motions used.**

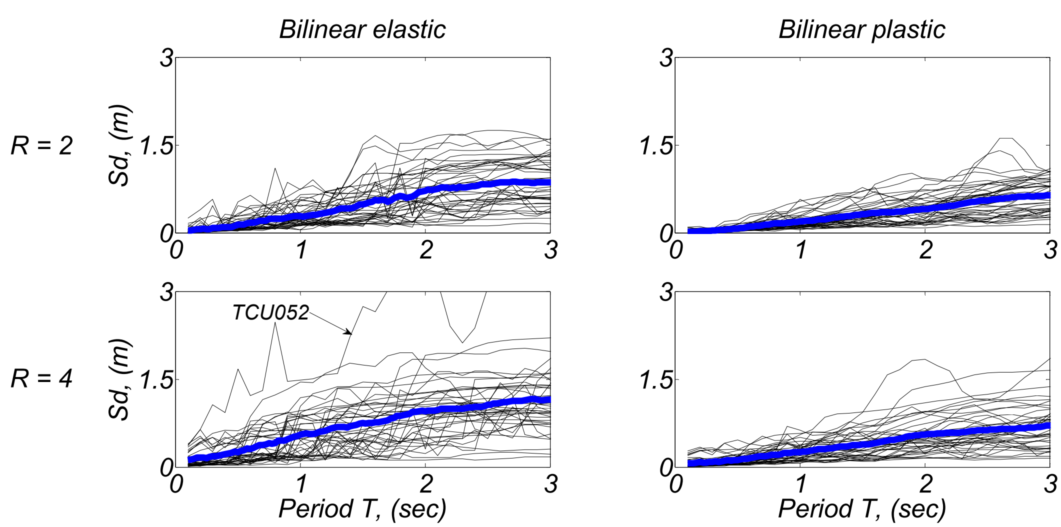

Figure 2.4 **Nonlinear displacement spectra for the near-fault ground motions (fault-normal component); damping ζ = 2%, and hardening ratio *r* = 0%.**

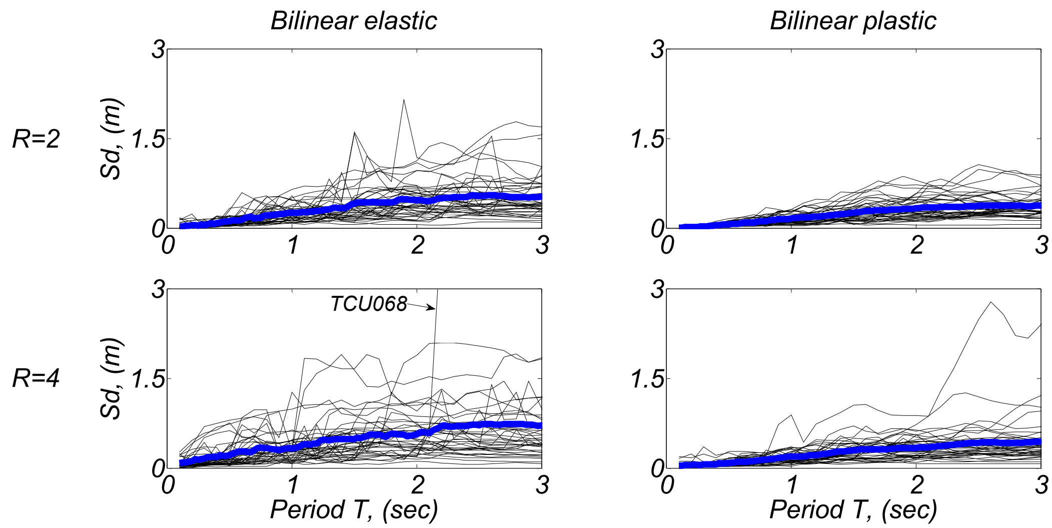

Figure 2.5 Nonlinear displacement spectra for the near-fault ground motions (fault-parallel component); damping ζ = 2% and hardening ratio r = 0%.

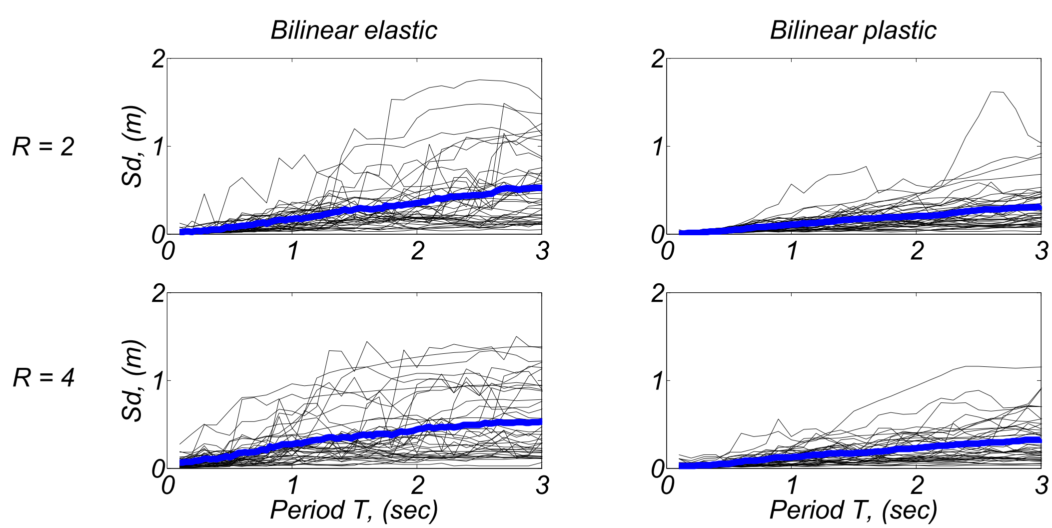

Figure 2.6 Nonlinear displacement spectra for the broadband set of ground motions; damping ζ = 2% and hardening ratio r = 0%.

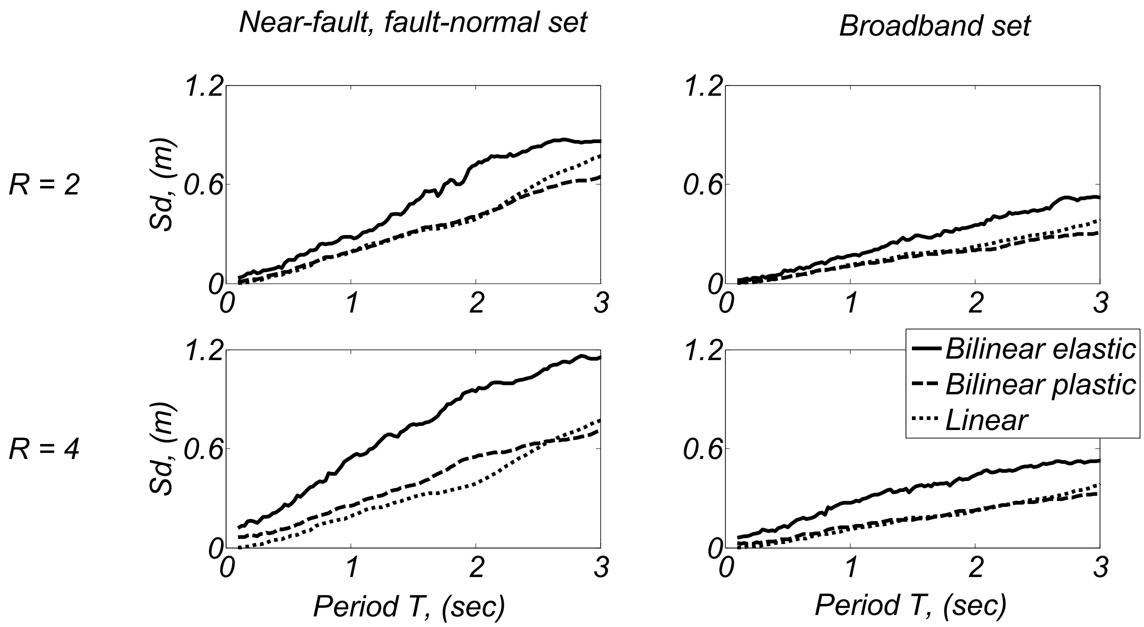

Figure 2.7 Mean linear and nonlinear displacement spectra comparison.

2.2 BENCHMARK BRIDGES

Figure 2.8 shows the structural layout of the eleven bridges considered; the characteristics of the bridges are listed in Table 2.3. Bridges with this layout were used by the Transportation Research Program of PEER (http://peer.berkeley.edu/transportation/projects/); two of these bridges are described in Ketchum et al. [2004].

Composed of five straight spans and single column bents, these bridges differed in terms of the following (i) column height, H_c; (ii) column diameter D_c; (iii) type of foundation design; (iv) type of connection between the top of the columns and the deck; (v) type of bearings supporting the deck at the abutments; and (vi) the deformation capacity of the expansion joints. Two different column heights H_c equal to 15.2 m (Bridges B15) and 6.7 m (bridges B7) were considered (see Figure 2.9). Three different design strategies were considered in terms of H_c for the two types of bridge; one bridge is composed of columns fixed at both ends, another bridge used columns supported on rocking pile foundations, and the third bridge used columns supported on rocking shallow foundations.

As shown in Table 2.3, the column diameter for the fixed-base (FB) bridge was 1.8 m and 2.1 m for the rocking pile (RP1) and shallow foundation (RS) designs. Bridges with rocking pile (RP) foundations with the same column diameter and abutment configuration as the fixed-base bridges were also considered for comparison's sake (termed "RP2a" bridges). In order to study the effect of the lead-plug rubber bearings at the abutments, an additional model (termed "RP2b") was analyzed. This model was identical to the RP1 model except for the bearings, which did not include lead plugs. For the fixed-base design with H_c = 6.7 m, two bridges with different longitudinal steel ratio of the columns were considered. For all bridges with rocking foundations, a pin connection in the longitudinal direction of the bridge between the top of the column and the deck was used. The deck was supported on three circular rubber bearings at each abutment (see Figure 2.10). The size and type of bearings and the type of the expansion joints differed between the fixed-base and rocking designs are described below and are summarized in Table 2.3. Shear keys in all designs were designed to resist a force equal to 667 kN, that is 30% of the vertical service loads at the abutments. The gravity loads included the factored dead load of the structural system of the bridge.

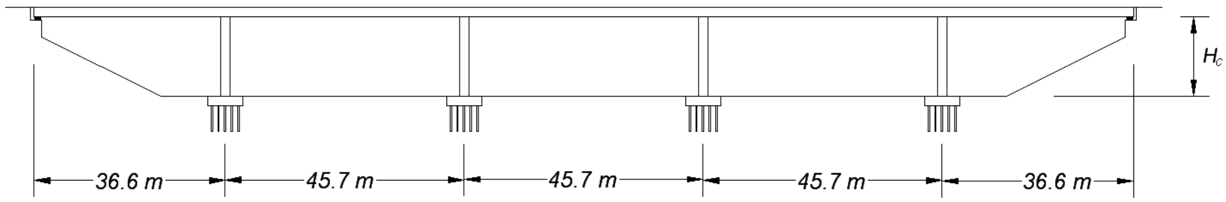

Figure 2.8 Side view of the structural system layout of the benchmark bridges. Two column heights were considered: H_c = 15.2 m and 6.7 m.

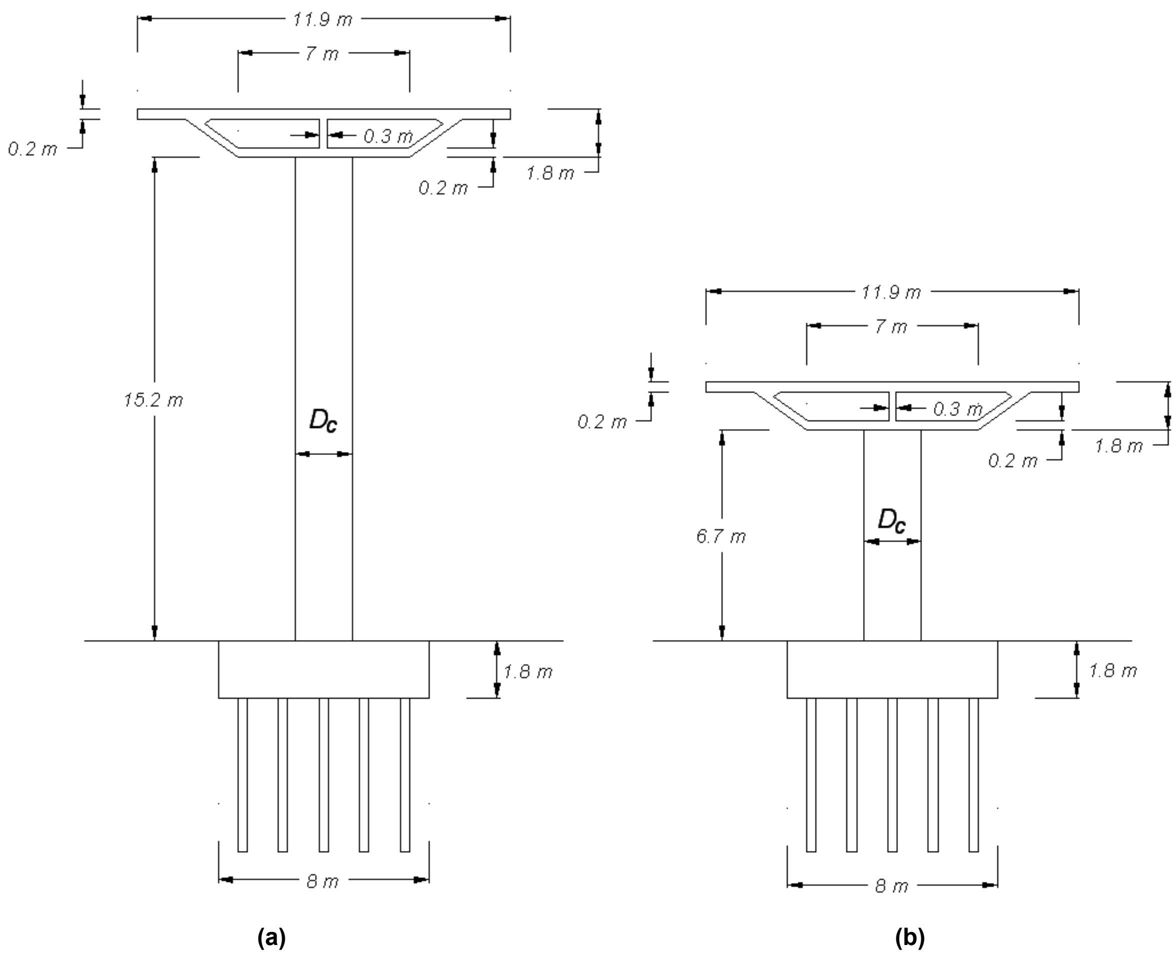

Figure 2.9 Foundation-column-deck elevation for the bridges considered: (a) the 15.2 m tall bridges and (b) the 6.7 m tall bridges.

Table 2.3 Characteristics of the eleven bridges considered.

Bridge number	Bridge name	Type of design	Column height H_c (m)	Column diameter D_c (m)	Column longitudinal reinforcement ratio (ρ_l)	Foundation width B (m)	Displacement capacity of expansion joint (m)	Type of bearings in abutments, [diameter (m), total rubber height (m)]	Total seismic weight W, (kN)	Gravity load at the base of columns N_{cG}, (kN)*
1	B15-FB1	Fixed-base	15.2	1.8	2%	N/A	0.10	RB [0.90, 0.22]	33826	7473 (6823)
2	B7-FB1	Fixed-base	6.7	1.8	2%	N/A	0.10	RB [0.90, 0.22]	31713	6945 (6295)
3	B7-FB2	Fixed-base	6.7	1.8	1.2%	N/A	0.10	RB [0.90, 0.22]	31713	6945 (6295)
4	B15-RP1	Rocking pile foundation	15.2	2.1	3%	6.5	0.40	LPRB [1.26, 0.36]	35194	7816 (7165)
5	B15-RP2a	Rocking pile foundation	15.2	1.8	3%	4.7	0.10	RB [0.90, 0.22]	33826	7473 (6823)
6	B15-RP2b	Rocking pile foundation	15.2	2.1	3%	6.5	0.40	RB [1.26, 0.36]	35194	7816 (7165)
7	B7-RP1	Rocking pile foundation	6.7	2.1	3%	6.5	0.40	LPRB [1.26, 0.36]	32314	7095 (6445)
8	B7-RP2a	Rocking pile foundation	6.7	1.8	3%	4.7	0.10	RB [0.90, 0.22]	31713	6945 (6295)
9	B7-RP2b	Rocking pile foundation	6.7	2.1	3%	6.5	0.40	RB [1.26, 0.36]	32314	7095 (6445)
10	B15-RS	Rocking shallow foundation	15.2	2.1	3%	6.5	0.40	LPRB [1.26, 0.36]	35194	7816 (7165)
11	B7-RS	Rocking shallow foundation	6.7	2.1	3%	6.5	0.40	LPRB [1.26 / 0.26]	32314	7095 (6445)

*Interior column, exterior in parentheses.

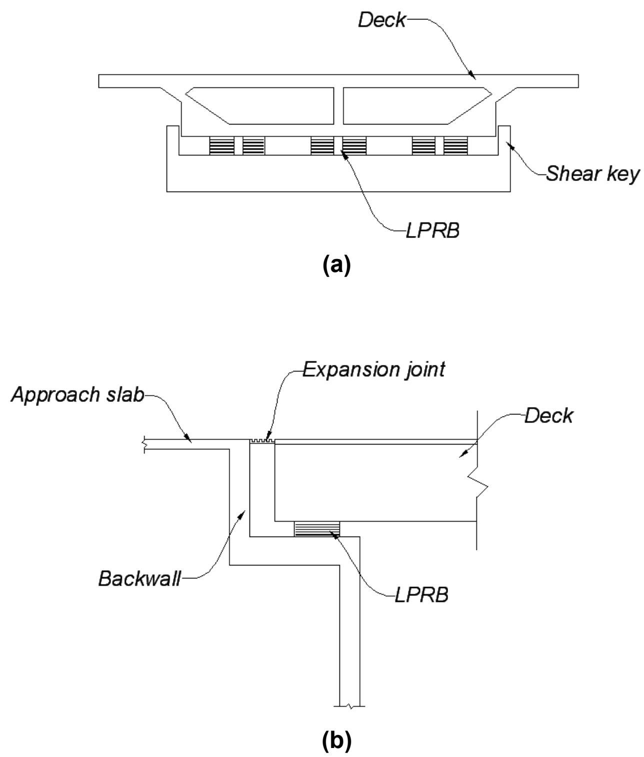

Figure 2.10 **(a) Configuration of bearings and shear keys at the abutment; and (b) side view of the region near the end of the deck and the abutment (drawing not in scale). Rubber bearings without lead plugs were used for the fixed-base designs.**

2.3 FIXED-BASE DESIGN

The majority of deformations in the design of the fixed-based bridge were concentrated in flexural plastic hinges that developed at the bottom and at the top of the columns. The columns were monolithically connected at their bottom and top to the foundation and the deck, respectively. The foundations consisted of an 8 × 8 × 1.8-m pile cap supported on 6 steel piles, with external diameter D_p = 0.61 m, thickness t_p = 0.013 m, length L_p = 18 m, and steel yield strength f_y = 414 MPa. The bearings supporting the deck at the abutments were 0.90 m in diameter and had a total height of rubber of 0.22 m.

Figure 2.11 presents the first mode pushover curves of the fixed-base bridges. For the pushover in the transverse direction, the force vector had the shape of the mode with the most predominant component of transverse displacement of the middle columns. The points where the reinforcement tensile strain, ε_s, reaches 0.5%, 1%, and 3% in the columns are also shown. Chapter 3 describes the numerical models used in this analysis.

Figure 2.12 shows the bilinear approximation of the pushover curves used to estimate the nonlinear displacement demand in the transverse direction of the bridges using SDOF analysis. The initial stiffness, K_y, of the bilinear approximations was defined based on two points of the pushover curves: the point at zero displacement and the point with displacement $\Delta_{\varepsilon,0.2\%}$, at which the longitudinal reinforcement in the column reached a tensile strain ε_s equal to 0.2%. The strength, F_y, of the bilinear approximation was determined from the monotonic response at the mean drift ratio computed from NRHA. Based on this approximation, K_y and the corresponding SDOF period, T_y, Δ_y, was determined using the effective seismic weight, W_{eff}, of the mode with the most predominant translational component in the transverse direction, as described in Chapter 4. Similarly, the force reduction factor, R_y, was calculated, defined as the linear seismic force, F_e, computed using the elastic spectral acceleration at T_y multiplied by the first-mode effective seismic mass, to F_y. Based on T_y and R_y, and using the nonlinear (bilinear plastic) SDOF displacement spectra shown in Figure 2.4, the nonlinear displacement demand, Δ_{NL}, was calculated, as shown in Table 2.4.

The corresponding drift ratios were 2.1% and 1.0%, for Bridges B15-FB1 and B7-FB1, respectively. The corresponding mean values computed using 3D NRHA of the bridges using two horizontal components of ground motion were 2.4% and 1.0%. In both cases the SDOF analysis resulted in very good agreement with the NRHA results. Even though this analysis used the mean drift ratio computed by NRHA, it can easily be used in an iterative way to estimate the nonlinear displacement demands.

Table 2.4 Pushover and SDOF analysis results in the transverse direction for two of the fixed-base bridges.

Name	$\Delta_{\varepsilon,0.2\%}$ / H (%)	$\Delta_{y,\mathrm{ideal}}$ / H (%)	Secant stiffness K_y at $\Delta_{\varepsilon,0.2\%}$ (kN/m)	Effective seismic weight W_{eff}, (kN)	T_{uncr} (sec)	T_y (sec)	R_y	SDOF analysis Δ_{NL} / H (%)	NRHA Δ_{NL} / H (%)
B15-FB1	0.70	1.30	31465	25708	1.30	1.81	1.5	2.1	2.4
B7-FB1	0.32	0.60	129940	11100	0.53	0.59	1.6	1.0	1.0

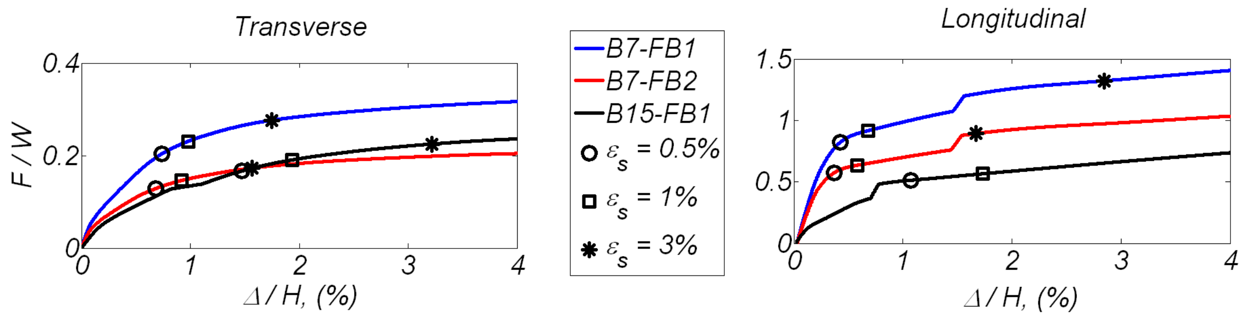

Figure 2.11 Fixed–based Bridges B7 and B15: system pushover curves.

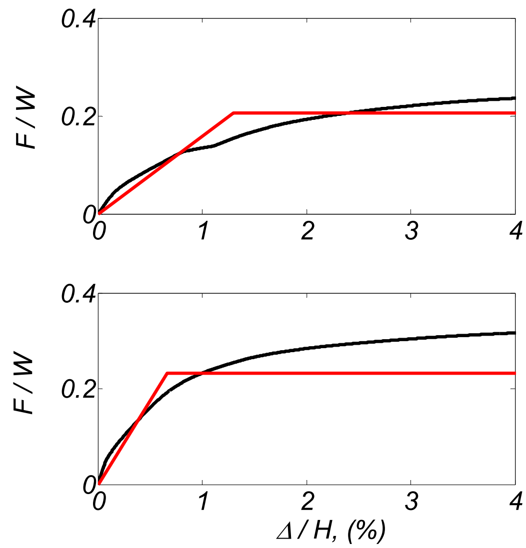

Figure 2.12 Fixed-based bridges: bilinear idealizations of the pushover curves.

2.4 ROCKING FOUNDATION DESIGNS

The majority of deformations for these designs were accommodated at the rocking interfaces. Two different designs using rocking foundations were considered: (a) pile foundations where the pile cap is designed to uplift on top of piles; and (b) shallow foundations designed to uplift on top of soil. The objective in both designs was to ensure that the columns remain essentially elastic. In the case of shallow foundation, the soil properties in the vicinity of the foundation were assumed to be such to prevent extensive inelastic response of the soil. To prevent the formation of a flexural plastic hinge at the top of the columns, a pin connection between the columns and the deck was used in the plane parallel to the longitudinal axis of the bridge. Three lead-plug rubber bearings—1.26 m in diameter and with a total rubber height of 0.36 m—were used at each abutment. The lead plug of each bearing was 0.35 m in diameter with a yield force of 1025 kN. The deformation capacity of the expansion joint was 0.40 m for all designs with rocking foundations except for Bridge RP2a, as described below.

2.4.1 Rocking Pile Foundations

The design considering a rocking pile foundation consisted of a square pile cap supported on four piles (see Figure 2.13). This design resulted in a nonlinear elastic moment-rotation behavior (approximately) of the rocking plane (see Figure 2.2). A comparison between the bilinear elastic versus bilinear plastic behavior for the same moment strength and same initial stiffness should result in an increase of about 80% of the displacement demand (see Figure 2.7). Moreover, comparing this design with the fixed-based design results in an increase in the periods of the longitudinal modes due to the pin connection between the top of the columns and the deck in the longitudinal direction. Thus, significant increase of the displacements of more than 100% is expected if rocking foundations are used compared to the fixed-base design with similar columns and bearings.

The maximum overturning capacity of the pile foundation was calculated as $M_{max} = N_{tot}B_d / 2$, where N_{tot} is the total vertical load including the effective weight of the deck (W_d), the weight of the column (W_c), and the weight of the foundation (W_f), as well as the variation of the vertical load due to framing (N_F) between the columns, the deck, and the abutment, as described below. The maximum distance of a pile from the centroid of the vertical load was B_d (see Figure 2.13). Aiming at an elastic response of the columns, the largest B_d was determined such that when M_{max} developed at the base of the foundation, the steel tensile strain in the column, ε_s, did not exceed 0.2%. Compared with the fixed-base bridge, where D_c was 1.8 m and ρ_l was equal to 2%, in the rocking foundation bridges the column diameter was increased to 2.1 m. A ρ_l = 3% was used as an upper bound for constructability as well as for performance, thus achieving a lateral strength of the bridge that was similar to the fixed-base design at 2% drift ratio. To ensure adequate performance of the piles when all the vertical load is resisted by a single pile, the piles were designed so that the corresponding axial load ratio of the pile $N_{tot} / f_c^{'} A_g$, where $f_c^{'}$ = 48 MPa, the compressive strength of concrete, and A_g (the cross-section area of the pile) is less than 0.25.

The total axial load at the base of the columns N_{tot}, including framing effects between the columns, the deck, and the abutment, was computed using monotonic static analysis of the bridges. Figure 2.14 and Figure 2.15 show the variation of the total axial force at the base of the column versus drift ratio for Bridges B15 and B7, respectively. The analysis results for loading in the transverse and the longitudinal direction are presented. As shown in Figure 2.14 for the response in the transverse direction with an increase in lateral drift, the framing effects increased the axial load in the exterior columns and decreased it in the interior columns. The total axial load for the exterior columns was less than the gravity load on the interior columns, N_{cG}, for loading in the transverse direction and for drift ratios up to 8%. In the longitudinal direction, the framing resulted in larger total axial load in the exterior columns than the gravity load for drift ratios larger than 4%. Nevertheless, the drift ratio in the longitudinal direction was expected to be less than 4%; thus, the axial load after this level of displacement was not critical for the design. Therefore, the axial load used for the design of the columns and the foundations was equal to the gravity load in the interior column (N_{cG} = 7819 kN).

The design of foundations of the interior and exterior columns were identical. The axial load used in the design of the foundation was N_{ftot} = 9647 kN [7816 (gravity load at the base of the interior column, N_{cG}) + 1831 (weight of footing, W_f)]. For N_{ftot} = 9647 kN and B_d = 6.8 m, $M_{max,d}$ = 32,800 kN-m, as shown in Table 2.5. Assuming a triangular bending moment diagram along the height of the column, the moment at the base of the column, $M_{col,max}$ was 94.6% of the moment at the base of the foundation for Bridge B15, and equal to 31028 kN-m. This is less than $M_{\varepsilon,0.2\%}$ = 31,100 kN-m, which is the moment capacity of the column section when the steel reinforcement reaches a tensile strain ε_s = 0.2% for the design axial load, N_{cG}. Because the shape of the bending moment diagram can be affected by the bending moment that develops at the top of the column in the transverse direction, it was not considered in this design. For the N_{ftot} defined above and the limit of the axial load ratio of the piles, the required pile diameter D_p was 1.05 m. Knowing the pile diameter, D_p, the diagonal distance between the piles, B_d, and using 0.30 m distance from the pile surface to the pile-cap edge, the length of the square pile cap was determined to be 6.5 m with a height of 1.8 m (see Figure 2.13).

Two additional rocking-on-piles bridges were analyzed (RP2a and RP2b) for Bridges B15 and B7, but only for the near-fault ground motions. The same design procedure was followed for the design of Model RP2a, which had a column diameter of 1.8 m, reinforcing steel ratio equal to 3%, and same bearings and expansion joints as the fixed-base designs (with expansion joints of 0.10 m and the same rubber bearings without lead plugs used in the fixed-base bridges). Here, the resulting foundation width was 4.7 m (see Table 2.5). Bridge RP2b was identical to bridge RP1 with a 6.5-m-wide foundation; the only difference was in the type of bearings used.

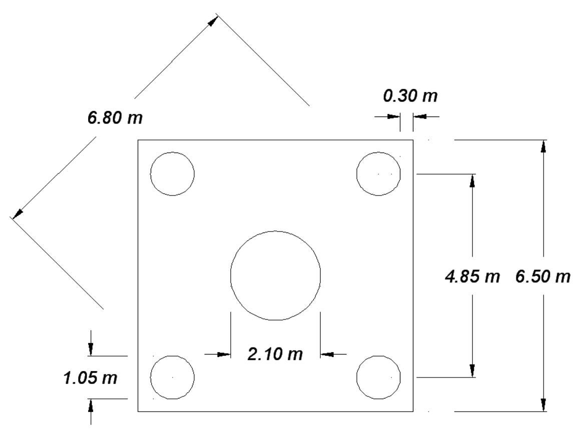

Figure 2.13 Plan view of the rocking pile foundation.

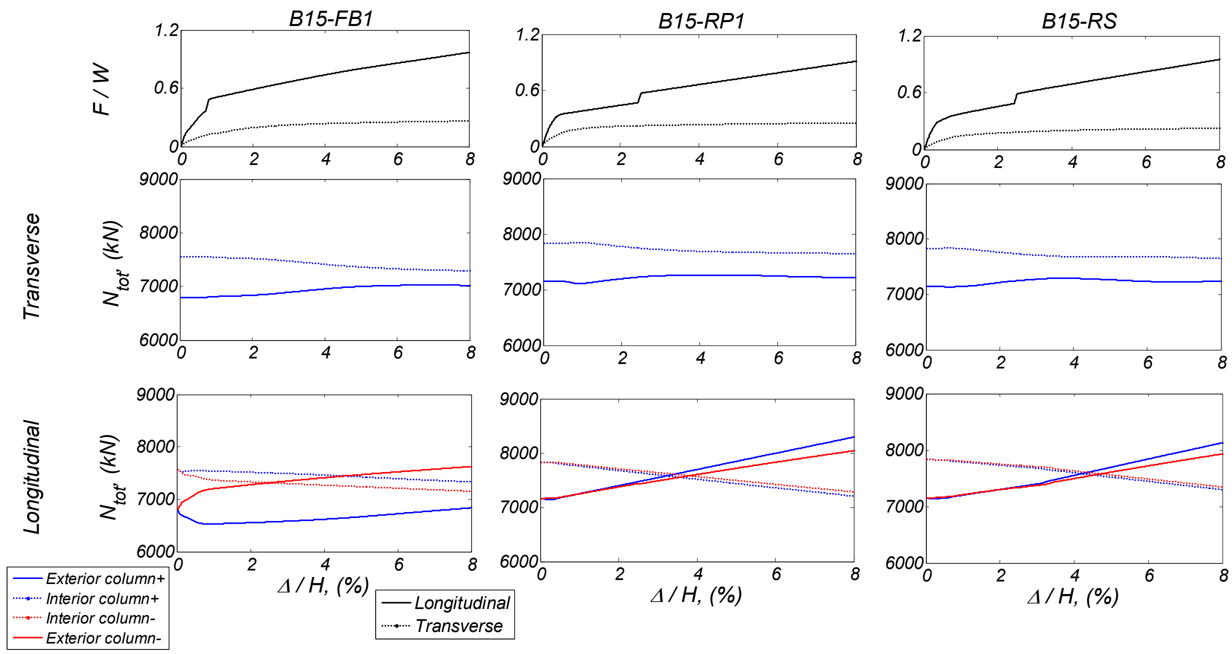

Figure 2.14 Static monotonic analysis of Bridges B15 and axial load at the base of columns versus drift ratio. The plus sign is for the column ahead and the minus sign for the column behind, with respect to the direction of loading.

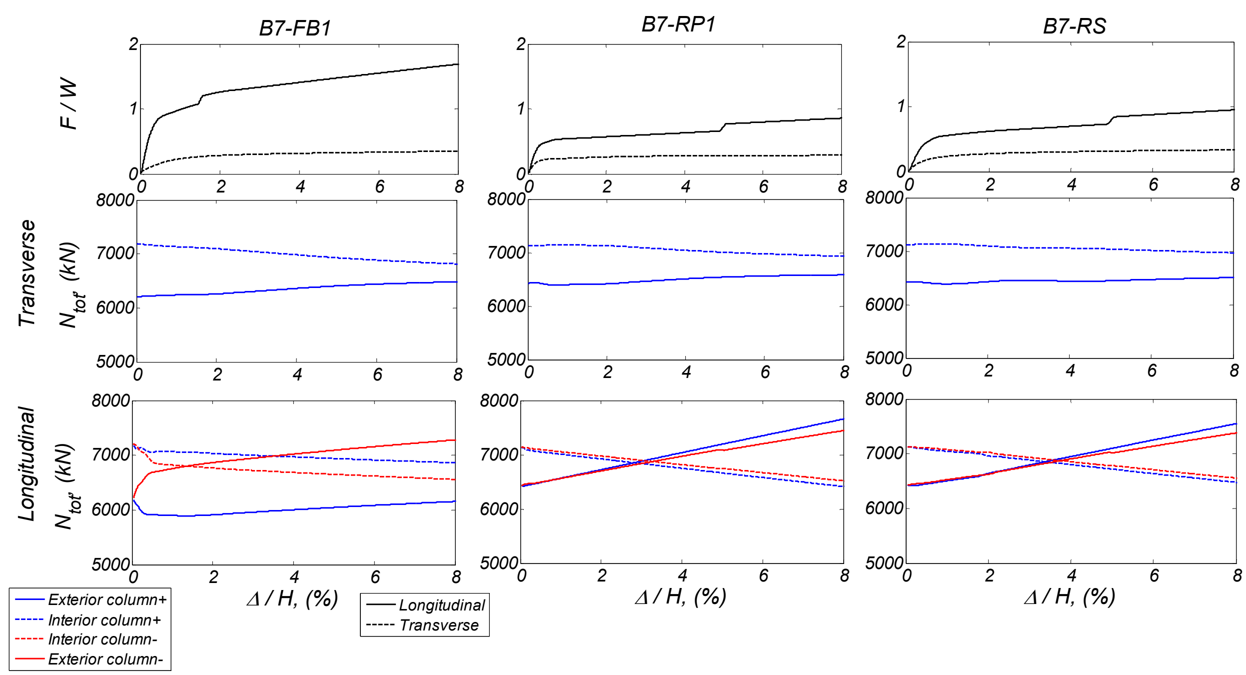

Figure 2.15 Static monotonic analysis results for the three B7 bridges and axial load at the base of columns versus drift ratio. The plus sign is for the column ahead and the minus sign for the column behind, with respect to the direction of loading.

Table 2.5 Design parameters for the rocking on piles footing.

Name	B_d (m)	N_{ftot} (kN)	N_{cG} (kN)	$M_{max,d}$ for N_{ftot} (kN-m)	$M_{col,max}$ for $M_{max,d}$ at foundation (kN-m)	$M_{\varepsilon,0.2\%}$ for $\rho_l = 3\%$ and N_{cG} (kN-m)
B15-RP1	6.8	9647	7816	32800	31028	31100
B15-RP2a	4.7	8426	7473	18160	17252	18972

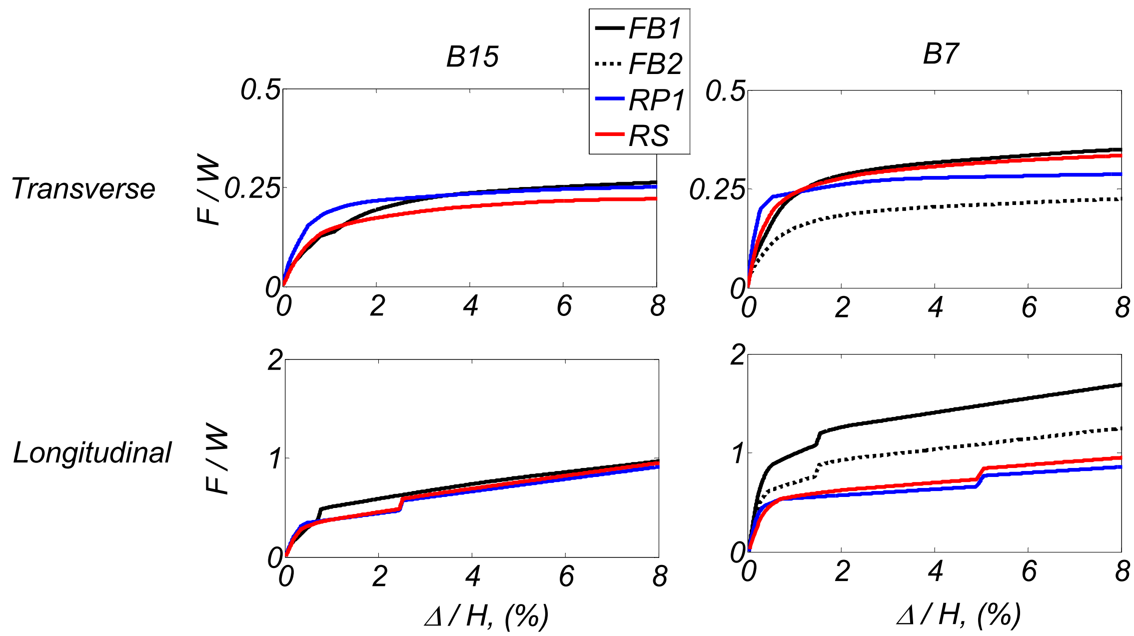

Figure 2.16 Static monotonic analysis results of seven bridges in terms of total horizontal force versus drift ratio.

The results of the static monotonic analysis in terms of total force versus drift ratio at the mid-length of the bridge deck for seven bridges are shown in Figure 2.16. For the response in the transverse direction, Bridges B15 and B7 with rocking pile foundations showed similar strength when compared to the corresponding fixed-based bridges. In the longitudinal direction, the soil behind the back wall of the abutment was activated at a drift ratio of 0.6% and 3.6% for the fixed-base and rocking designs, respectively.

Figure 2.17 shows the bilinear idealization of the pushover curves used in the SDOF nonlinear analysis. The initial stiffness was assumed to be 50% of the initial stiffness obtained from the monotonic static analysis of the bridge; the strength was computed from the monotonic analysis at a drift ratio equal to the mean response computed with NRHA. Based on this idealization, Δ_y, T_y, and R_y were determined (see Table 2.6), and the Δ_{NL} / H was calculated using the nonlinear elastic displacement spectra shown in Figure 2.4. The computed Δ_{NL} / H was equal to 2.6% for Bridge B15-RP1 and 1.4% for Bridge B7-RP1. These results are in very good agreement with the mean values computed by NRHA (see Chapter 4), which were 2.4% and 1.6%, respectively.

Figure 2.18 shows the static cyclic analysis results for the RP bridges for two cycles at drift ratios of 2.5% and 5%, respectively; the bilinear elastic SDOF behavior approximates well the transverse response. In the longitudinal direction, the lead-plug rubber bearings at the abutments increased the hysteretic energy dissipation and did not impede re-centering.

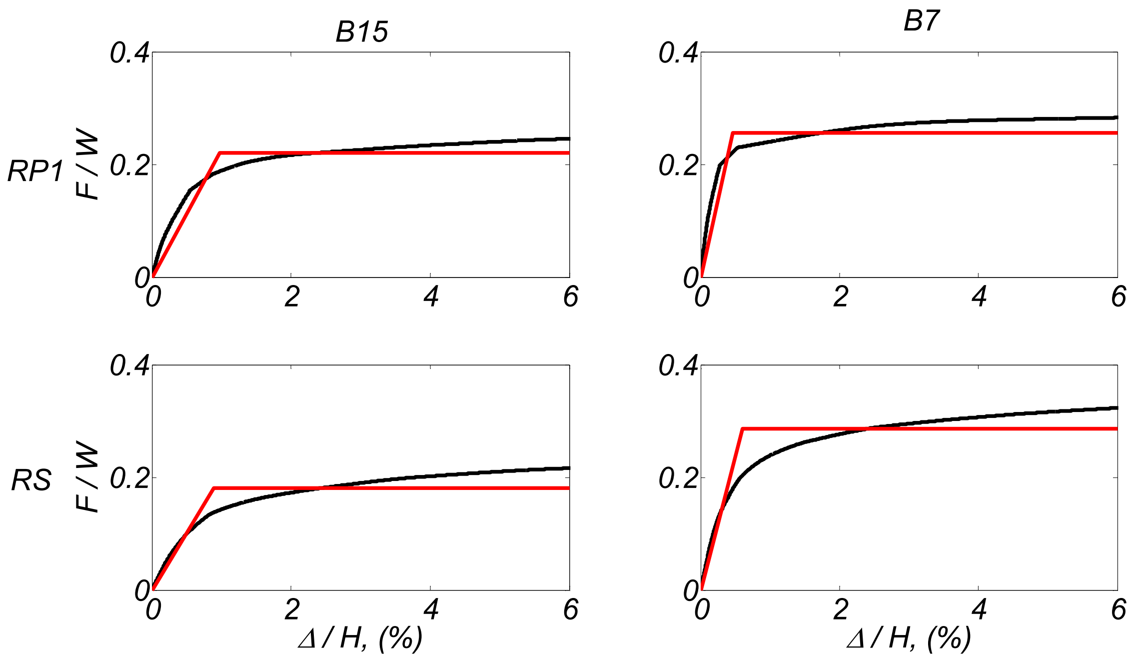

Figure 2.17 Bilinear idealization of the horizontal force-drift ratio response (transverse direction) for the rocking bridges.

Table 2.6 Pushover and SDOF analysis results. Design parameters in the transverse direction for the rocking bridges.

Name	$\Delta_{y,ideal}$ / H (%)	Secant stiffness K_y (kN/m)	Effective seismic weight W_{eff}, (kN)	T_{uncr} (sec)	T_y (sec)	R_y	SDOF analysis Δ_{NL} / H (%)	NRHA Δ_{NL} / H (%)
B15-RP1	0.98	46554	24988	1.05	1.47	1.8	2.6	2.4
B7-RP1	0.42	209520	15188	0.45	0.54	1.9	1.4	1.6
B15-RS	0.89	41893	26396	1.26	1.59	2.1	3.1	2.6
B7-RS	0.56	177950	20681	0.60	0.68	2.1	2.3	2.4

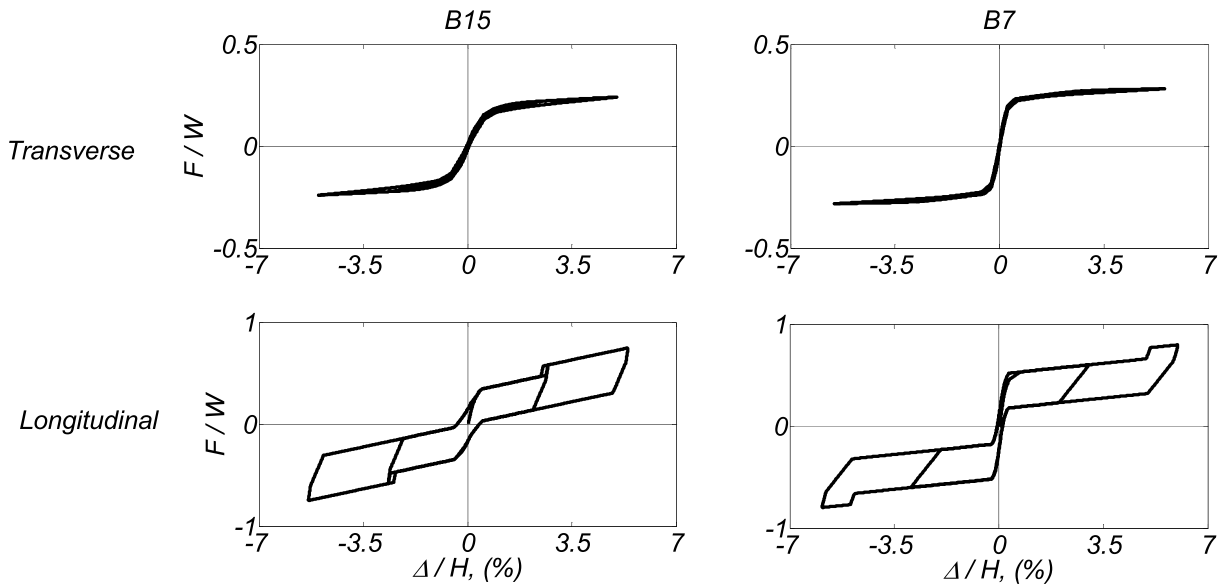

Figure 2.18 Cyclic static analysis results for the rocking pile foundation bridges (RP1).

2.4.2 Rocking Shallow Foundations

For the design of the shallow foundations, the soil in the vicinity of the footings for was assumed to be a clean sand with critical state friction angle φ_c = 28^o, specific weight γ = 18.6 kN / m^3, Poisson's ratio v = 0.2, minimum void ratio e_{min} = 0.5, maximum void ratio e_{max} = 0.8, and relative density DR = 80%. The square footings were the same for Bridges B15 and B7, with a width equal to 6.5 m and a height of 2.0 m.

The maximum moment capacity of the shallow foundations was calculated as $M_{max} = N_{ftot}(B\text{-}L_c)/2$, where B is the length of the footing parallel to the plane of loading, and L_c is the length of the contact between the soil and the footing area. The calculation of L_c and M_{max} is an iterative procedure. First, a value of L_c is assumed, and the corresponding mean effective vertical stress is calculated, which results into the dilatancy index, IR. Then the peak angle of friction, φ_p, is calculated using Bolton's equation [Salgado 2006] and based on that, the ultimate stress capacity of the soil, q_u, within the contact area is calculated [Salgado 2006]. The above procedure is repeated until convergence of the vertical force capacity to the N_{ftot}. The main parameters of the last iteration of this procedure are shown in Table 2.7. The footing of Bridge B15 with N_{ftot} = 9.9 MN resulted in L_c = 0.42 m, φ_p = 41.1^o and M_{max} = 29.8 MN-m. The corresponding values for the footing of Bridge B7 with N_{ftot} = 8.4 MN were L_c = 0.34 m, φ_p = 40.7^o, and M_{max} = 26 MN-m.

The safety factor against gravity loads for the foundations is $FS_v = N_{ftot} / (A_f q_u)$, where A_f the area of the footing. Assuming full contact of the footing with the soil, FS_v was calculated equal to 9.2 and 10.7 for the footings of Bridges B15 and B7, respectively.

Using the model described in Chapter 3, Figure 2.19 shows the computed cyclic moment rotation response of the shallow foundation for moment parallel to one of its two primary axes.

The design procedure was similar to that performed for the rocking pile foundations aiming at elastic response of the column when the foundation at its base developed the moment M_{max}. As shown in Figure 2.14 and Figure 2.15, the framing effects for the bridges with rocking shallow foundations are lower than the ones of the rocking pile foundations. Even for drift ratios up to 6%, the total axial load at the base of any of the columns is smaller than the initial gravity load at the base of the interior column. Thus, the initial gravity load of the interior column was used for the design of the footings of all columns.

Table 2.6 lists the computed nonlinear displacements using SDOF nonlinear analysis for the bilinear idealizations shown in Figure 2.17. The initial stiffness in this case was assumed to be 80% of the initial stiffness obtained from the monotonic static analysis of the bridge. The lateral strength of the bilinear idealization was computed from the monotonic analysis at a drift ratio equal to the mean response computed with NRHA. Because the large FSv of the footings in this study limit the soil inelasticity, a bilinear elastic behavior results in a good approximation of the force displacement curve. This approximation is shown in Figure 2.4, resulting in an Δ_{NL} / H equal to 3.1% and 2.3%, for Bridges B15 and B7, respectively. These were in good agreement with the results of NRHA (2.6% and 2.4% for Bridges B15 and B7, respectively, see Chapter 4). Figure 2.20 plots the first-mode cyclic static analysis curves for the shallow foundation designs for cycles with peak drift ratios 3% and 6%. These designs resulted in limited soil inelasticity and hysteretic energy dissipation associated with this in the transverse direction, whereas the lead-plug rubber bearings provided significant hysteretic dissipation in the longitudinal direction.

Table 2.7 Design parameters for the rocking shallow foundations.

Name	Design axial load of the footing N_{ftot} (kN)	$\underline{B}$ (m)	FS_v for N_{ftot}	M_{max} (kN-m)	$M_{col,max}$ (kN-m)	$M_{\varepsilon,0.2\%}$ for ρ_l = 3% and N_{cG} (kN-m)
B15-RS	9806	6.5	9.2	29830	28220	31650
B7-RS	8435	6.5	10.7	25988	20958	29970

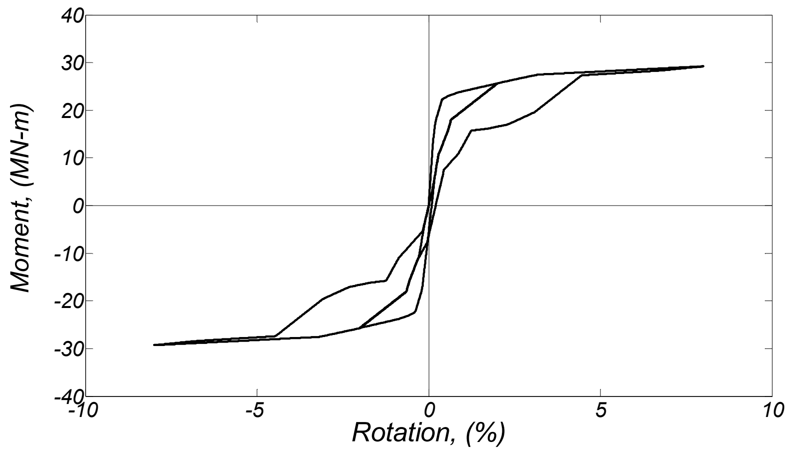

Figure 2.19 Moment-rotation response for the shallow foundation of Bridge B15-RS.

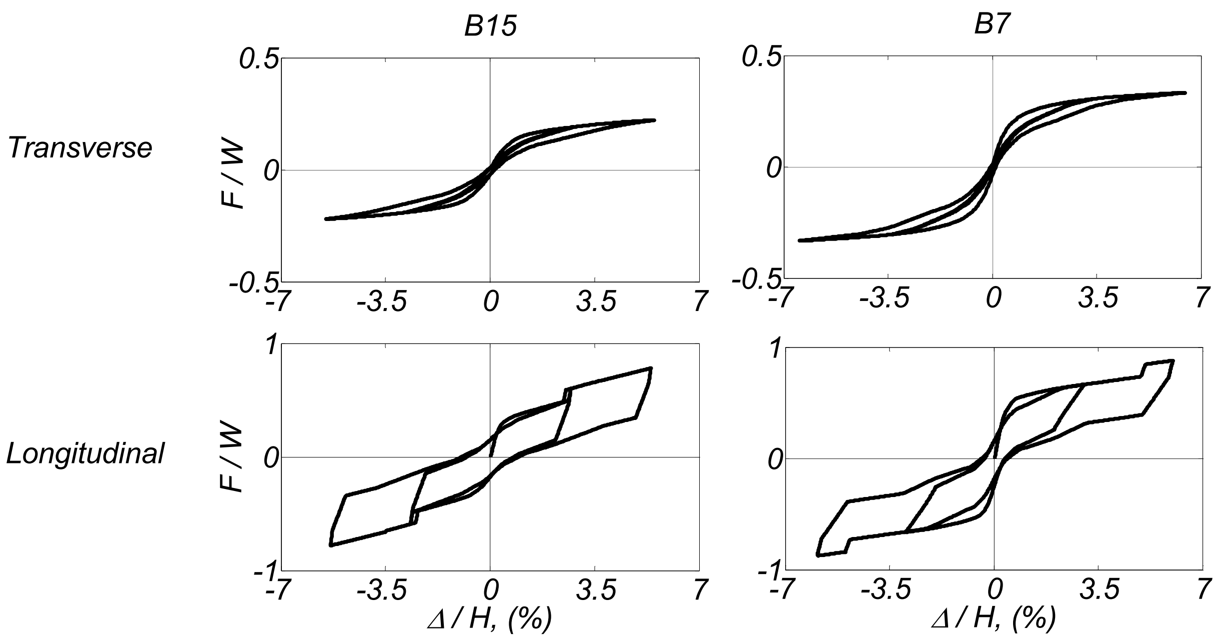

Figure 2.20 Cyclic static analysis results for the shallow foundation bridges (RS).

3 Numerical Modeling

The analyses were conducted using the Open System for Earthquake Engineering Simulation [OpenSees 1999] computer software. The 3D model developed is shown in Figure 3.1; a side of view of the column and foundation part of model is shown in Figure 3.2. Fiber-section nonlinear Euler Bernoulli beam-column (frame) elements were used to model the columns and the deck, with 6 and 8 integration points per element, respectively. Existing material models in OpenSees—*Concrete03* and *Steel02*—were used to model the concrete and steel, respectively. The compressive strength of concrete was 35 MPa, and the yielding stress of steel was 450 MPa with a 2% hardening ratio. The post-tensioning of the deck was modeled using the initial strain material and co-rotational truss members in parallel. A linear elastic stiff element was used to connect the top of the columns with the centroid of the deck (see Figure 3.2), as well as the foundation centroid with the bottom of the column and the bottom of the foundation. The bearings at the abutments were modeled with zero-length spring elements, with a linear elastic force-displacement behavior (for the bearings without lead plugs) in two horizontal directions and stiffness equal to1870 kN/m for the fixed-base models. The lead-plug rubber bearings for the rocking models had an initial stiffness of 2450 kN/m, a yielding force of 1025 kN, and post-yield stiffness equal to 10% of the initial stiffness, see Figure 3.3(c). In the vertical direction, the bearings were modeled to have zero tensile strength and a linear elastic behavior in compression with stiffness equal to 1,050,000 kN/m and 6,500,000 kN/m for the fixed-base and rocking models, respectively. The abutment wall and the backfill soil were modeled according to Caltrans Seismic Design Criteria [2010] using a zero-length spring with zero tensile strength and a trilinear behavior with gap in compression, see Figure 3.3(b). The shear keys were modeled using zero-length spring elements with the tri-linear force-displacement relationship shown in Figure 3.3(d).

The soil underneath each shallow foundation was modeled using 81 zero length springs distributed in a non-uniform 9×9 grid. The vertical force-displacement relation was modeled using the QzSimple1 F-D relation, see Figure 3.3(a). The initial stiffness of the vertical springs in the middle and end region was determined according to Harden et al. [2005], which were calibrated to match the vertical and rotational stiffness of the shallow footings [Gazetas 1983]. Because the combined horizontal resistance at the bottom and sides of the footing due to friction and passive reaction of the surrounding soil was significantly higher than the expected peak base shear, the horizontal translations at the base of the foundation were restrained. Each pile of the rocking pile-foundations was modeled using a zero-length spring having a zero-tension and linear elastic behavior in compression with stiffness equal to $E_c A_p / L_p$, where E_c = 27,500 MPa, L_p the length of the pile, and A_p the cross-section area of the piles. This modeling is appropriate for end bearing piles.

The mass was assigned at the abutments, the intersection of the columns with the deck, and at the centroid of the foundations. The corresponding mass moments of inertia at each of these locations were also assigned. The gravity load was assigned as point loads in the above locations. An initial stiffness Rayleigh damping of 2% was used in mode 1.

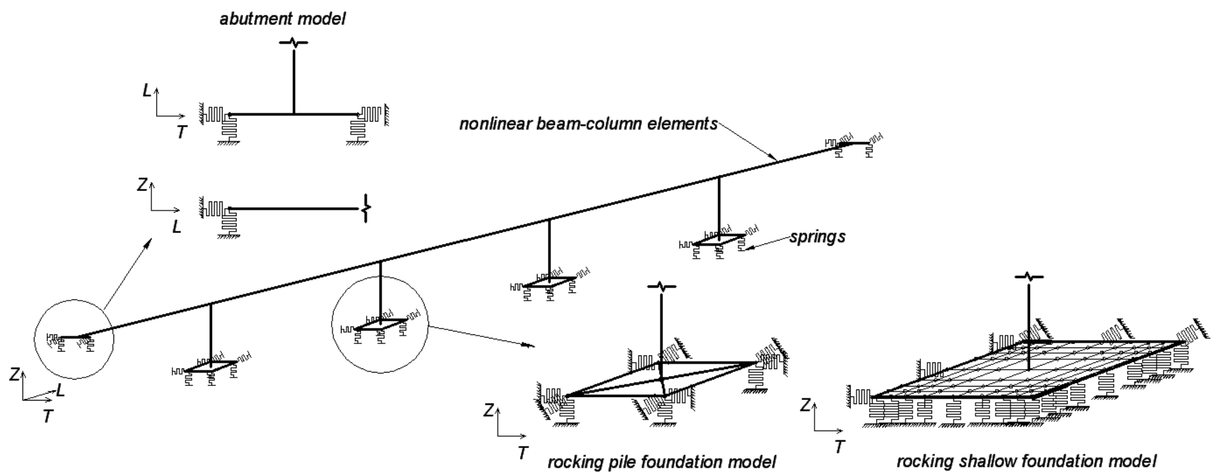

Figure 3.1 Three-dimensional bridge model in OpenSees (drawing not to scale).

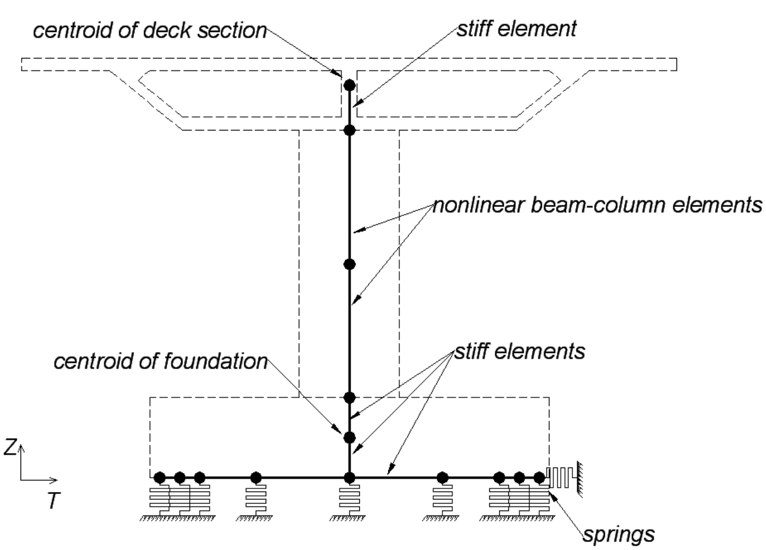

Figure 3.2 Modeling of the bridge column supported on rocking shallow foundation. (drawing not to scale).

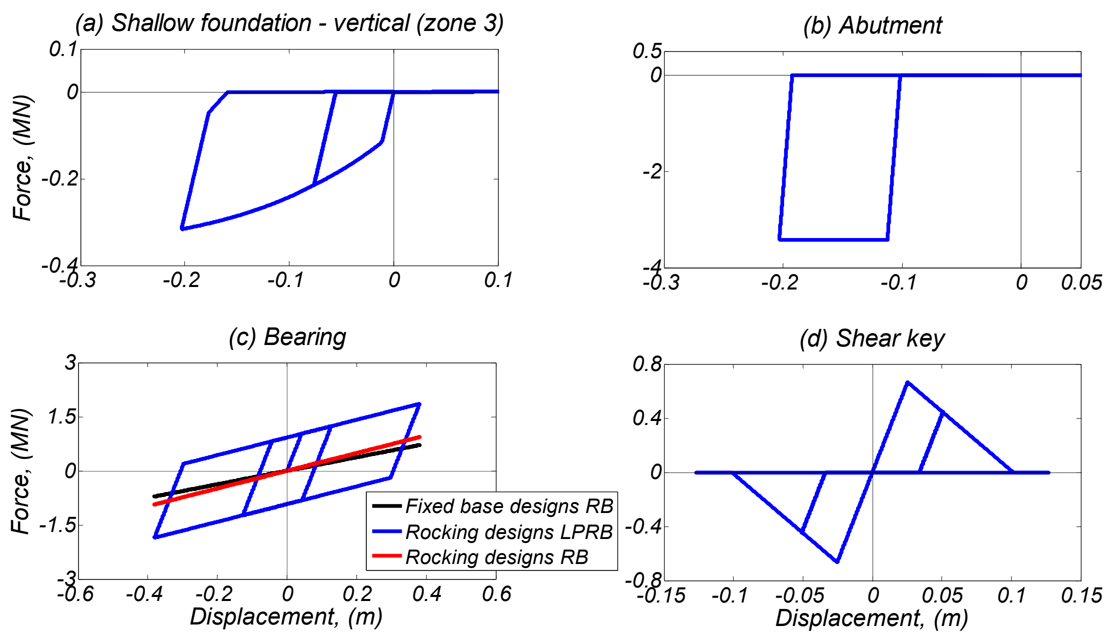

Figure 3.3 **Nonlinear force/stress-displacement relationships: (a) contact behavior of the soil-foundation system in the vertical direction; (b) abutment (longitudinal direction); (c) bearings; and (d) shear keys.**

4 Numerical Analysis Results

4.1 MODAL ANALYSIS

Table 4.1 lists the modal periods $T_{1,t,}$ and $T_{1,l}$ of the two modes with the most predominant translational component of the interior columns in the transverse and longitudinal directions, respectively. The plan and side view of the first ten mode shapes in and the corresponding periods of Bridges B15-FB1, B7- FB1, B15-RP1, B7-RP1, B15-RS, and B7-RS, see Table 2.3, are shown in Figure 4.1 to Figure 4.6. In these figures, only the translational components are plotted. The modal masses normalized to the total horizontal seismic mass are also shown for some of the modes, with predominant translational component in the transverse (M_T*) or longitudinal direction (M_L*).

The modal periods were computed using the initial stiffness matrix. Mode period $T_{1,t}$ is larger than $T_{1,l}$ for all bridges except Bridges B7- FB1 and B7-FB2. The periods $T_{1,t}$, $T_{1,l}$ of Bridge RP1 are smaller than those of the fixed-base bridges, primarily due to the larger initial stiffness of the bearings. For Bridge B7-RS, the $T_{1,t}$ was slightly larger than the fixed-base design, whereas the $T_{1,l}$ was 34% smaller. The B7 bridges had three modes of similar period with predominant the translational component in the transverse direction. Table 4.1 shows the ratio of the moment at the base of the foundation due to the concentrated modal moment at the top of the internal column to the modal force at the same location times the height from the foundation level. This ratio, M_r / M_{FI}, indicates the relative contribution of the rotatory and horizontal inertia forces to the moment at the base of the foundation. Note the significant contribution of the rotatory inertia for the B7 bridges.

Table 4.1 Modal periods of primary modes and relative contribution of rotatory and horizontal inertia to the moment at the base of the foundations.

	B15				B7				
	FBI	RP1	RP2a	RS	FBI	FB2	RP1	RP2a	RS
$T_{1,t}$ (sec)	1.30	1.05	1.34	1.26	0.53	0.55	0.45	0.59	0.60
$T_{1,l}$ (sec)	0.77	0.72	0.87	0.79	0.68	0.69	0.36	0.46	0.45
M_r / M_{FI} (%)	5.7	5.3	5.5	4.6	26.8	26.8	27.2	25.3	18.3

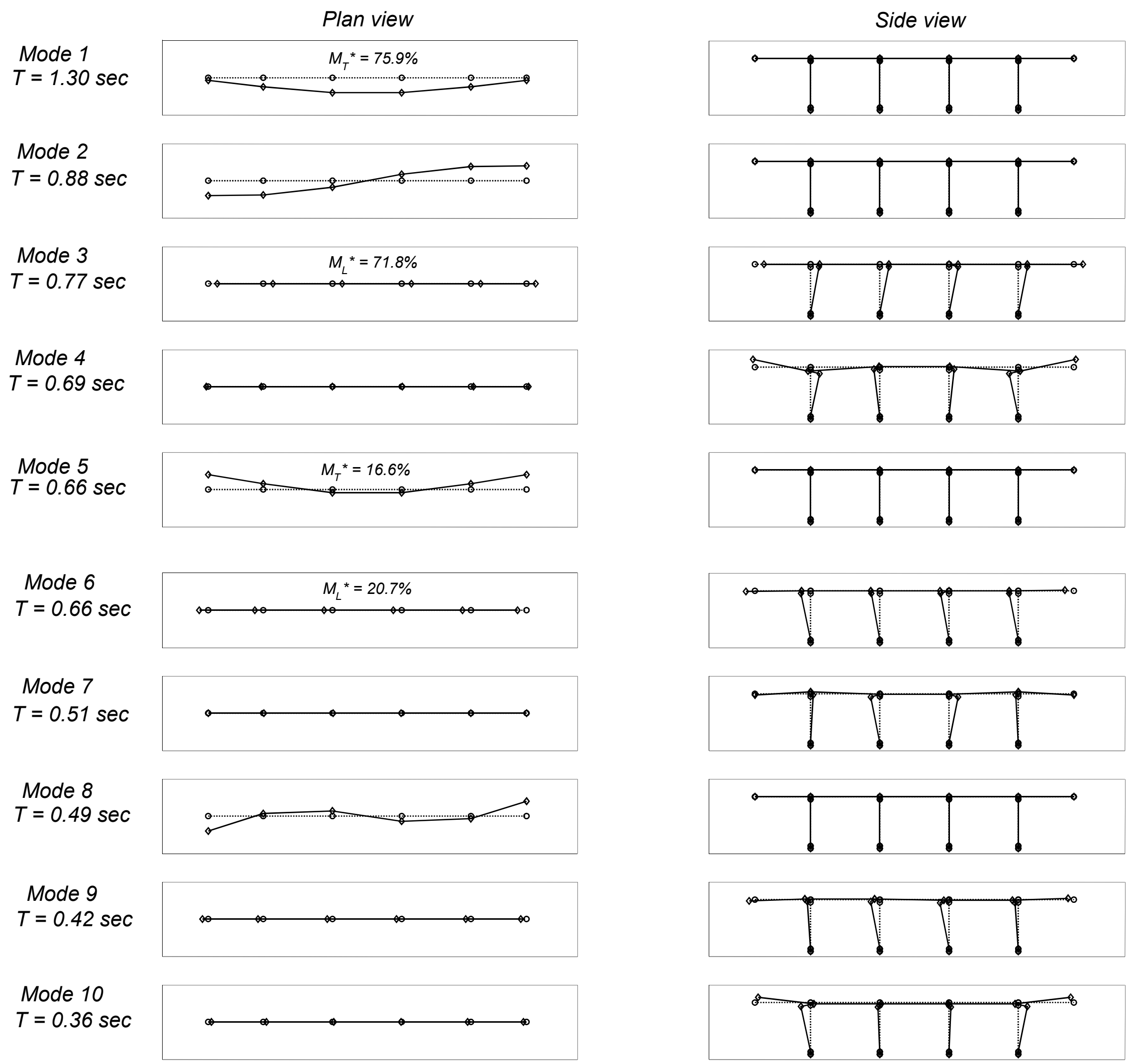

Figure 4.1 Mode shapes and periods of the first ten modes of Bridge B15-FB1.

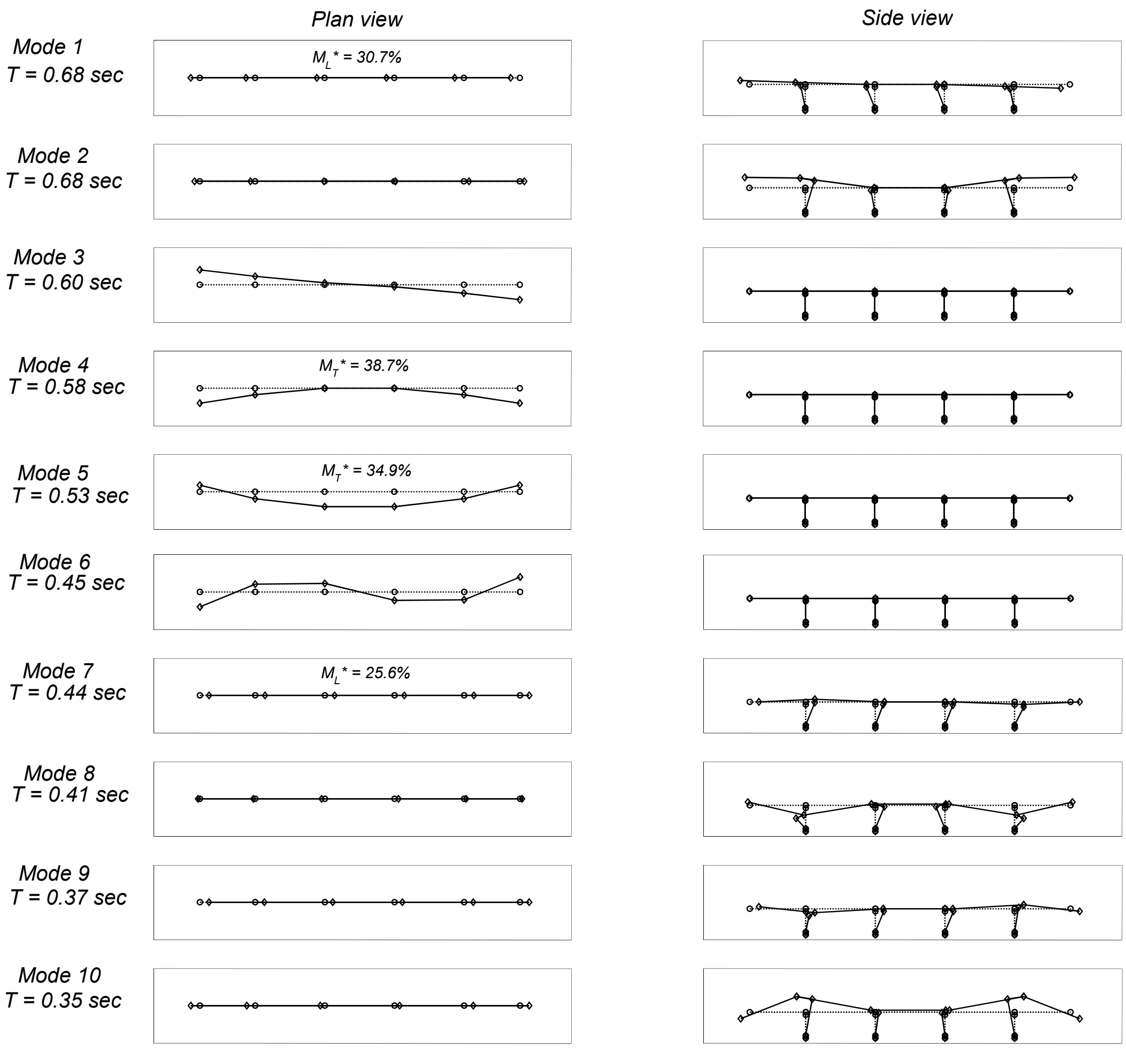

Figure 4.2 Mode shapes and periods of the first ten modes of Bridge B7-FB1.

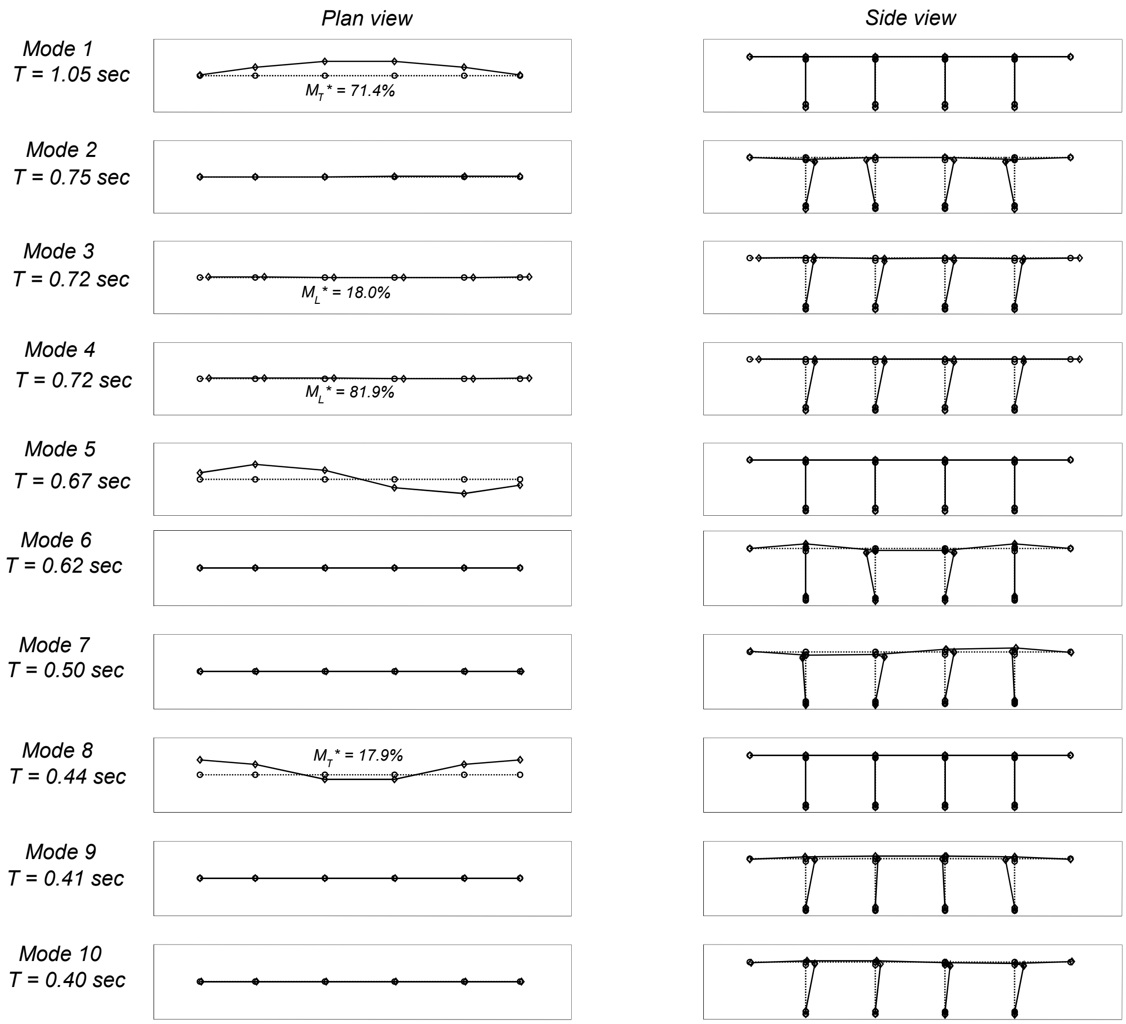

Figure 4.3 Mode shapes and periods of the first ten modes of Bridge B15-RP1.

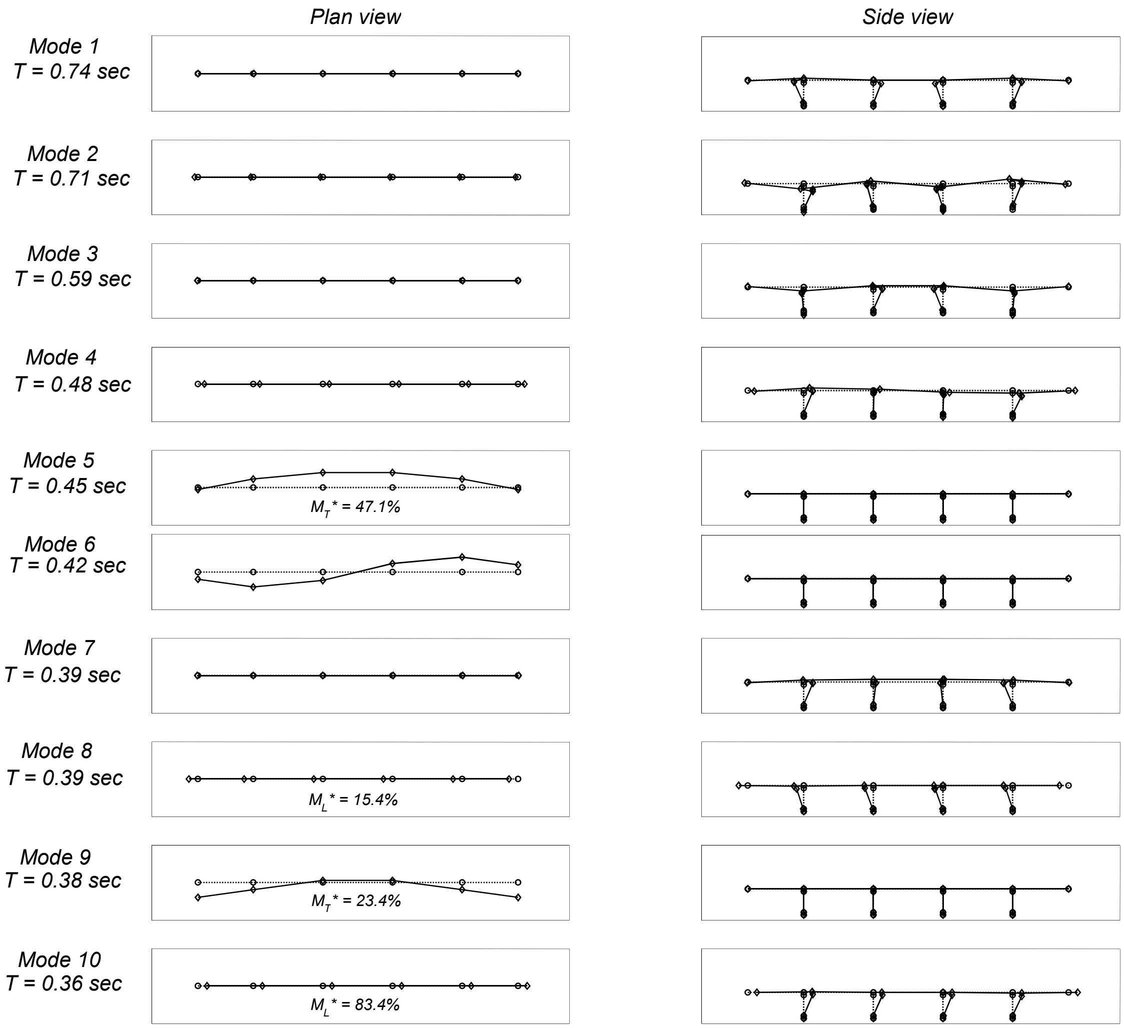

Figure 4.4 Mode shapes and periods of the first ten modes of Bridge B7-RP1.

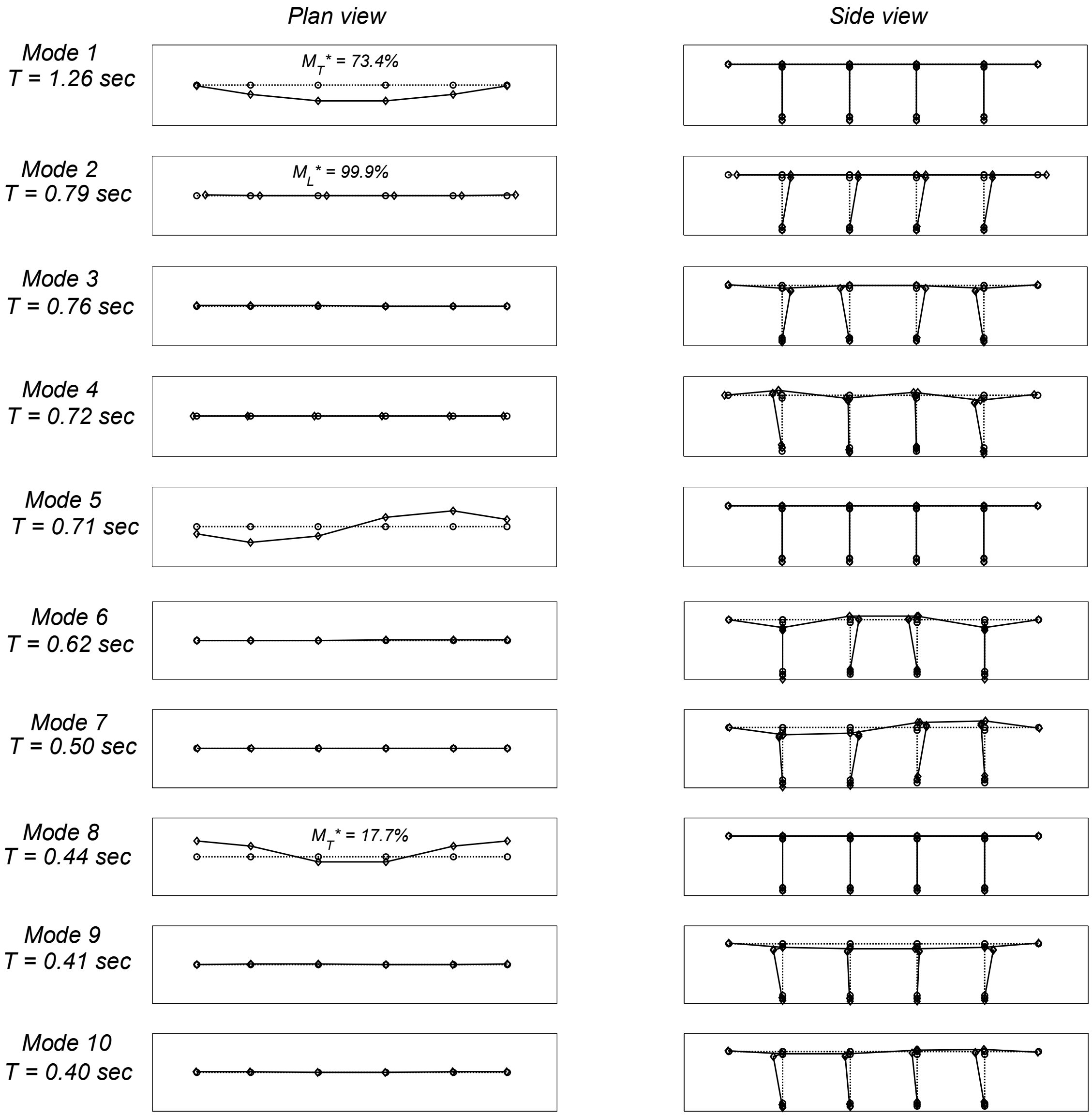

Figure 4.5 Mode shapes and periods of the first ten modes of Bridge B15-RS.

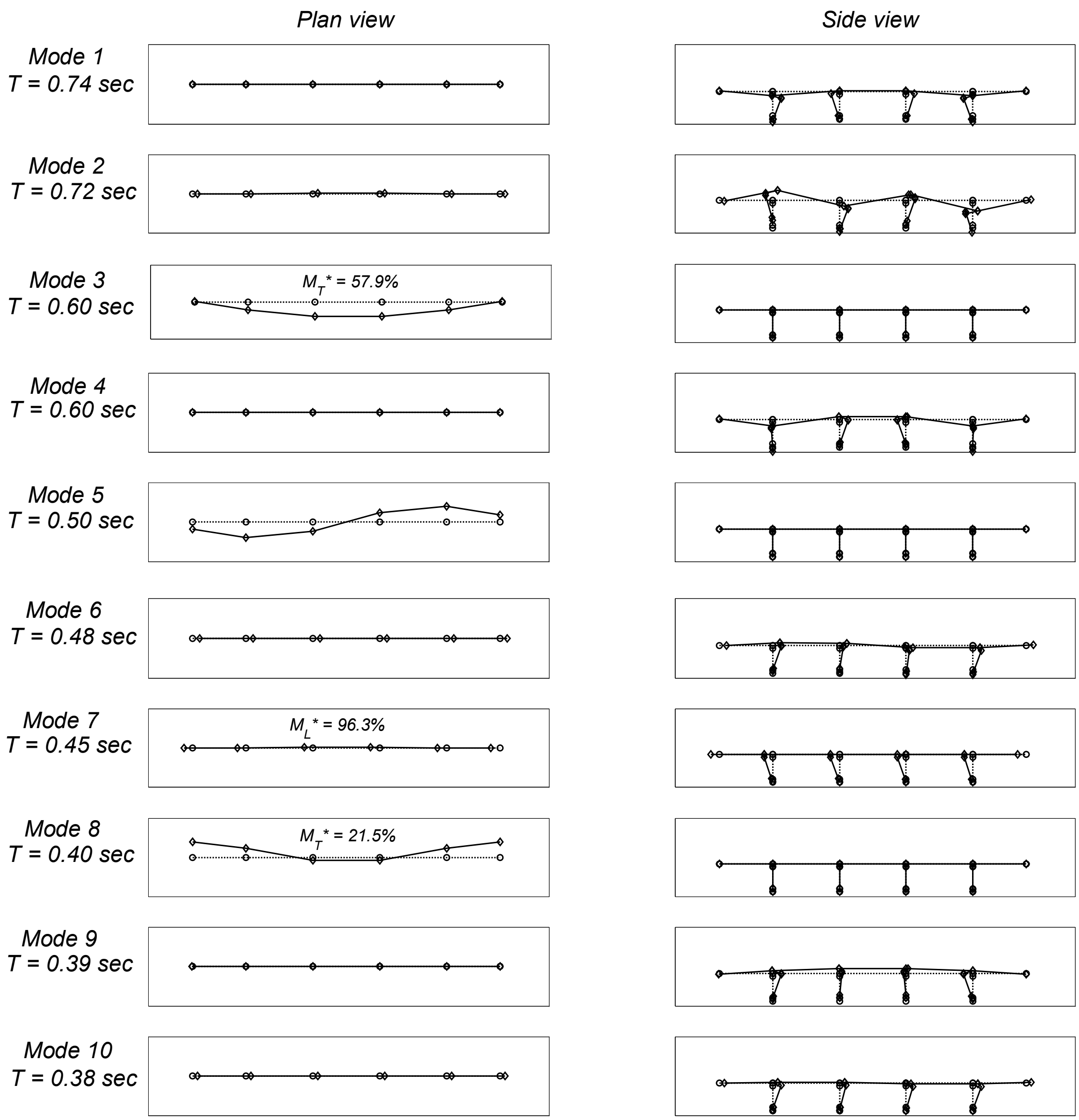

Figure 4.6 Mode shapes and periods of the first ten modes of Bridge B7-RS.

4.2 NONLINEAR RESPONSE HISTORY ANALYSIS

This section presents the results of NRHA for the two sets of ground motions described in Chapter 2. The peak values obtained for the following response parameters for each of the ground motions are as follows:

- drift ratio of the columns, defined as the ratio of the peak lateral displacement (in any direction) at the centroid of the deck to the height of this point from the base of the columns for fixed-base bridges and from the base of the foundation for bridges with rocking foundations
- rocking drift ratio, defined as the peak rotation of the foundation (in any direction)
- displacement in the longitudinal direction of the bridge at the end of the deck
- displacement of the bearings (in any direction)
- tensile strains at the base of the interior and exterior columns
- tensile strains at the top of the interior and exterior columns
- peak settlements at the edges of the rocking shallow foundations due to plastic deformation of the soil
- variation of vertical force at the base of the foundation normalized by the axial load due to gravity loads
- variation of the vertical force at the base of the foundation due to framing effects N_F normalized by the vertical force due to gravity.

Table 4.2 lists the mean values of the above response parameters for the near-fault ground motions as well as their corresponding peak values in parentheses for three B15 bridges (FB1, RP1, RS) and four B7 bridges (FB1, FB2, RP1 and RS). Table 4.3 compares the drift ratios as well as the drift ratios in the transverse and longitudinal directions of Bridges FB1, RP1, RP2a, and RP2b, B15 and B7. For the analyses using the near-fault ground motion set, the fault-normal and fault-parallel component were used in the transverse and longitudinal direction, respectively.

4.2.1 Mean Response: B15 Bridges subjected to Near-Fault (Set 1) Ground Motions

Analysis of Bridge RP1 resulted in mean displacement responses, except for the bearing displacements, similar to those for the fixed-base bridge (drift ratios and displacement of expansion joints), while for the RS bridge the mean displacement response was about 8% to 20% larger, respectively. Compared to Bridge FB1, however, the peak drift ratios were 47% and 32% larger for Bridges RP1 and RS, respectively.

Table 4.4 compares the drift ratio response of Bridges RP1 with RP2a; note that using larger foundations, columns and lead-plug rubber bearings for the RP1 bridge resulted in a 31% smaller drift ratio than for Bridge RP2a. The corresponding difference in the peak drift ratio for all near-fault motions was 32%. A comparison between Bridges RP2b and RP2a demonstrates that increasing only the foundation and column size did not reduce the mean drift ratio; however, it did reduce the peak drift ratio by 19%, indicating the significant effect that the larger bearings had in reducing displacements of the bridges with rocking pile foundations. Using lead-plug rubber bearings reduced the peak longitudinal drift ratios for Bridge B15 by 65%. Note that for Bridge RP2, the longitudinal drifts were similar to those calculated for the RP1 bridges; the smaller expansion joint allowed the mobilization of the back-wall soil at small longitudinal drifts.

Bridges RP1 and RS, which had the same type of expansions joints, resulting in about 19% larger peak displacement of the expansion joints compared to Bridge FB1. The peak displacement of the bearings in rocking designs with lead-plug rubber bearings was about half that exhibited by the fixed-base design. The mean and peak settlements at the edge of the foundations of the RS bridge were 0.04 m, and 0.11 m, respectively, corresponding to settlements normalized to the width of the foundation *B*, equal to 0.6% and 1.7%, respectively. Note that these are not mean residual settlements at the middle of the foundations.

In the fixed-base design, significant tensile strains developed at the base of the columns, with the mean values being 2.47%, and 2.03% for the interior and exterior columns, respectively. The corresponding mean values at the top of the columns were significantly smaller and less than 0.65%. The rocking foundation designs significantly reduced the inelastic response of the columns compared to the fixed-base design, with the mean strain in the columns being less than 0.20% for a peak value of 0.42%. Bridge B15 with rocking shallow foundations resulted in peak tensile strains less than 0.19%. The increase in axial load of the exterior columns due to framing effects was 9% and 5% for Bridges FB1 and RP1, respectively. The axial load variation ratio was higher and equal to 30%, and 32% because of the significant contribution of the vertical inertia effects. All the axial forces reported were filtered using a finite impulse response low-pass filter [Matlab R2008a], with cut-off frequency equal to 5 Hz, This is done to ensure that spurious numerical spikes due to sudden change of stiffness during impact of the foundation are eliminated [Wiebe and Christopoulos 2010].

4.2.2 Mean Response: Bridges B7 Subjected to Near-Fault (Set 1) Ground Motions

With the fixed-base design as the benchmark, use of rocking foundations in the B7 bridges resulted in larger displacements compared to the B15 bridges. The increase of mean drift ratios was 60% and 140% for the rocking on piles and shallow foundations designs, respectively, compared to the fixed-base bridge. Due to the use of lead-rubber plug bearings, the mean displacement of the bearings of the RP1 and RS bridges was 0.07 m and 0.10 m, respectively, compared to the 0.13 m of the fixed-base bridge. Compared to the negligible expansion joint displacements of 0.01 m of Bridge B7-FB1, the RP1 and RS bridges developed displacements of 0.03 m and 0.07 m, respectively.

As shown in Table 4.3, using smaller foundations, columns, and bearings resulted in total drift ratios 2.2 times larger in Bridge RP2a compared to Bridge RP1. The increase in the peak total drift ratio was 180%. Comparing the responses of Bridges RP1, RP2a, and RP2b, the most important factor for reducing the total drift ratios was the size of the foundation rather than the size of the bearings.

In terms of inelastic response in the columns of the B7 bridges, the rocking designs resulted in mean strains less than 0.30% while the mean values for the exterior columns of Bridges FB1 and FB2 were 2.16% and 3.05%, respectively. The peak strains were 6.28% and 7.75% for Bridges FB1 and FB2, respectively. For Bridge RP1, the peak strain was 1.33% and 0.39% for the external and internal columns, respectively, while the equivalent values for Bridge RS were less than 0.20%.

The axial load variation due to framing was nearly constant for all four bridges with a mean value of about 12% for the exterior column. The effect of framing was larger in the B7 bridges than found in the B15 bridges due to the larger axial rigidity of the columns. Note that for the rocking designs the peak value of the increase in vertical force due to framing was equal to 32%, which is significantly higher than that computed from monotonic static analysis. This is because the latter was conducted using a force vector of a specific mode, resulting in significantly different response in terms of framing effects than when computed using 3D NRHA.

Table 4.2 Mean, and peak (in parentheses) values for different response parameters for the near-fault set of ground motions.

	B15			B7			
	FB1	**RP1**	**RS**	**FB1**	**FB2**	**RP1**	**RS**
Drift ratio (%)	2.4 (6.8)	2.4 (10.0)	2.6 (9.0)	1.0 (3.9)	1.3 (4.2)	1.6 (6.6)	2.4 (7.4)
Rocking drift ratio (%)	N/A	1.9 (9.5)	2.1 (8.4)	N/A	N/A	1.4 (6.4)	2.2 (7.1)
Expansion joint displacement (m)	0.11 (0.27)	0.11 (0.31)	0.12 (0.32)	0.01 (0.04)	0.01 (0.05)	0.03 (0.14)	0.07 (0.24)
Bearing displacement (m)	0.27 (0.65)	0.14 (0.34)	0.16 (0.34)	0.13 (0.44)	0.13 (0.41)	0.07 (0.17)	0.10 (0.27)
ε_s, interior column base (%)	2.47 (7.42)	0.20 (0.42)	0.15 (0.19)	1.73 (6.15)	2.79 (7.53)	0.30 (1.33)	0.14 (0.20)
ε_s, exterior column base (%)	2.03 (6.45)	0.18 (0.37)	0.13 (0.17)	2.16 (6.28)	3.05 (7.75)	0.19 (0.39)	0.13 (0.20)
ε_s, interior column top (%)	0.64 (2.55)	-	-	0.29 (1.27)	0.60 (2.95)	-	-
ε_s, exterior column top (%)	0.65 (2.28)	-	-	0.39 (1.34)	0.79 (3.03)	-	-
Peak foundation edge settlement (m)	N/A	N/A	0.04 (0.11)	N/A	N/A	N/A	0.04 (0.13)
Axial load variation ratio, interior column*	0.27 (0.53)	0.32 (0.85)	0.53 (0.71)	0.28 (0.75)	0.32 (0.86)	0.57 (1.39)	0.60 (1.45)
Framing effect in axial load variation ratio, interior column N_F / N_G	0.03 (0.06)	0.03 (0.08)	0.02 (0.04)	0.04 (0.14)	0.01 (0.07)	0.07 (0.13)	0.06 (0.15)
Axial load variation ratio, exterior column*	0.30 (0.56)	0.25 (0.76)	0.23 (0.56)	0.43 (0.96)	0.47 (1.05)	0.41 (0.93)	0.45 (1.16)
Framing effect in axial load variation ratio, exterior column N_F / N_G	0.09 (0.13)	0.05 (0.13)	0.04 (0.09)	0.11 (0.26)	0.01 (0.18)	0.12 (0.32)	0.11 (0.27)

*Filtered at 5 Hz.

Table 4.3 **Mean, and peak (in parentheses) values for the drift ratios for the near-fault ground motions of the fixed-base and rocking-on-piles bridges.**

	Total (%)	Transverse (%)	Longitudinal (%)
B15-FB1	2.4 (6.8)	2.4 (6.8)	0.8 (1.7)
B15-RP1	2.4 (10.0)	2.4 (10.0)	0.7 (1.9)
B15-RP2a	3.5 (14.6)	3.3 (14.6)	0.8 (2.1)
B15-RP2b	3.5 (11.8)	3.1 (11.0)	1.8 (5.5)
B7-FB1	1.0 (3.9)	1.0 (3.9)	0.2 (0.6)
B7-RP1	1.6 (6.6)	1.5 (6.6)	0.6 (1.8)
B7-RP2a	3.7 (18.3)	3.5 (18.3)	1.2 (3.2)
B7-RP2b	2.2 (8.0)	1.7 (7.2)	1.4 (5.9)

4.2.3 Mean Response: B15 Bridges Subjected to Broadband Set (Set 2) of Ground Motions

For the broadband set of ground motions, the mean drift ratios in Bridges B15 were 17% smaller for the rocking-on-piles bridges and equal for the shallow foundations designs compared to the fixed-base bridge. The peak drift ratio increased by 33% and 40% for the two rocking designs, respectively. The mean tensile strains of the longitudinal steel at the base of the columns of the fixed-base bridge were less than 0.67%, with a peak of 5.62%. The corresponding numbers for the top of the columns were less than 0.22%. The rocking designs had strains less than 0.21% for all cases. The mean and peak foundation edge settlements of the shallow foundation design were 0.02 and 0.08 m, respectively.

4.2.4 Mean Response: B7 Bridges Subjected to Broadband Set (Set 2) Ground Motions

Bridges B7-RP1 and B7-RS developed 20% and 100% larger drifts compared to the fixed-base designs, respectively, with peak drifts roughly twice for both rocking bridges. The mean expansion joints were negligible for all cases; both the mean and peak bearing displacements were again significantly reduced in the rocking designs. The tensile strains at the columns of Bridge B7-FB1 were similar to those strains recorded for Bridge B15-FB1, and they were less than 0.47% for all rocking designs. The mean and peak foundation edge settlements of the shallow foundation design were 0.02 and 0.07 m, respectively.

Table 4.4 Mean, and peak (in parentheses) values for different response parameters for the broadband set of ground motions.

	B15			B7			
	FB1	**RP1**	**RS**	**FB1**	**FB2**	**RP1**	**RS**
Drift ratio, (%)	1.2 (5.5)	1.0 (7.3)	1.2 (7.7)	0.5 (3.0)	0.6 (3.6)	0.6 (6.2)	1.0 (6.2)
Rocking drift ratio, (%)	N/A	0.7 (6.8)	0.8 (7.1)	N/A	N/A	0.4 (6.0)	0.8 (5.9)
Expansion joint displ., (m)	0.01 (0.09)	0.01 (0.06)	0.01 (0.07)	0.00 (0.00)	0.00 (0.00)	0.00 (0.01)	0.01 (0.03)
Bearing displacement, (m)	0.13 (0.47)	0.04 (0.16)	0.05 (0.16)	0.06 (0.33)	0.06 (0.28)	0.03 (0.07)	0.03 (0.07)
ε_s, int. column base, (%)	0.67 (5.62)	0.13 (0.21)	0.11 (0.18)	0.43 (4.97)	0.68 (5.89)	0.12 (0.47)	0.10 (0.17)
ε_s, ext. column base, (%)	0.50 (4.18)	0.10 (0.18)	0.08 (0.16)	0.66 (5.11)	0.87 (5.27)	0.12 (0.19)	0.08 (0.14)
ε_s, int. column top, (%)	0.04 (0.20)	-	-	0.05 (0.13)	0.06 (0.18)	-	-
ε_s, ext. column top, (%)	0.06 (0.22)	-	-	0.13 (0.17)	0.16 (0.24)	-	-
Peak foundation edge settlement, (m)	N/A	N/A	0.02 (0.08)	N/A	N/A	N/A	0.02 (0.07)
Axial load variation ratio, interior column*	0.13 (0.34)	0.18 (0.71)	0.16 (0.52)	0.16 (0.53)	0.18 (0.63)	0.24 (1.58)	0.27 (1.23)
Framing effect in ALVR, interior column N_F / N_G	0.01 (0.03)	0.01 (0.05)	0.01 (0.04)	0.02 (0.03)	0.01 (0.03)	0.01 (0.08)	0.02 (0.08)
Axial load variation ratio, exterior column*	0.13 (0.41)	0.13 (0.47)	0.10 (0.32)	0.21 (0.90)	0.22 (0.95)	0.16 (0.77)	0.17 (0.55)
Framing effect in ALVR, exterior column N_F / N_G	0.04 (0.09)	0.02 (0.07)	0.02 (0.06)	0.03 (0.08)	0.04 (0.10)	0.03 (0.17)	0.04 (0.17)

*Filtered results at 5 Hz.

4.2.5 Response to Individual Ground Motions

This section presents the responses to the 40 individual ground motions of each of the two sets considered. Figure 4. shows the peak drift ratios for all bridges. For the B15 bridges with rocking foundations for all motions except near-fault ground motions (number 19, 21, 28 and 31 and broadband motions number 10, 18 and 19), the drift was less than 7%. Four of these ground motions—two from the Northridge 1979 earthquake and two from the Chi-Chi 1999 earthquake—include strong pulses of long predominant period T_p. The peak drift ratio for the B15 bridges with rocking-pile and shallow foundations occurred when subjected to the TCU052 station record ground motion 28 (the 1999 Mw 7.6 Chi-Chi, Taiwan, earthquake), which was equal to 10%, and 9.0%, respectively.

Figure 4. shows the drift ratios of Bridges B7-FB1 and B7-FB2. The mean drift ratio for Bridge B7-FB2 was about 30% larger than that of Bridge B7-FB1, which had 25% more lateral strength at 2% drift ratio based on monotonic static analysis. As shown in Table 4.2, the mean tensile strains at the base of the columns of Bridge B7-FB2 were 70% larger than the corresponding mean strain of Bridge B7-FB1.

Figure 4. shows the peak tensile strain of the steel at the base of the interior columns of Bridges B15 and B7 for the two sets of ground motions, and Figure 4. plots the corresponding results for the exterior columns. For Bridge B15-FB1, the number of near-fault ground motions that resulted in strains at the base of the interior larger than 3% and 4%, was 16 and 11, respectively. The corresponding numbers for Bridge B7-FB1 were 10 and 8.

The tensile strains for the B15 bridges with rocking foundations were less than 0.5% for all ground motions considered herein. For Vridge B7 with rocking pile foundations, six near-fault records resulted in strains larger than 0.5%. This was due to the 3D response of the bridge, which resulted in large moments at the top of the columns of equal sign with the moments at the base, as opposed to zero top column moments assumed in the design (triangular moment diagram).

The maximum tensile strains near the top of the columns of the fixed-base bridges are shown in Figure 4.1. For the near-fault ground motions and for Bridge B15-FB1, 11 motions resulted in strains larger than 1%, while seven motions resulted in strains larger than 1% for Bridge B7-FB1. For ground-motion Set 2, the strains were less than 0.24% for every motion for both B15 and B7 fixed-base bridges.

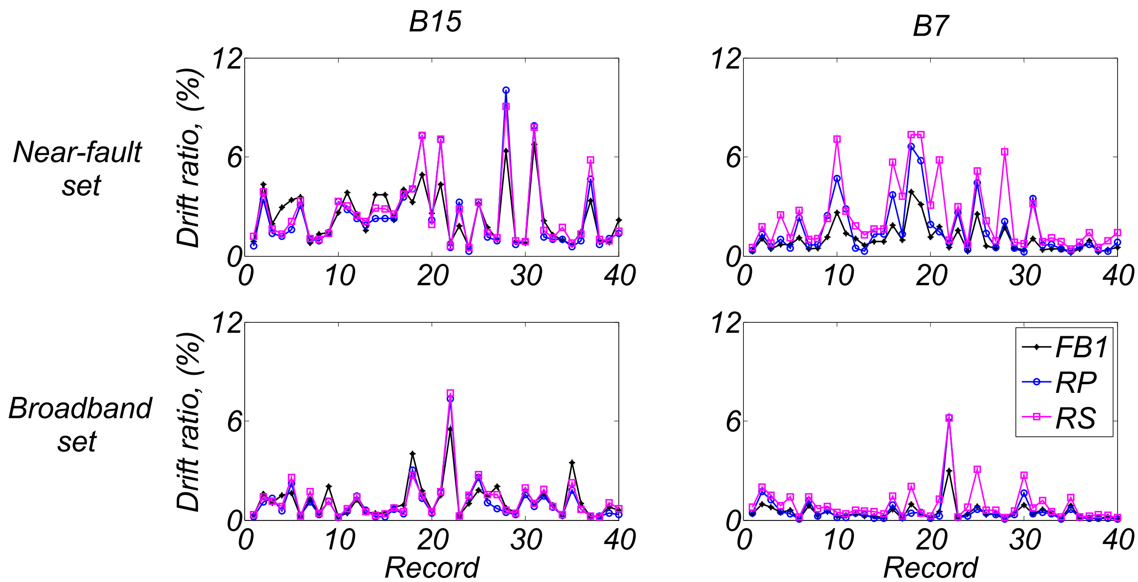

Figure 4.7 Drift ratios of the six main bridges considered.

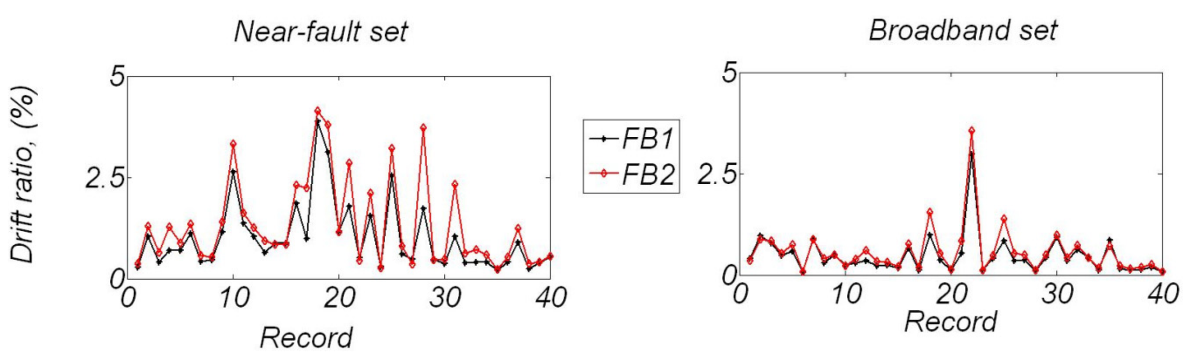

Figure 4.8 Comparison of the drift ratios for the two fixed-base B7 bridges.

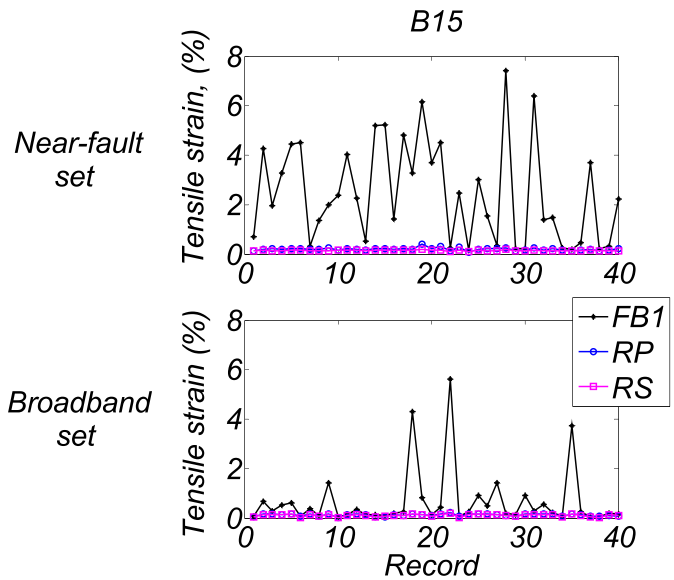

Figure 4.9 Maximum tensile strains near the base of the interior columns.

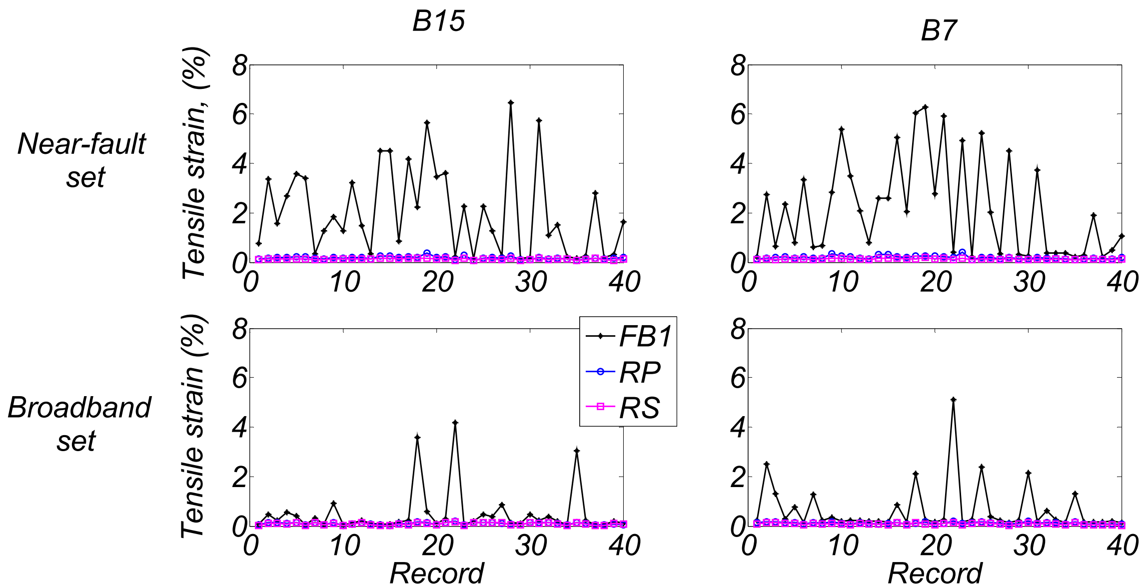

Figure 4.10 Maximum tensile strains near the base of the exterior columns.

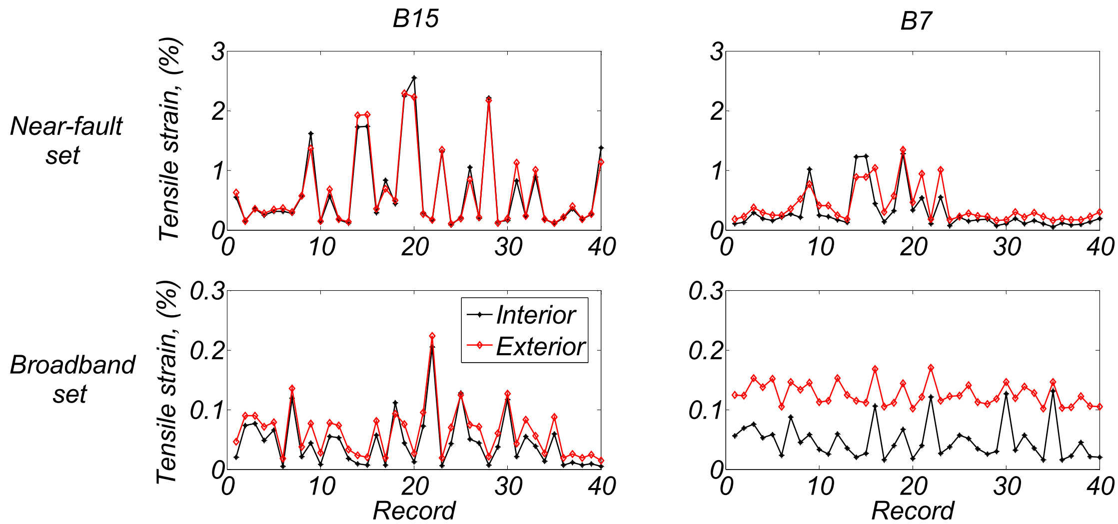

Figure 4.1 Maximum tensile strains at the top of the columns for the FB1 bridges.

Figure 4.2 and Figure 4.3 plot the unfiltered axial load variation in the interior and exterior columns, respectively, while Figure 4.4 and Figure 4.5 plot the filtered axial load variations using the low-pass filter (described in Section 2) with a cut-off frequency of 5Hz. The axial load variation is due to the combined effects of vertical inertia and framing effects between the columns, deck, and abutment. Filtering reduces significantly the axial load variation primarily for the bridges with rocking-pile foundations, while it reduces somewhat the variation for bridges with shallow foundations. This is because in the case of rocking-pile foundations the stiffness recovers due to the impact of the foundation on the piles; therefore, it is modeled with high axial rigidity, resulting in high-frequency spikes of vertical acceleration and thus inertia forces.

Figure 4.16 and Figure 4.17 plot the unfiltered increase in axial load due to framing normalized to the vertical force due to gravity for the interior and the exterior columns, respectively. The effect of framing is more important in the B7 bridges due to the larger axial stiffness of the columns. The effect is negligible for interior columns for most motions of Set 2. For the interior columns subjected to near-fault ground motions, the effect of framing is generally larger for bridges with rocking pile foundations. For the exterior columns, the effect is more important than for the interior for both sets of motions, which is in agreement with the pushover analysis results presented in Chapter 2. For Bridge B7, the axial load variation due to framing effects is more than 0.2 for seven and six near-fault ground motion motions for Bridges RP1 and RS, respectively. Figure 4.18 presents the peak displacement of the expansion joints for each individual ground motion for Bridges FB1, RP1, and RS.

Despite the use of a pin connection between the column and the deck in the longitudinal direction, the use of lead-plug rubber bearings with larger initial stiffness and strength at the abutments of the rocking bridges resulted in similar deformations of the expansion joint compared to the fixed-base bridge. In general, the lead-plug rubber bearings reduced the longitudinal drifts of the rocking bridges. Figure 4.19 plots the peak displacement of the bearings, which are higher for the fixed-base bridges, as discussed above. Finally, Figure 4.20 presents the edge settlements of the shallow foundations, where peak edge settlement of more than 0.10 m corresponding to 1.5% of the foundation width *B* was computed for three and one near-fault ground motions in Bridges B15 and B7, respectively.

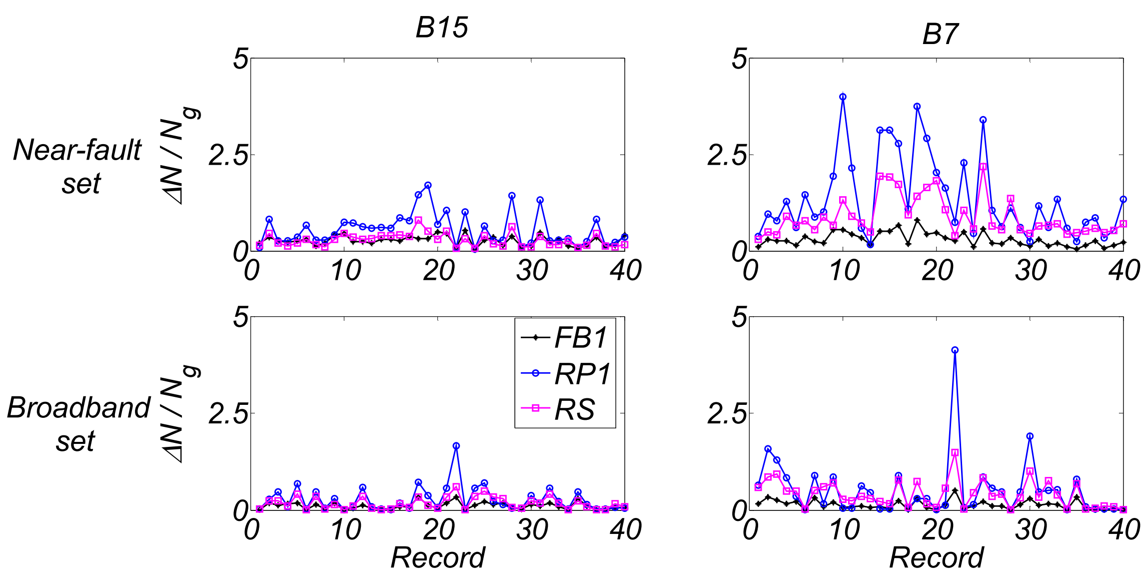

Figure 4.2 Unfiltered axial load variation in the interior columns.

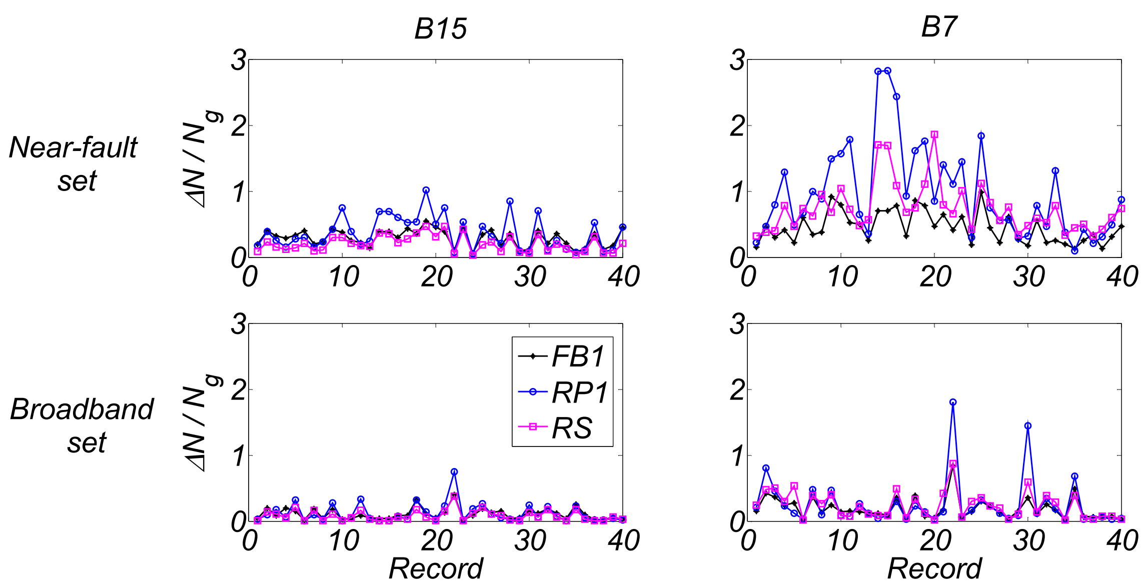

Figure 4.3 Unfiltered axial load variation in the exterior columns.

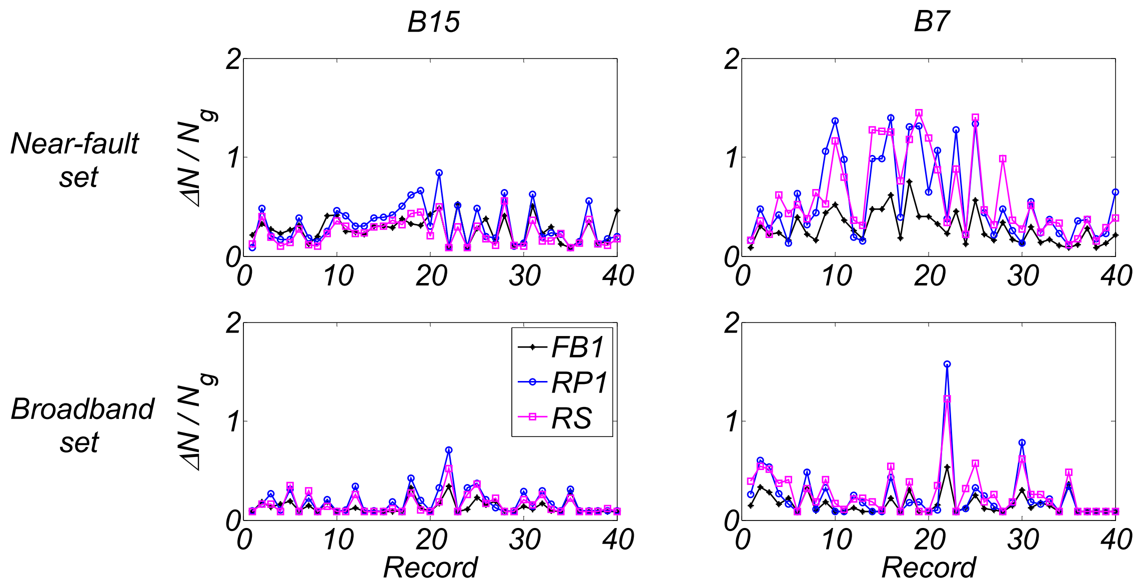

Figure 4.4 **Low-pass filtered axial load variation in the interior columns (with a cut-off frequency of 5 Hz).**

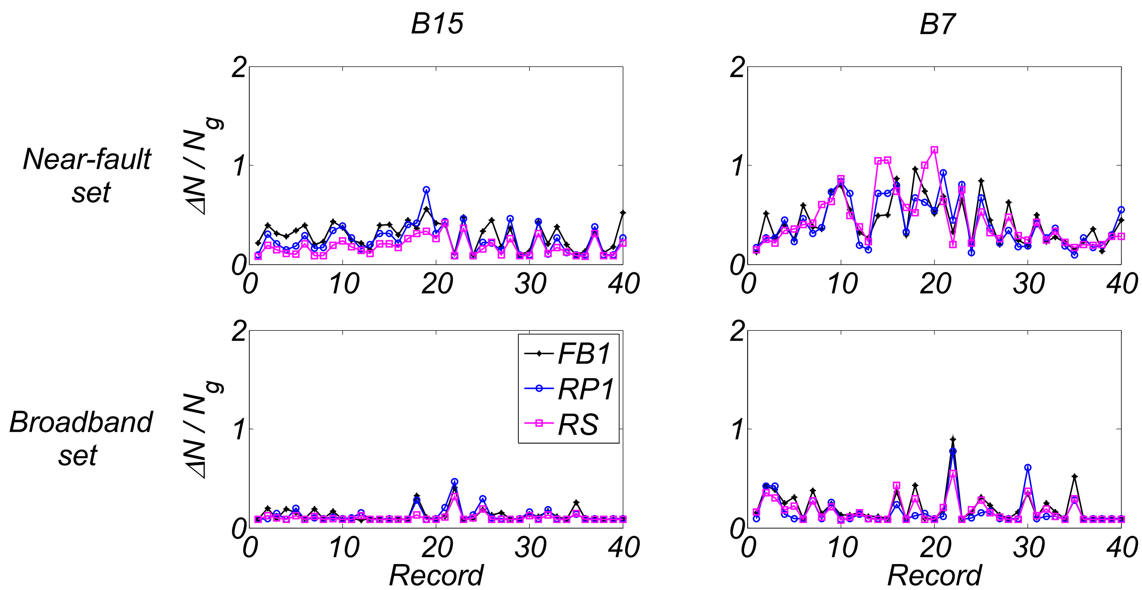

Figure 4.5 **Low-pass filtered axial load variation in the exterior columns (with a cut-off frequency of 5 Hz).**

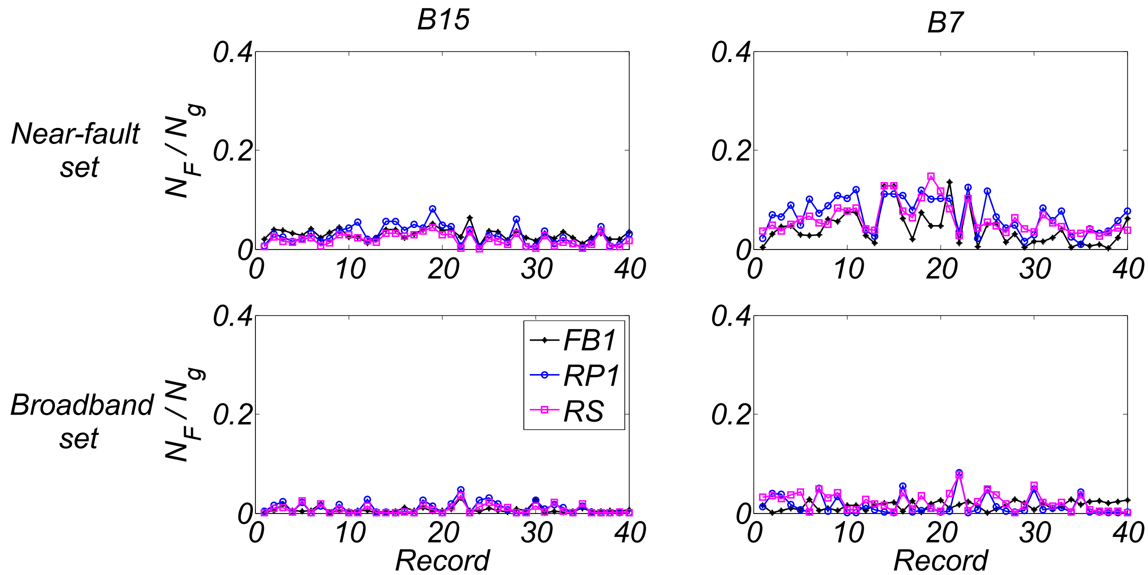

Figure 4.6 Increase in axial load of the interior columns due to framing effects.

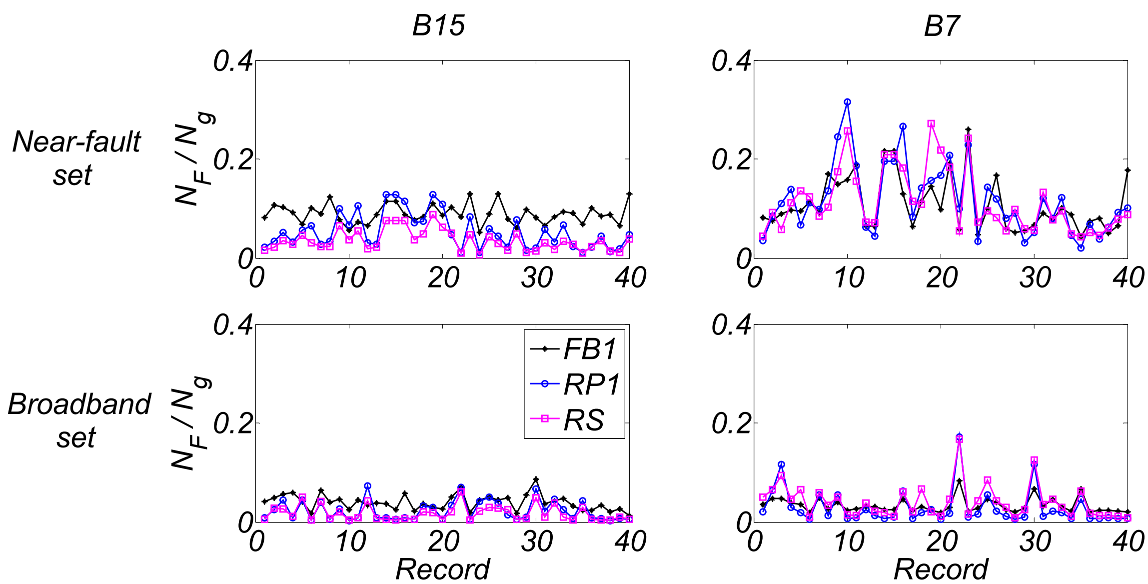

Figure 4.7 Increase in axial load of the exterior columns due to framing effects.

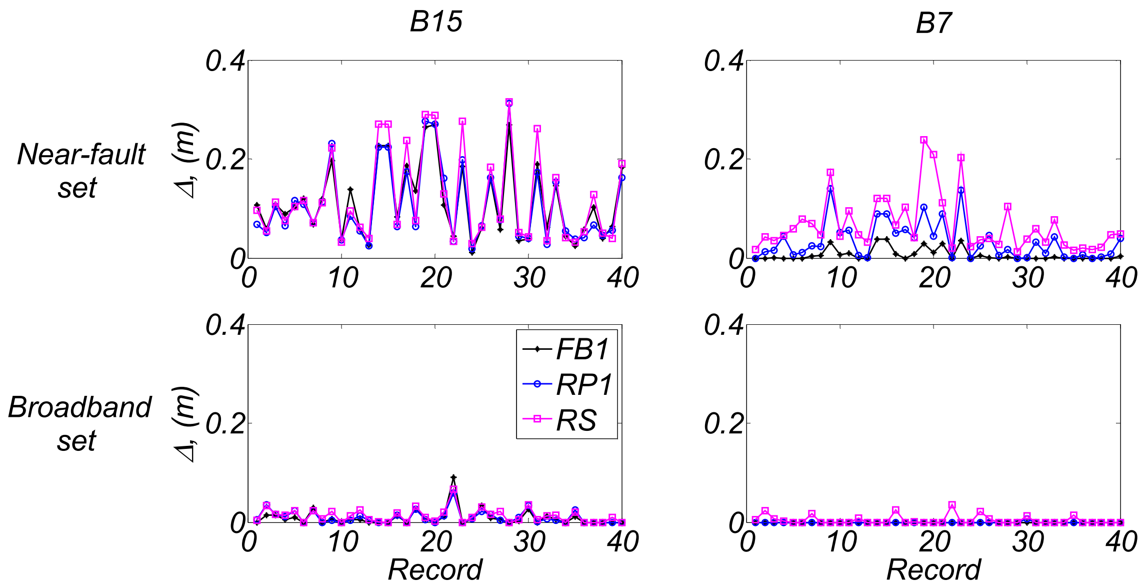

Figure 4.8 Peak expansion joint displacement for the six main bridges.

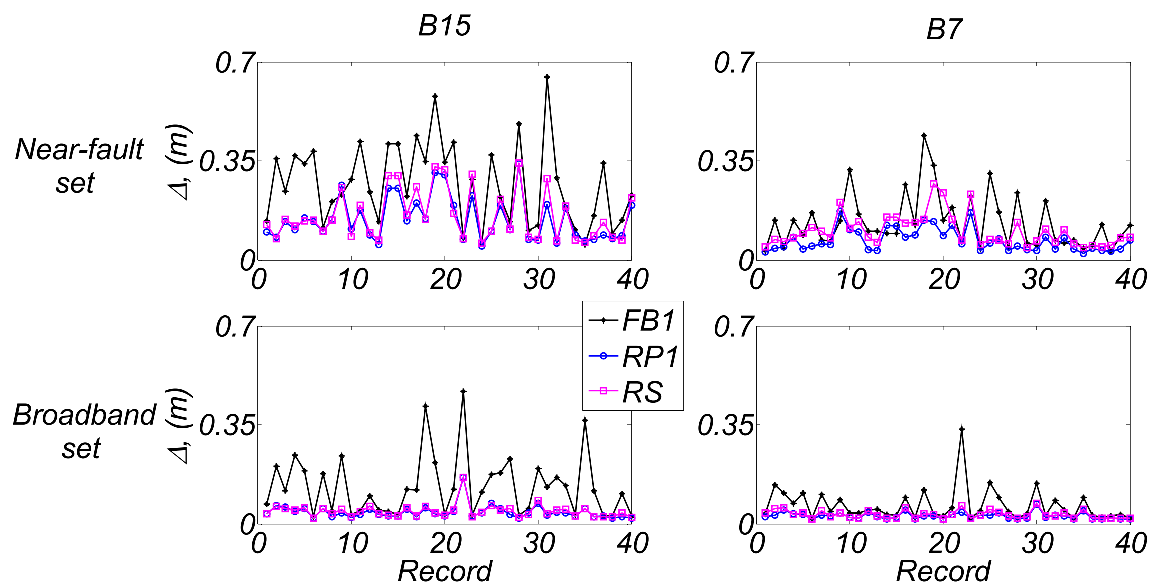

Figure 4.9 Peak bearings displacement for the six main bridges.

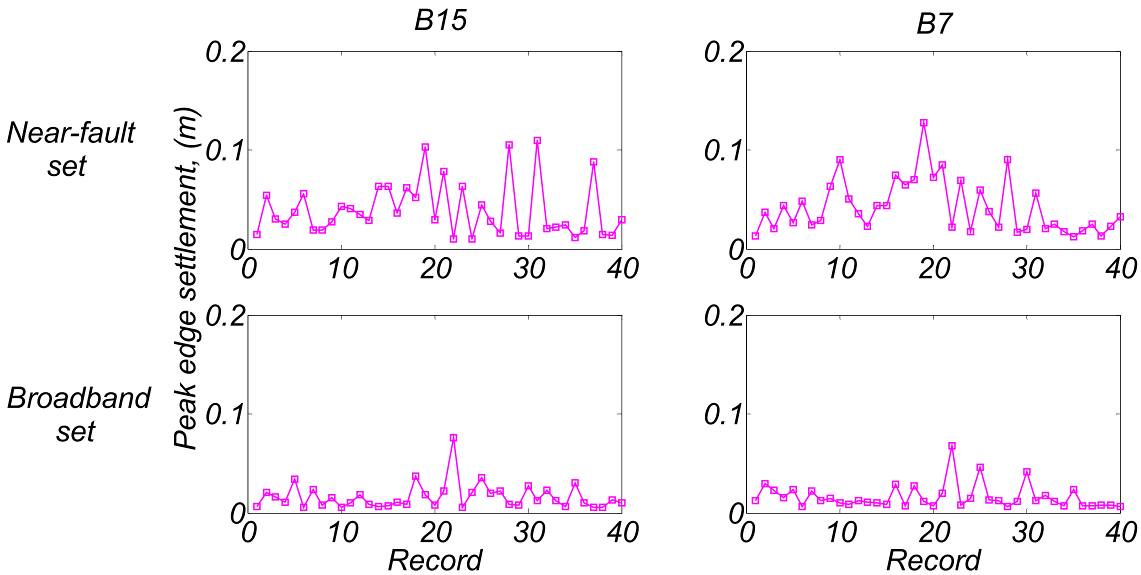

Figure 4.20 Maximum settlements at the edge of the footings for the shallow foundation bridges (RS).

5 Probabilistic Seismic Performance Evaluation

This chapter presents the probabilistic seismic performance evaluation of nine of the eleven bridges described in Chapter 2, conducted using PEER's PBEE methodology developed by Mackie et al. [2008]. The results are presented in terms of post-earthquake repair cost versus seismic hazard intensity measure, which in this study is the linear spectral acceleration S_a at period $T = 1$ sec with a 2% damping ratio.

5.1 DESCRIPTION OF METHODOLOGY

The method used in this study was developed by Mackie et al. [2008] based on the PEER PBEE methodology [Cornell and Krawinkler 2000]. The PEER PBEE framework utilizes the total probability theorem and involves intermediate probabilistic models that include seismic hazard intensity measures (*IMs*), engineering demand parameters (*EDPs*), damage measures (*DMs*), and socio-economic decision variables (*DVs*). The *DVs* are then related to the seismic hazard *IMs* considering randomness and uncertainties in all the intermediate models.

Mackie et al. [2008], classifies structural components into performance groups according to their repair method corresponding to their damage states. This allows for a detailed calculation of the post-earthquake repair cost and duration by considering in a discrete manner the damage developed in the main components of the bridge.

As implemented here, the method starts with a *Demand Model*, which relates the seismic hazard *IM* of the ground motions and the elastic spectral acceleration S_a ($T = 1$ sec), to different *EDP*s, which have been calculated from NRHA. The next intermediate probabilistic model of the method is the *Damage Model* for the different components of the bridge, which relates the probability of exceedance of a discrete damage state (*DS*) of each component to the *EDP* selected to describe the damage of this component. Five components of the bridge were considered:

- columns
- combined expansion joints, abutment back-wall, and approach slab
- bearings

- shear keys at the abutments
- shallow foundations.

As shown in Table 5.1, a different *EDP* was used for each of the five components.

The next part of the method relates the damage states of the different components with appropriate repair methods, which require different quantities (*Q*) of materials with specific unit costs. The total repair cost is calculated based on the *Q* quantities and their unit costs. Therefore, the *Decision Model*, which traditionally relates the damage states to different decision variables *DV,* is quantified through the *Qs*. In this study, the second of the three approaches considered by Mackie et al. [2008] was adopted, which uses continuous functions between *IM-EDP*, *EDP-DS* and *DS-Q*, and integrates them by using the closed form solution described below.

Table 5.1 Engineering demand parameters for the components considered.

Component	Engineering Demand Parameter
Column	Flexural drift ratio
Exp. joint, abutment back-wall, approach slab	Expansion joint displacement
Bearing	Bearing displacement
Abutment shear key	Transverse deck displacement at abutment
Shallow foundation	Settlement of footing along the four sides of its perimeter

5.1.1 Demand Model

The *Demand Model* relates the *EDPs* to the *IM*. For each of the ground motions considered the different *EDPs* are calculated using NRHA, see Chapter 4. Figure 5.1 shows the demand models of three *EDPs* for near-fault ground motions (Set 1) of Bridges B15-FB1 and B15-RP1. The same demand models with the addition of the shallow foundation are shown in Figure 5.2 for Bridge B15-RS for the near-fault set of ground motions. A power law relation between *EDPs* and *IM* is developed in linear and logarithmic scale using a least squares fitting based on Equations (5.1) and (5.2), respectively, where $a = \exp(A)$ and $b = B$.

$$EDP = a(IM)^b \tag{5.1}$$

$$\ln(EDP) = A + B\ln(IM) \tag{5.2}$$

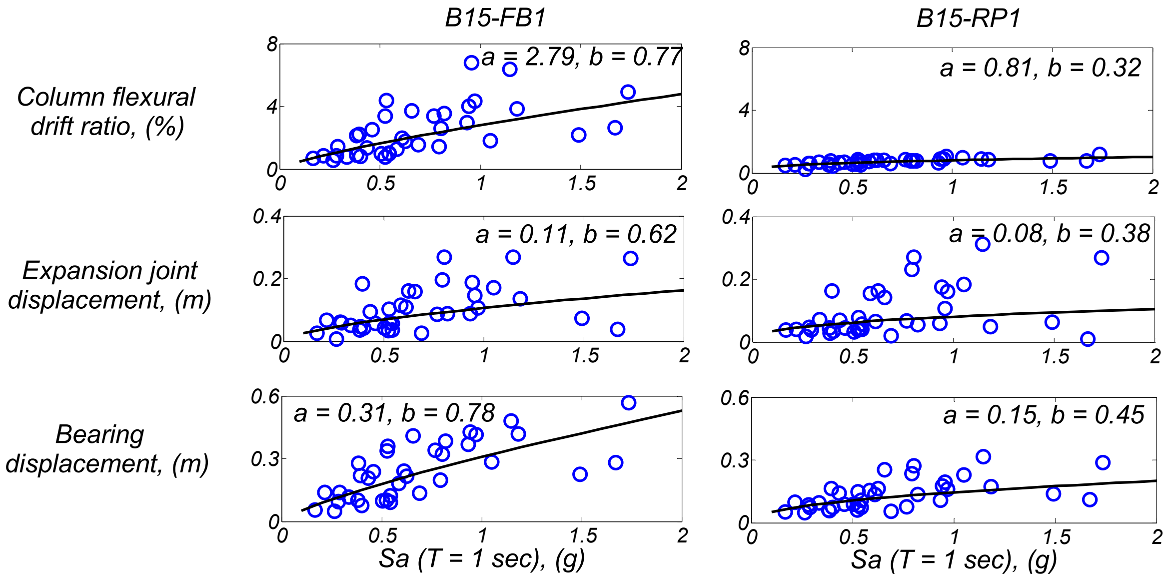

Figure 5.1 Three of the five demand models for Bridges B15-FB1 and B15-RP1 for the near-fault set of ground motions.

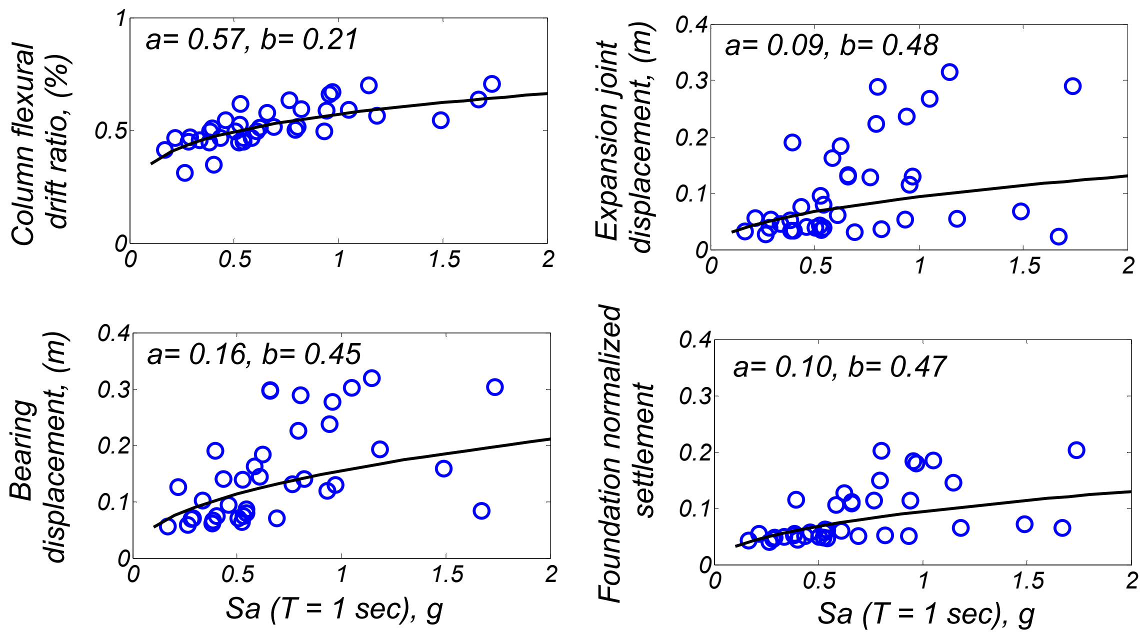

Figure 5.2 Four of the five demand models for Bridge B15-RS for the near-fault set of ground motions.

5.1.2 Damage Models

This model relates the probability of exceedance of a discrete *DS* of a component to a characteristic *EDP*. The damage models of the columns, shear keys, combined components of expansion joint-abutment back wall-approach slab, and bearings were similar to those described in Mackie et al. [2008]. A new damage model for the shallow foundations was developed and is described below.

The damage models were assumed continuous, and the following power law relation between the *DM* and *EDP* was used:

$$DM = c\left(EDP\right)^{d} \tag{5.3}$$

$$\ln\left(DM\right) = C + D\ln\left(EDP\right) \tag{5.4}$$

with $c = \exp(C)$ and $d = D$

While the damage states are discrete, the damage models are assumed continuous, whereby $C = 0$ and $D = 1$. Figure 5.3 shows the four damage models used in this study (with the exception of the shallow foundations). The damage model of the rocking and fixed-base bridges for the bearings and combined expansion joint-back wall-approach slab presented herein differs from that described in Mackie et al. [2008] because different bearings and expansion joints were used. The damage states considered for each of these four components and the value of *EDP* for which the probability of exceedance of each *DS* is 50% are shown in Tables A.1 to A.4 of Appendix A.

The repair methods for each performance group were assigned according to the damage state. The repair work required different materials such as epoxy, concrete, reinforcing steel, removal of concrete, etc., and the amount of materials required was related to the geometry of the bridge. These are summarized in the Tables A.1 to A.4 and are similar to those used by Mackie et al. [2008]. The unit costs (at 2008 prices) for each repair quantity are shown in Table A.5 of Appendix A.

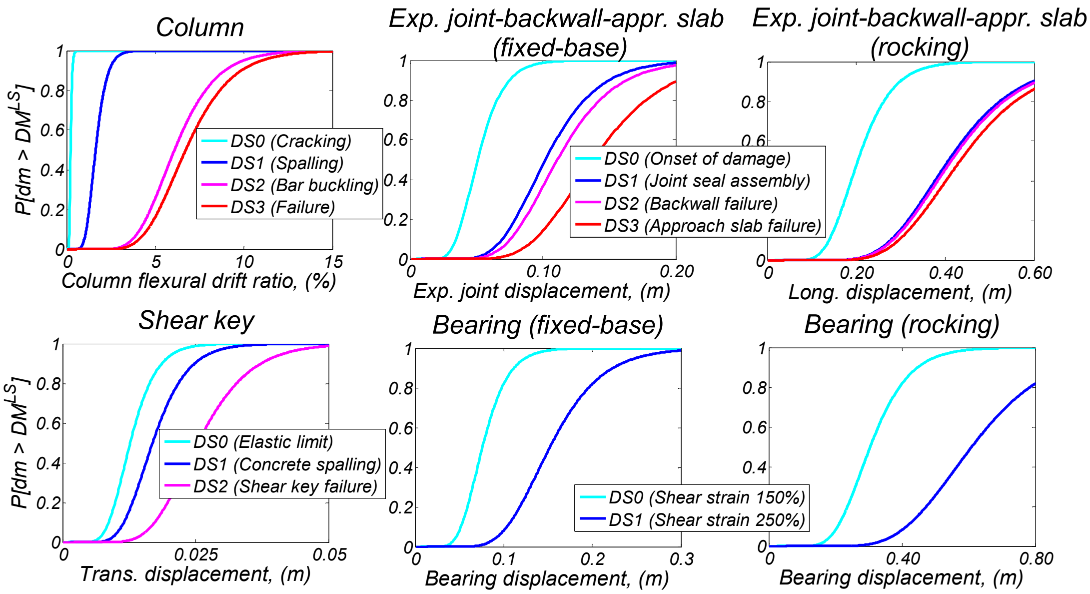

Figure 5.3 Damage models of the components considered (except for shallow foundations).

5.1.3 Damage Model for Shallow Foundations

The damage indicator and thus the *EDP* used for the shallow foundations in this study was z / z_y, where z is the settlement of the foundation and z_y the settlement at first yield of the soil. The damage of the foundation was assumed to be related only to the soil under the footing; no damage was associated with the concrete footing itself. As shown in Figure 5.4, the yield settlement, z_y, was defined based on the uniaxial vertical soil stress versus settlement relation and is 2.5 times the settlement z_{50}. This is the settlement at vertical stress $q = 0.5q_{ult}$, where q_{ult} is the ultimate stress. Figure 5.4 also plots the settlements at which the four discrete damage states are defined.

Response parameter z was computed from NRHA. For each side of the perimeter of the foundation, see Figure 5.5, the average of the settlements at the two ends of this side describes the overall damage and quantifies the repair works and the associated cost. The repair methods associated with this type of damage include improving the soil condition in the vicinity of the shallow foundation by using compaction of the soil and/or replacement.

For the repair methods for each of the four damage states described below, a bilinear profile of the settlement along a cut passing from the centroid of foundation, O, was considered (see Figure 5.5). The bilinear approximation of the actual curved profile shown in Figure 5.5 estimated adequately the quantity of damaged soil requiring remediation.

Four damage states were defined for the shallow foundation based on the magnitude of z / z_y, see Table 5.2. The damage model was assumed to be lognormal with dispersion equal to 0.3 and is shown in Figure 5.6 for the different damage states. The first damage state (DS0) occurs for $z = 0.4z_y$ and involves settlements under essentially elastic behavior of the soil and negligible damage. In DS1 $z = 0.8z_y$; some limited damage is expected, which is repaired with compaction of the soil near the perimeter of the footing. The surface area requiring compaction is up to 1.2 m away from the footing perimeter. No excavation and soil replacement is considered as necessary for this damage state.

The third damage state (DS2) is defined as z / z_y = 1.2, corresponding to limited inelasticity in the soil. To repair the soil in this case, the volume of soil shown in Figure 5.7 is replaced. This repair work requires temporary support of the deck and the column above the foundation. For shallow foundations of vertical load factor (FS_v) larger than 5, the required temporary support was assumed to be designed for 20% of the service load on the footing; thus repair work can be conducted at different times on each side of the footing. The area of soil surface that needs replacement extends 1.8 m away from the perimeter of the footing, and the corresponding depth of this area is equal to the foundation height (H_f) plus the maximum settlement (z). The crew can then access the edge of the footing, place the required temporary support, and restore the soil beneath. The surrounding soil is replaced and compacted. Once that is completed, the next side of the foundation perimeter is repaired. The last damage state (DS3) occurs for z / z_y = 1.6, which corresponds to more inelasticity in the soil. The repair work required is similar to the previous damage state, but in this case requires a temporary support able to carry 50% of the design axial load of the footing.

Table 5.2 Damage states repair works and quantities for the shallow foundations.

Damage State	Description	Normalized settlement z/z_y	Repair item	Quantity
DS0	Elastic soil	0.4	N/A	N/A
DS1	Onset of damage	0.8	Compact soil around foundation (SM*)	(Width of footing) × 1.2 m + 2 x 2.4 m × 1.2 m
DS2	Limited inelasticity	1.2	Structure excavation (CM**) Structure backfill (CM) Temporary support (SM)	Volume as shown in Figure 5.7 (same with excavation) 0.2*(Tributary length) × (deck width)
DS3	Some inelasticity	1.6	Structure excavation (CM) Structure backfill (CM) Temporary support (SM)	Volume as shown in Figure 5.7 (same with excavation) 0.5*(Tributary length) × (deck width)

*Square meters (SM), ** Cubic meters (CM).

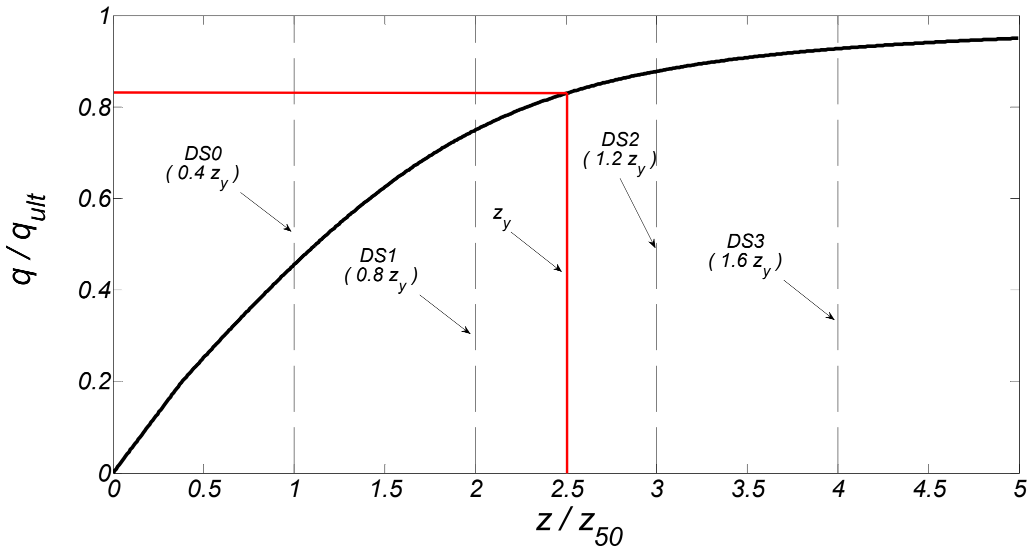

Figure 5.4 **Definition of the yield settlement z_y based on the uni-axial stress-displacement relation used in the springs representing the soil under the foundation.**

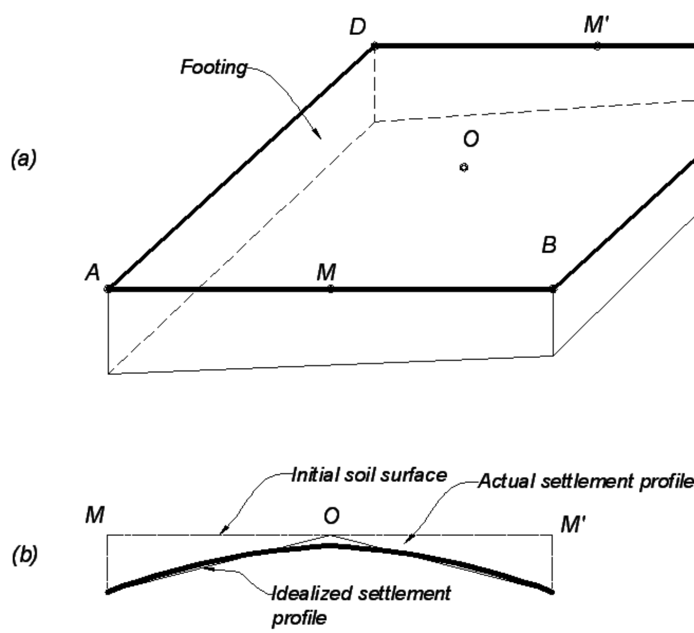

Figure 5.5 **(a) Three-dimensional settlement profile of a rocking shallow foundation subjected to cyclic loading, and (b) 2D profile of settlement for a cut passing from the centroid, O.**

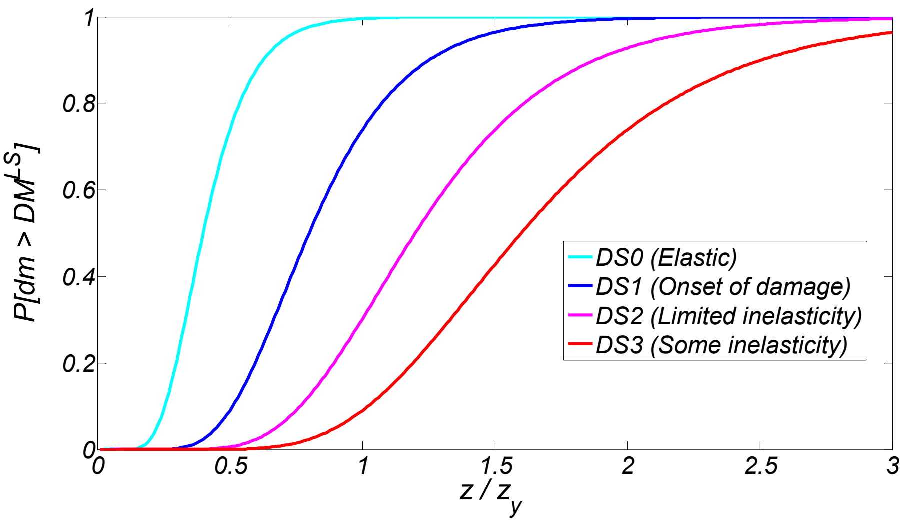

Figure 5.6 Shallow foundation damage model.

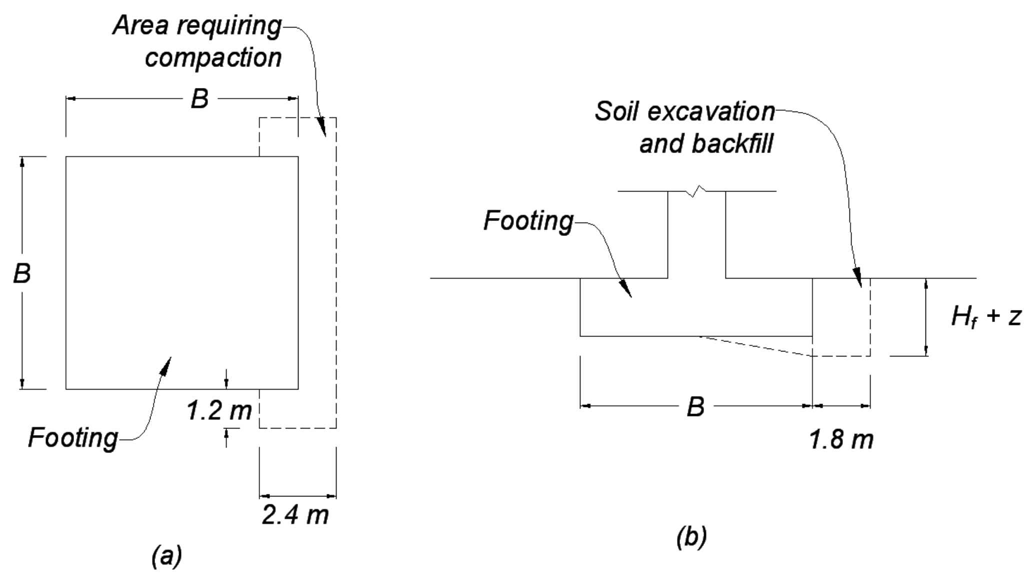

Figure 5.7 Foundation repair work: (a) DS1 (plan view) and (b) DS2 and DS3 (side view).

5.1.4 Decision Model

The *Decision Model* relates the *DM*s to the *DVs*, which is the total repair cost. The intermediate variable of repair quantities Q and their unit costs (see Table A.5 in Appendix A) are used to calculate the total repair cost. The median relationship between the damage measure (DM) and the DV can be approximated with the power law relation Equation (5.5) in linear space and the linear relation Equation (5.6) in logarithmic space, with $e = \exp(E)$ and $f = F$.

$$DV = e\left(DM\right)^{f} \tag{5.5}$$

$$\ln\left(DV\right) = E + F\ln\left(DM\right) \tag{5.6}$$

5.1.5 Integration of Intermediate Models

Assuming the intermediate *IM-EDP*, *EDP-DM*, *DM-DV* models to be lognormal, with associated dispersions $\sigma_{EDP|IM}$, $\sigma_{DM|EDP}$ and $\sigma_{DV|DM}$, and computing the closed form solution in the *IM-EDP-DM-Q* space instead of the *IM-EDP-DM-DV* space, as described in Mackie et al. [2008], the following fragility curves can be calculated:

$$P\left(Q > q^{LS} \mid IM = im\right) = 1 - \Phi\frac{\ln\left(q^{LS}\right) - \left[E + FC + FDA + FDB\ln\left(im\right)\right]}{\sqrt{d^2 f^2 \sigma^2_{EDP|IM} + f^2\sigma^2_{DM|EDP} + \sigma^2_{Q|DM}}} \tag{5.7}$$

Using the above curves and for each *IM*, the expected values $q_{n,l}$ for every repair item n and performance group l are calculated. Some repair materials are used in several repair methods for different components, while the cost of the materials can change with the quantity required. Summing up over the repair quantities of each material needed and then multiplying it with the cost corresponding to its required quantity leads to material costs that are then summed up to result into a total median repair cost for the *IM* used. The final results of the probabilistic performance evaluation are presented in terms of median repair cost versus *IM*.

5.2 PERFORMANCE-BASED EVALUATION RESULTS

Figure 5.8 shows the total repair cost versus *IM* (S_a for T = 1 sec) for the fixed-base bridges (FB1, FB2), rocking on piles bridges (RP1, RP2a), and shallow foundation (RS) bridges. Bridge B15-FB1 was also evaluated for the case where damage in the expansion joint, back-wall and approach slab is avoided by using larger expansion joints, see FB1* in Figure 5.8.

For the near-fault set of ground motions and the B15 bridges, the repair cost of the fixed-base bridge is significant even for small values of the *IM*. For S_a (T = 1 sec) equal to 0.5g and 0.65g reflecting that the shear keys have broken, whereas after 0.4g the columns repair cost exhibits a step increase (see also Figure 5.9, for the cost disaggregation). At S_a = 1.5g, one of the expansion joints, abutment back-walls, and approach slabs are damaged, increasing the cost by 35% (see also the FB1*, which ignores the costs in FB1 associated with the abutments). The rocking on pile bridge (RP1) and the shallow foundation (RS) bridge require negligible repair, even for very large values of S_a. Finally, the RP2a model, which had identical bearings, expansion joints, and column diameter as the fixed-base designs, had significant repair costs for S_a > 1.8g, which was associated with the expansion joint damage. Nevertheless, for values smaller than that, the overall repair cost was similar to those calculated for Bridge RP1 and four times on average smaller than that for Bridge FB1.

For the same set of ground motions, the B7 bridges developed smaller overall damage and required smaller repair costs. The main cost contribution of the fixed-base models was from the columns and the shear keys, while the 0.10-m expansion joint was adequate for the whole range of S_a used in this study. Model FB2 model required slightly larger costs compared to Model FB1, which was expected due to the cost associated with repairing the cracks and spalling in the columns. The repair cost of the shallow foundation (RS) bridge was larger than the rocking on piles (RP1) bridge due to the damage associated with the soil underneath the footing. For the broadband set of ground motions, the repair cost was significantly smaller than those calculated for bridges subjected to the near-fault ground motions.

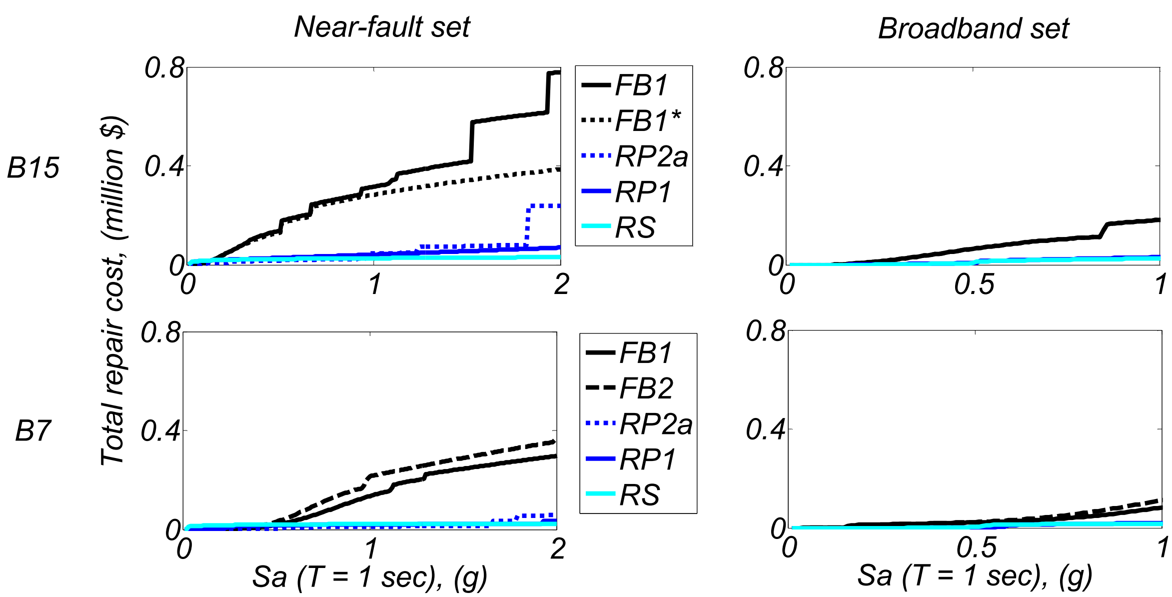

Figure 5.8 Total repair cost for the fixed-base, rocking on piles, and shallow foundation bridges.

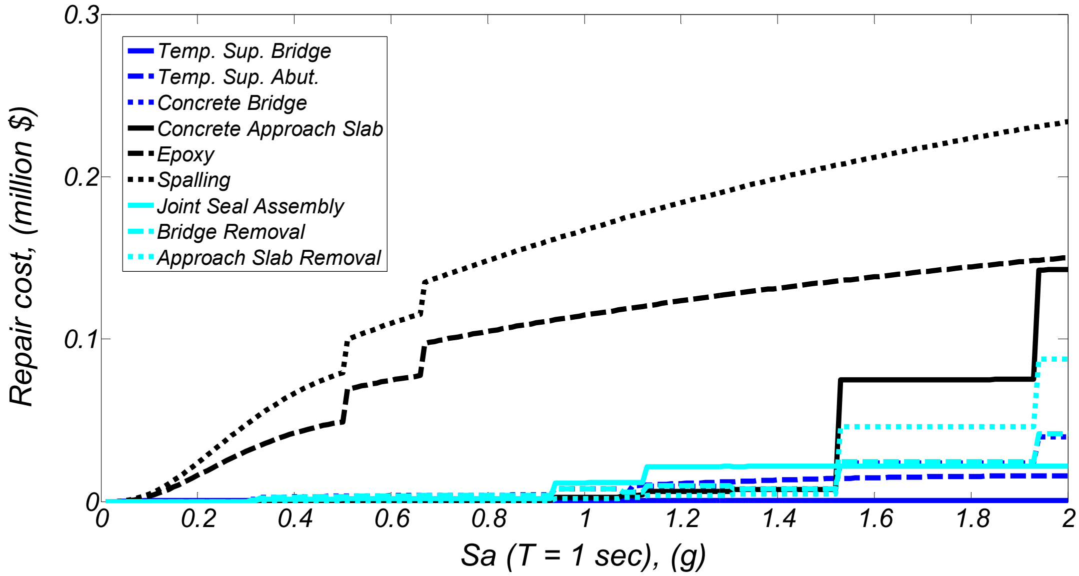

Figure 5.9 **Cost disaggregation for Bridge B15-FB1 for the near-fault set of ground motions.**

6 Conclusions

This study considered the seismic design, response, and performance of bridges with columns supported on rocking foundations and compared their computed seismic response with the response of traditionally designed bridges expected to develop significant inelastic deformations in the columns. Two bridges with different column heights were studied and subjected to two sets of forty ground motions each, one consisting of strong pulse-type near-fault ground motions and the other containing a mix of near- and far-fault ground motions. Three design strategies were considered for each of the two bridges studied. The first used conventional fixed-end columns, with 1.8-m-diameter columns designed to develop flexural plastic hinges at both ends. The other two designs used rocking pile and shallow foundations, respectively, with all columns designed to remain elastic.

The designs with rocking foundations used either 2.1-m- or 1.8-m-diameter columns, which were pinned at their top in the longitudinal direction; the fixed-base designs used 1.8-m-diameter columns. The fixed-based bridges used 0.9-m-diameter bearings and either 0.9-m- or 1.26-m-diameter bearings for the bridges with rocking foundations. The fixed-base designs used expansion joints with 0.10-m displacement capacity, while the corresponding displacement capacity in the rocking foundation designs was 0.4 m.

The vertical load factor of safety for the shallow foundations was 9.2 and 10.7 for Bridges B15 and B7, respectively. Each bridge was subjected to the two sets of ground motions using two horizontal components for each ground motion. In addition to comparing the seismic responses in terms of displacements, forces, and strain parameters, a comparison of the seismic performance of the bridges in terms of post-earthquake repair cost was conducted using the PEER performance based earthquake engineering method. Existing damage models for the columns, bearings, and the shear keys were used, and a new damage model for rocking shallow foundations was developed. The structural components were classified into different performance groups, with discrete damage states and repair methodologies. Repair costs were calculated from the repair quantities of different materials used in the repair methods of every performance group. Based on the results of this study, the following conclusions were drawn:

1. Using columns supported on rocking pile-foundations (pile cap width B = 6.5 m for both the tall and short RP1 bridges), 2.1-m-diameter columns with 3% longitudinal reinforcement steel ratio, 1.26-m-diameter lead plug rubber bearings, and 0.4-m

expansions joints resulted in an essentially elastic response of the columns for Bridges B15 and B7, with the mean strains to be less than 0.3%.The mean drift ratios for the rocking pile foundations subjected to near-fault ground motions compared to the fixed-base bridge were the same (2.4%) for Bridge B15-RP1 and 60% larger (drift ratio = 1.6%) for Bridge B7-RP1. Among the 40 near-fault motions, the increase of peak drift ratio was larger for Bridges B15-RP1 and B7-RP1. The peak drift ratio for these two bridges was 10% and 6.6%, respectively, in response to the TCU052 ground motion (the 1999 M7.6 Chi-Chi, Taiwan, earthquake). Bridge B15-RP1 developed 48% smaller mean deformation of the bearings (0.14 m) compared to the fixed-base bridge (0.27 m). The mean displacement of Bridge B15-RP1 was same as that of the fixed-base bridge (0.11 m).

2. For Bridge B15-RP2a (with 1.8-m-diameter columns) supported on rocking pile foundations (pile cap width B = 4.7 m), 1.26-m-diameter bearings, and expansion joints with 0.1-m deformation capacity, the mean drift ratios for near fault ground motions increased to 3.5% compared to 2.4% for Bridge B15-RP1. The corresponding values of the peak drift increased to 14.6% for the TCU052 motion.
3. For Bridge B7-RP2a with 1.8-m-diameter columns supported on rocking pile foundations (pile cap width B = 4.7 m), 1.26-m-diameter bearings, and expansion joints with 0.1-m deformation capacity, the mean drift ratios for near fault ground motions increased to 3.7% compared to 1.6% in Bridge B7-RP1. The corresponding values of the peak drift increased to 18.3% for the TCU052 motion compared to 6.6% for Bridge B7-RP1.
4. The absence of the 0.35-m diameter lead in the bearings of RP1 bridges resulted in 46% and 38% increase of the drift ratios in Bridges B15 and B7, respectively. The corresponding increase in the mean longitudinal drift ratios was 157%, and 133%, respectively.
5. Use of rocking shallow foundations compared to rocking pile foundations resulted in an increase of the mean drift ratios of 8%, and 50% in Bridges B15 and B7, respectively, with the mean drift ratios being less than 2.6% for Bridges B15 and B7. The displacements of the bearings and the expansion joints were similar in the bridges with columns on rocking pile and rocking shallow foundations, except for the expansion joint displacement of the B7 bridges.
6. Framing effects between the columns the deck and the abutments were more important in the B7 bridges due to the larger axial rigidity of the columns. This effect resulted in a mean variation of the vertical axial force of the columns less than 5%, and 12% for Bridges B15 and B7 with rocking pile foundations, respectively. The corresponding peak values (among the 40 near-fault motions) were less than 13% and 32%, respectively. These effects were quantified based on 3D nonlinear response history analysis, while the monotonic static analysis significantly underestimated them.

7. Bilinear idealization of the nonlinear static monotonic force-displacement response of the bridge in the transverse direction and use of nonlinear SDOF displacement spectra resulted in very good estimation of the nonlinear displacement demand of all bridges.
8. The PEER probabilistic methodology developed by Mackie et al. [2008] was used to investigate the post-earthquake assessment of the different bridge designs. The traditional fixed-base design resulted into significant repair costs for near-fault motions with intensity S_a (T = 1 sec) of about 0.5g. This cost was mainly due to the damage associated with inelastic flexural deformations of the columns and damage in the shear keys. An increased expansion joint would decrease that cost associated with damage of the expansion joint-abutment back-wall and approach slab for values of S_a (T =1 sec) larger than 0.45g. The rocking designs resulted in negligible post-earthquake damage, even in the case of shallow foundations because the inelasticity of the soil was intentionally limited in the designs considered herein.

REFERENCES

Anooshehpoor A., Heaton T.H., Shi B., Brune J.M. (1999). Estimates of the ground accelerations at Point Reyes station during the 1906 San Francisco earthquake, *Bull. Seismol. Soc. Am.,* 89(4): 845–853.

Apostolou M., Gazetas G., Garini E. (2007). Seismic response of slender rigid structures with foundation uplifting, *Soil Dyn. Earthq. Eng.,* 27: 642–654.

Astaneh-Asl A., Shen J., Cho S. (1995). Seismic behavior and retrofit design of steel long span bridges, *Proceedings, National Seismic Conf. on Bridges and Highways*, "Progress in Research and Practice," Federal Highway Administration, pp. 1995-2012, San Diego, CA.

Baker J., Lin T., Shahi S., Jayaram N. (2011). New ground motion selection procedures and selected motions for the PEER transportation research program, *Report No. 2011/03*, Pacific Earthquake Engineering Research Center, University of California, Berkeley CA.

Bartlett P.E. (1976). Foundation rocking on a clay soil, *Report No. 154*, ME Thesis, School of Engineering, University of Auckland, Auckland, New Zealand.

Beck J. L., Skinner R.I. (1974). The seismic response of a reinforced concrete bridge pier designed to step, *Earthq. Eng. Struct. Dyn,* 2: 343–358.

Boore D.M., Atkinson G.M. (2008). Ground-motion prediction equations for the average horizontal component of PGA, PGV, and 5%-damped PSA at spectral periods between 0.01 s and 10.0 s, *Earthq. Spectra,* 24(1): 99-138.

Caltrans (2010). Seismic Design Criteria, California Department of Transportation, Version 1.6, Sacramento, CA.

Chen Y., Liao W., Lee C., Wang, Y. (2006). Seismic isolation of viaduct piers by means of a rocking mechanism, *Earthq. Eng. Struct. Dyn,.* 35: 713–736.

Chopra A.K., Yim S.C. (1985). Simplified earthquake analysis of structures with foundation uplift, *J. Struct. Eng.,* 111(4): 906–930.

Clough R.W., Huckelbridge A.A. (1977). Preliminary experimental study of seismic uplift of a steel frame*, Report No. UCB/EERC-77/22*, Earthquake Engineering Research Center, University of California, Berkeley, CA.

Cornell C.A., Krawinkler H. (2000). Progress and challenges in seismic performance assessment, Pacific Earthquake Engineering Research Center Newsletter, Volume 3, No. 2., University of California, Berkeley, CA.

Cremer C., Pecker, A., Davenne L. (2001). Cyclic macro-element for soil-structure interaction: material and geometrical non-linearities, *Inter. J. Numerical Analytical Methods Geomech.,* 25: 1257–1284.

Cremer C., Pecker A., Davenne L. (2002). Modeling of nonlinear dynamic behavior of a shallow strip foundation with a macro-element, *J. Earthq. Eng.,* 6(2): 175–211.

Deng L., Kutter B.L. (2011). Characterization of rocking shallow foundations using centrifuge model tests, *Earthq. Eng. Struct. Dyn.*, 41(5): 1043–1060.

Deng L., Kutter B.L., Kunnath S.K. (2011). Probabilistic seismic performance of rocking-foundation and hinging-column bridges, *Earthq. Spectra,* 28(4): 1423-1446.

Dowdell D.J., Hamersley B.A. (2000). Lion's Gate Bridge north approach – seismic retrofit, *Proceedings, STESSA 2000, Third International Conf. on Behavior of Steel Structures in Seismic Areas*, pp. 319–326, Balkema Publishers, Rotterdam.

Dynamic Isolator Systems. http://www.dis-inc.com/.

Espinoza A., Mahin S.A. (2008). Shaking table and analytical investigation of reinforced concrete bridge piers with foundations allowed to uplift during earthquakes*, Report No. UCB/SEMM-08/03*, Department of Civil and Environmental Engineering, University of California, Berkeley, CA.

Faccioli E., Paolucci R., Vivero, G. (2001). Investigation of seismic soil-footing interaction by large scale cyclic tests and analytical models, *Proceedings, Fourth International Conference Recent Advances in Geotechnical Earthquake Engineering and Soil Dynamics. Special Presentation Lecture,* Paper No. SPL-05, San Diego, CA.

Gajan S., Hutchinson T., Kutter B.L., Raychowdhurry P., Ugalde J.A., Stewart J.P. (2008). Numerical models for analysis and performance-based design of shallow foundations subjected to seismic loading*, Report No. 2007/04*, Pacific Earthquake Engineering Research Center, University of California, Berkeley, CA.

Gazetas G. (1983). Analysis of machine foundation vibrations: state of the art. *Soil Dyn. Earthq. Eng.,* 2(1): 2–42.

Georgiadis M., Butterfield R. (1988). Displacement of footings on sand under eccentric and inclined loads, *Canadian Geotech. J.,* 25: 199–212.

Harden C., Hutchinson T., Martin G. R., Kutter B.L. (2005). Numerical modeling of the nonlinear cyclic response of shallow foundations, *Report No. 2005/04*, Pacific Earthquake Engineering Research Center, University of California, Berkeley, CA.

Housner G.H. (1963). The behavior of inverted pendulum structures during earthquakes, *Bull. Seismol. Soc. Am.,* 53(2): 403–417.

http://www.opensha.org/glossary-attenuationRelation-BOORE_ATKIN_2008.

Ingham T.J., Rodriguez S., Nader M., Taucer F. (1995). Seismic retrofit of the Golden Gate Bridge, *Proceedings, Eleventh World Conf. on Earthquake Engineering,* Paper No. 1396, Acapulco, Mexico.

Ishiyama Y. (1983). Motions of rigid bodies and criteria for overturning by earthquake excitations, *Earthq. Eng. Struct. Dyn.*, 10: 635–650.

Jones M.H., Holloway L.J., Toan V., Hinman, J. (1997). Seismic retrofit of the 1927 Carquinez bridge by a displacement capacity approach, *Proceedings, National Seismic Conference on Bridges and Highways,* pp. 445–456, Sacramento, CA.

Kelly J.M., Tsztoo D.F. (1977). Earthquake simulation testing of a stepping frame with energy-absorbing devices, *Report No. UCB/EERC-77/17*, Earthquake Engineering Research Center, University of California, Berkeley, CA.

Ketchum M., Chang V., Shantz T. (2004). Influence of design ground motion level on highway bridge costs*, Report No. Lifelines 6D01*, Pacific Earthquake Engineering Research Center, University of California, Berkeley, CA.

Kirkpatrick P. (1927). Seismic measurements by the overthrow of columns, *Bull. Seismol. Soc. Am.,* 17: 95–109.

Kutter B.L., Martin G.R., Hutchinson T., Harden C., Gajan S., Phalen J. (2006). Workshop on modeling of nonlinear cyclic load-deformation behavior of shallow foundations*, Report No. 2005/14*, Pacific Earthquake Engineering Research Center, University of California, Berkeley, CA.

Mackie K.R., Wong J.M., Stojadinovic B. (2008). Integrated probabilistic performance-based evaluation of benchmark reinforced concrete bridges*, Report No. 2007/09*, Pacific Earthquake Engineering Research Center, University of California, Berkeley, CA.

Makris N., Konstantinidis, D. (2003). The rocking spectrum and the limitations of practical design methodologies, *Earthq. Eng. Struct. Dyn.*, 32: 265–289.

Makris N., Roussos Y.S. (2000). Rocking response of rigid motions under near-source ground motions, *Géotechnique,* 50(3): 243–262.

Makris N., Zhang J. (2001). Rocking response of free-standing blocks under cycloidal pulses, *J. Eng. Mech.,* 127(5): 473–483.

MATLAB (2008). The MathWorks Inc., Natick, MA.

Meek J.W. (1978). Dynamics response of tipping core buildings, *Earthq. Eng. Struct. Dyn.*, 6: 437–454.

Mergos P.E., Kawashima K. (2005). Rocking isolation of a typical bridge pier on spread foundation, *J. Earthq. Eng.,* 9(2): 395–414.

Milne J., Omori F. (1893). On the overturning and fracturing of brick columns by horizontal applied motion, *Seismol. J. Japan*, 17: 59–86.

Muto K., Takahasi R., Aida I., Ando N., Hisada T., Nakagawa K., Omemura H., Osawa, Y. (1960). Nonlinear response analyzers and application to earthquake resistant design, *Proceedings, Second World Conf. on Earthquake Engineering,* Japan, 2: 649–668.

OPENSEES (1999). *http://opensees.berkeley.edu/.*

Paolucci R., di Prisco C., Vecchiotti M., Shirato M., Yilmaz M.T. (2007). Seismic behaviour of shallow foundations: Large scale experiments vs. numerical modelling and implications for performance based design, *Proceedings, First US-Italy Seismic Bridge Workshop*, Pavia, Italy.

Pecker A., Pender, M.J. (2000). Earthquake resistant design of foundations: new construction, Invited Paper, *GeoEng2000*, 1: 313–332, Melbourne, Australia.

Pecker A. (ed.) (2006). Enhanced seismic design of shallow foundations: example of the Rion Antirion Bridge, Fourth Athenian Lecture on Geotechnical Engineering, *Bull. Hellenic Geotech. Soc.,* Athens, Greece.

Priestley M.J.N., Evison R.J., Carr A.J. (1978). Seismic response of structures free to rock on their foundations, *Bull. NZ Nat. Soc. Earthq. Eng.,* 11(3): 141–150.

Psycharis I.N., Jennings P.C. (1983). Rocking of slender rigid bodies allowed to uplift, *Earthq. Eng. Struct. Dyn.*, 11: 57–76.

Rutenberg A., Jennings P.C., Housner G.H. (1982). The response of Veteran's Hospital Building 41 in the San Fernando earthquake, *Earthq. Eng. Struct. Dyn.*, 10: 359–379.
Saiidi M., Gopalakrishnan B., Siddharthan R. (2002). Shake table studies of effects of foundation flexibility on seismic demand in substandard bridge piers, *Am. Conc. Institute Special Publication*, 209: 553–570.
Sakellaraki D., Kawashima K. (2006). Effectiveness of seismic rocking isolation of bridges based on shake table test, *Proceedings, First European Conf. on Earthquake Engineering and Seismology*, Paper No. 364, Geneva, Switzerland.
Salgado R. (2006). *The Engineering of Foundations*, McGraw-Hill, New York, NY.
Shi B., Anooshehpoor A., Zeng Y., Brune J. (1996). Rocking and overturning of precariously balanced rocks by earthquakes, *Bull. Seismol. Soc. Am.,* 86(5): 1364–1371.
Spanos P.D., Koh A. (1984). Rocking of rigid blocks due to harmonic shaking, *J. Eng. Mech.,* 110(11): 1627–1642.
Tso W.K., Wong C.M. (1989). Steady state rocking response of rigid blocks. Part 1: analysis, *Earthq. Eng. Struct. Dyn.*, 18: 89–106.
Ugalde J.A., Kutter B.L., Jeremić B. (2010). Rocking response of bridges on shallow foundations*, Report No. 2010/101*, Pacific Earthquake Engineering Research Center, University of California, Berkeley, CA.
Wiebe L., Christopoulos C. (2010). Characterizing acceleration spikes due to stiffness changes in nonlinear systems, *Earthq. Eng. Struct. Dyn,*, 39: 1653–1670.
Wiessing P.R. (1979). Foundation rocking on sand*, Report No. 203*, Master's Thesis, School of Engineering, University of Auckland, Auckland, New Zealand.

APPENDIX A: Damage States and Repair Methods for the Different Performance Groups

Table A.1 Damage states and repair methods for the columns.

	Description	Column flexure drift ratio (%)	Repair item	Unit computation
DS0	Negligible damage, cracking	0.23	N/A	N/A
DS1	Concrete spalling	1.64	Epoxy inject cracks (LM)	2 × (column height)
			Repair minor spalls (CM)	10% × (surface area) x (cover + 0.025 m)
DS2	Bar buckling	6.09	Epoxy inject cracks (LM)	4 × (column height)
			Repair minor spalls (CM)	25% × (surface area) x (cover + 0.025 m)
DS3	Column failure	6.72	Structural concrete, bridge (CM)	(column height) × (column cross section)
			Reinforcing steel bars (KG)	(column gross volume)x 268 kg / m^3
			Temporarily support (SM)	Tributary length × (deck width)
			Structure excavation (CM)	1 m embedment plus 1.2 m concentric circle around columns
			Structure backfill (CM)	same as structure excavation

Table A.2 Damage states and repair methods for the abutments.

	Description	Expansion joint displacement, (m)	Repair item	Unit computation
DS0	Onset of damage	0.05 (0.20)*	N/A	N/A
DS1	Replace joint seal assembly	0.10 (0.40)*	Joint seal assembly (LM)	(deck width)
			Structural concrete , bridge (CM)	(blockout volume)
			Reinforcing steel bar, (KG)	(blockout volume) × 48 kg / m^3
			Bridge removal (CM)	(blockout volume)
DS2	Replace joint seal assembly and back-wall	0.11 (0.41)*		same as before plus
			Epoxy inject cracks (LM)	2 × (back-wall height)
			Repair minor spalls (CM)	10% × (back-wall height) x deck width)
			Structure excavation (CM)	(deck width) x (deck depth) × 0.3 m
			Structure backfill (CM)	(deck width) x (deck depth) × 0.3 m
DS3	Replace joint seal assembly, back-wall and approach slab	0.14 (0.44)*		same as before plus
			Structural concrete, approach slab (CM)	(approach slab volume)
			Aggregate base approach slab (CM)	1/2 × (settlement due to 1/62.5 gradient) × approach slab area)
			Approach slab removal (CM)	(approach slab volume)

*The values in parentheses correspond to the rocking bridges that had larger expansion joints.

Table A.3 Damage states and repair methods for the shear keys.

	Description	Displacement (m)	Repair item	Unit computation
DS0	Elastic limit	0.01	N/A	N/A
DS1	Concrete spalling	0.015	Repair minor spalls (CM)	10% x (shear key volume)
			Epoxy inject cracks (LM)	2 × (shear key height) × (number of shear keys)
DS2	Shear key failure	0.025	Structural concrete (CM)	(shear key volume)
			Reinforcing steel bars (KG)	(concrete volume) × 48 kg/m^3
			Bridge removal (CM)	(shear key volume)

Table A.4 Damage states and repair methods for bearings.

	Description	Displacement (m)	Repair item	Unit computation
DS0	Shear strain 150%	0.33 (0.60)*	N/A	N/A
DS1	Shear strain 250%	0.55 (0.90)*	Replace bearings	(Number of bearings)

*The values in parentheses correspond to the rocking bridges that had larger rubber bearings.

Table A.5 Repair quantities, units, and unit costs.

Quantity	Unit	Unit cost, ($ / unit)
Structure excavation	Cubic meters, CM	165
Structure backfill	CM	220
Temporary support, bridge	Square meters, SM	407
Temporary support, abutment	SM	407
Structural concrete, bridge	CM	2225
Structural concrete, approach slab	CM	1625
Aggregate base	CM	325
Steel rebars, bridge	Kilograms, KG	2.7
Epoxy	Linear meters, LM	650
Spalling	SM	5100
Joint seal assembly	LM	825 (8250)
Bearing	Each, EA	6000 (15000)
Bridge removal, column	CM	3405
Bridge removal, portion	CM	2355
Approach slab removal	CM	1000
Soil compaction	SM	100

PEER REPORTS

PEER reports are available as a free PDF download from http://peer.berkeley.edu/publications/peer_reports_complete.html. Printed hard copies of PEER reports can be ordered directly from our printer by following the instructions at http://peer.berkeley.edu/publications/peer_reports.html. For other related questions about the PEER Report Series, contact the Pacific Earthquake Engineering Research Center, 325 Davis Hall mail code 1792, Berkeley, CA 94720. Tel.: (510) 642-3437; Fax: (510) 665-1655; Email: peer_editor@berkeley.edu

PEER 2013/21 *Seismic Design and Performance of Bridges with Columns on Rocking Foundations.* Grigorios Antonellis and Marios Panagiotou. September 2013.

PEER 2013/20 *Experimental and Analytical Studies on the Seismic Behavior of Conventional and Hybrid Braced Frames.* Jiun-Wei Lai and Stephen A. Mahin. September 2013.

PEER 2013/19 *Toward Resilient Communities: A Performance-Based Engineering Framework for Design and Evaluation of the Built Environment.* Michael William Mieler, Bozidar Stojadinovic, Robert J. Budnitz, Stephen A. Mahin and Mary C. Comerio. September 2013.

PEER 2013/18 *Identification of Site Parameters that Improve Predictions of Site Amplification.* Ellen M. Rathje and Sara Navidi. July 2013.

PEER 2013/17 *Response Spectrum Analysis of Concrete Gravity Dams Including Dam-Water-Foundation Interaction.* Arnkjell Løkke and Anil K. Chopra. July 2013.

PEER 2013/16 *Effect of hoop reinforcement spacing on the cyclic response of large reinforced concrete special moment frame beams.* Marios Panagiotou, Tea Visnjic, Grigorios Antonellis, Panagiotis Galanis, and Jack P. Moehle. June 2013.

PEER 2013/15 *publication pending*

PEER 2013/14 *publication pending*

PEER 2013/13 *publication pending*

PEER 2013/12 *Nonlinear Horizontal Site Response for the NGA-West2 Project.* Ronnie Kamai, Norman A. Abramson, Walter J. Silva. May 2013.

PEER 2013/11 *Epistemic Uncertainty for NGA-West2 Models.* Linda Al Atik and Robert R. Youngs. May 2013.

PEER 2013/10 *NGA-West 2 Models for Ground-Motion Directionality.* Shrey K. Shahi and Jack W. Baker. May 2013.

PEER 2013/09 *Final Report of the NGA-West2 Directivity Working Group.* Paul Spudich, Jeffrey R. Bayless, Jack W. Baker, Brian S.J. Chiou, Badie Rowshandel, Shrey Shahi, and Paul Somerville. May 2013.

PEER 2013/08 *NGA-West2 Model for Estimating Average Horizontal Values of Pseudo-Absolute Spectral Accelerations Generated by Crustal Earthquakes.* I. M. Idriss. May 2013.

PEER 2013/07 *Update of the Chiou and Youngs NGA Ground Motion Model for Average Horizontal Component of Peak Ground Motion and Response Spectra.* Brian Chiou and Robert Youngs. May 2013.

PEER 2013/06 *NGA-West2 Campbell-Bozorgnia Ground Motion Model for the Horizontal Components of PGA, PGV, and 5%-Damped Elastic Pseudo-Acceleration Response Spectra for Periods Ranging from 0.01 to 10 sec.* Kenneth W. Campbell and Yousef Bozorgnia. May 2013.

PEER 2013/05 *NGA-West 2 Equations for Predicting Response Spectral Accelerations for Shallow Crustal Earthquakes.* David M. Boore, Jonathan P. Stewart, Emel Seyhan, Gail M. Atkinson. May 2013.

PEER 2013/04 *Update of the AS08 Ground-Motion Prediction Equations Based on the NGA-West2 Data Set.* Norman Abrahamson, Walter Silva, and Ronnie Kamai. May 2013.

PEER 2013/03 *PEER NGA-West2 Database.* Timothy D. Ancheta, Robert B. Darragh, Jonathan P. Stewart, Emel Seyhan, Walter J. Silva, Brian S.J. Chiou, Katie E. Wooddell, Robert W. Graves, Albert R. Kottke, David M. Boore, Tadahiro Kishida, and Jennifer L. Donahue. May 2013.

PEER 2013/02 *Hybrid Simulation of the Seismic Response of Squat Reinforced Concrete Shear Walls.* Catherine A. Whyte and Bozidar Stojadinovic. May 2013.

PEER 2013/01 *Housing Recovery in Chile: A Qualitative Mid-program Review.* Mary C. Comerio. February 2013.

PEER 2012/08 *Guidelines for Estimation of Shear Wave Velocity.* Bernard R. Wair, Jason T. DeJong, and Thomas Shantz. December 2012.

PEER 2012/07 *Earthquake Engineering for Resilient Communities: 2012 PEER Internship Program Research Report Collection.* Heidi Tremayne (Editor), Stephen A. Mahin (Editor), Collin Anderson, Dustin Cook, Michael Erceg, Carlos Esparza, Jose Jimenez, Dorian Krausz, Andrew Lo, Stephanie Lopez, Nicole McCurdy, Paul Shipman, Alexander Strum, Eduardo Vega. December 2012.

PEER 2012/06 *Fragilities for Precarious Rocks at Yucca Mountain.* Matthew D. Purvance, Rasool Anooshehpoor, and James N. Brune. December 2012.

PEER 2012/05 *Development of Simplified Analysis Procedure for Piles in Laterally Spreading Layered Soils.* Christopher R. McGann, Pedro Arduino, and Peter Mackenzie–Helnwein. December 2012.

PEER 2012/04 *Unbonded Pre-Tensioned Columns for Bridges in Seismic Regions.* Phillip M. Davis, Todd M. Janes, Marc O. Eberhard, and John F. Stanton. December 2012.

PEER 2012/03 *Experimental and Analytical Studies on Reinforced Concrete Buildings with Seismically Vulnerable Beam-Column Joints.* Sangjoon Park and Khalid M. Mosalam. October 2012.

PEER 2012/02 *Seismic Performance of Reinforced Concrete Bridges Allowed to Uplift during Multi-Directional Excitation.* Andres Oscar Espinoza and Stephen A. Mahin. July 2012.

PEER 2012/01 *Spectral Damping Scaling Factors for Shallow Crustal Earthquakes in Active Tectonic Regions.* Sanaz Rezaeian, Yousef Bozorgnia, I. M. Idriss, Kenneth Campbell, Norman Abrahamson, and Walter Silva. July 2012.

PEER 2011/10 *Earthquake Engineering for Resilient Communities: 2011 PEER Internship Program Research Report Collection.* Eds. Heidi Faison and Stephen A. Mahin. December 2011.

PEER 2011/09 *Calibration of Semi-Stochastic Procedure for Simulating High-Frequency Ground Motions.* Jonathan P. Stewart, Emel Seyhan, and Robert W. Graves. December 2011.

PEER 2011/08 *Water Supply in regard to Fire Following Earthquake.* Charles Scawthorn. November 2011.

PEER 2011/07 *Seismic Risk Management in Urban Areas. Proceedings of a U.S.-Iran-Turkey Seismic Workshop.* September 2011.

PEER 2011/06 *The Use of Base Isolation Systems to Achieve Complex Seismic Performance Objectives.* Troy A. Morgan and Stephen A. Mahin. July 2011.

PEER 2011/05 *Case Studies of the Seismic Performance of Tall Buildings Designed by Alternative Means.* Task 12 Report for the Tall Buildings Initiative. Jack Moehle, Yousef Bozorgnia, Nirmal Jayaram, Pierson Jones, Mohsen Rahnama, Nilesh Shome, Zeynep Tuna, John Wallace, Tony Yang, and Farzin Zareian. July 2011.

PEER 2011/04 *Recommended Design Practice for Pile Foundations in Laterally Spreading Ground.* Scott A. Ashford, Ross W. Boulanger, and Scott J. Brandenberg. June 2011.

PEER 2011/03 *New Ground Motion Selection Procedures and Selected Motions for the PEER Transportation Research Program.* Jack W. Baker, Ting Lin, Shrey K. Shahi, and Nirmal Jayaram. March 2011.

PEER 2011/02 *A Bayesian Network Methodology for Infrastructure Seismic Risk Assessment and Decision Support.* Michelle T. Bensi, Armen Der Kiureghian, and Daniel Straub. March 2011.

PEER 2011/01 *Demand Fragility Surfaces for Bridges in Liquefied and Laterally Spreading Ground.* Scott J. Brandenberg, Jian Zhang, Pirooz Kashighandi, Yili Huo, and Minxing Zhao. March 2011.

PEER 2010/05 *Guidelines for Performance-Based Seismic Design of Tall Buildings.* Developed by the Tall Buildings Initiative. November 2010.

PEER 2010/04 *Application Guide for the Design of Flexible and Rigid Bus Connections between Substation Equipment Subjected to Earthquakes.* Jean-Bernard Dastous and Armen Der Kiureghian. September 2010.

PEER 2010/03 *Shear Wave Velocity as a Statistical Function of Standard Penetration Test Resistance and Vertical Effective Stress at Caltrans Bridge Sites.* Scott J. Brandenberg, Naresh Bellana, and Thomas Shantz. June 2010.

PEER 2010/02 *Stochastic Modeling and Simulation of Ground Motions for Performance-Based Earthquake Engineering.* Sanaz Rezaeian and Armen Der Kiureghian. June 2010.

PEER 2010/01 *Structural Response and Cost Characterization of Bridge Construction Using Seismic Performance Enhancement Strategies.* Ady Aviram, Božidar Stojadinović, Gustavo J. Parra-Montesinos, and Kevin R. Mackie. March 2010.

PEER 2009/03 *The Integration of Experimental and Simulation Data in the Study of Reinforced Concrete Bridge Systems Including Soil-Foundation-Structure Interaction.* Matthew Dryden and Gregory L. Fenves. November 2009.

PEER 2009/02 *Improving Earthquake Mitigation through Innovations and Applications in Seismic Science, Engineering, Communication, and Response. Proceedings of a U.S.-Iran Seismic Workshop.* October 2009.

PEER 2009/01 *Evaluation of Ground Motion Selection and Modification Methods: Predicting Median Interstory Drift Response of Buildings.* Curt B. Haselton, Ed. June 2009.

PEER 2008/10 *Technical Manual for Strata.* Albert R. Kottke and Ellen M. Rathje. February 2009.

PEER 2008/09 *NGA Model for Average Horizontal Component of Peak Ground Motion and Response Spectra.* Brian S.-J. Chiou and Robert R. Youngs. November 2008.

PEER 2008/08 *Toward Earthquake-Resistant Design of Concentrically Braced Steel Structures.* Patxi Uriz and Stephen A. Mahin. November 2008.

PEER 2008/07 *Using OpenSees for Performance-Based Evaluation of Bridges on Liquefiable Soils.* Stephen L. Kramer, Pedro Arduino, and HyungSuk Shin. November 2008.

PEER 2008/06 *Shaking Table Tests and Numerical Investigation of Self-Centering Reinforced Concrete Bridge Columns.* Hyung IL Jeong, Junichi Sakai, and Stephen A. Mahin. September 2008.

PEER 2008/05 *Performance-Based Earthquake Engineering Design Evaluation Procedure for Bridge Foundations Undergoing Liquefaction-Induced Lateral Ground Displacement.* Christian A. Ledezma and Jonathan D. Bray. August 2008.

PEER 2008/04 *Benchmarking of Nonlinear Geotechnical Ground Response Analysis Procedures.* Jonathan P. Stewart, Annie On-Lei Kwok, Yousseff M. A. Hashash, Neven Matasovic, Robert Pyke, Zhiliang Wang, and Zhaohui Yang. August 2008.

PEER 2008/03 *Guidelines for Nonlinear Analysis of Bridge Structures in California.* Ady Aviram, Kevin R. Mackie, and Božidar Stojadinović. August 2008.

PEER 2008/02 *Treatment of Uncertainties in Seismic-Risk Analysis of Transportation Systems.* Evangelos Stergiou and Anne S. Kiremidjian. July 2008.

PEER 2008/01 *Seismic Performance Objectives for Tall Buildings.* William T. Holmes, Charles Kircher, William Petak, and Nabih Youssef. August 2008.

PEER 2007/12 *An Assessment to Benchmark the Seismic Performance of a Code-Conforming Reinforced Concrete Moment-Frame Building.* Curt Haselton, Christine A. Goulet, Judith Mitrani-Reiser, James L. Beck, Gregory G. Deierlein, Keith A. Porter, Jonathan P. Stewart, and Ertugrul Taciroglu. August 2008.

PEER 2007/11 *Bar Buckling in Reinforced Concrete Bridge Columns.* Wayne A. Brown, Dawn E. Lehman, and John F. Stanton. February 2008.

PEER 2007/10 *Computational Modeling of Progressive Collapse in Reinforced Concrete Frame Structures.* Mohamed M. Talaat and Khalid M. Mosalam. May 2008.

PEER 2007/09 *Integrated Probabilistic Performance-Based Evaluation of Benchmark Reinforced Concrete Bridges.* Kevin R. Mackie, John-Michael Wong, and Božidar Stojadinović. January 2008.

PEER 2007/08 *Assessing Seismic Collapse Safety of Modern Reinforced Concrete Moment-Frame Buildings.* Curt B. Haselton and Gregory G. Deierlein. February 2008.

PEER 2007/07 *Performance Modeling Strategies for Modern Reinforced Concrete Bridge Columns.* Michael P. Berry and Marc O. Eberhard. April 2008.

PEER 2007/06 *Development of Improved Procedures for Seismic Design of Buried and Partially Buried Structures.* Linda Al Atik and Nicholas Sitar. June 2007.

PEER 2007/05 *Uncertainty and Correlation in Seismic Risk Assessment of Transportation Systems.* Renee G. Lee and Anne S. Kiremidjian. July 2007.

PEER 2007/04 *Numerical Models for Analysis and Performance-Based Design of Shallow Foundations Subjected to Seismic Loading.* Sivapalan Gajan, Tara C. Hutchinson, Bruce L. Kutter, Prishati Raychowdhury, José A. Ugalde, and Jonathan P. Stewart. May 2008.

PEER 2007/03 *Beam-Column Element Model Calibrated for Predicting Flexural Response Leading to Global Collapse of RC Frame Buildings.* Curt B. Haselton, Abbie B. Liel, Sarah Taylor Lange, and Gregory G. Deierlein. May 2008.

PEER 2007/02 *Campbell-Bozorgnia NGA Ground Motion Relations for the Geometric Mean Horizontal Component of Peak and Spectral Ground Motion Parameters.* Kenneth W. Campbell and Yousef Bozorgnia. May 2007.

PEER 2007/01 *Boore-Atkinson NGA Ground Motion Relations for the Geometric Mean Horizontal Component of Peak and Spectral Ground Motion Parameters.* David M. Boore and Gail M. Atkinson. May. May 2007.

PEER 2006/12 *Societal Implications of Performance-Based Earthquake Engineering.* Peter J. May. May 2007.

PEER 2006/11 *Probabilistic Seismic Demand Analysis Using Advanced Ground Motion Intensity Measures, Attenuation Relationships, and Near-Fault Effects.* Polsak Tothong and C. Allin Cornell. March 2007.

PEER 2006/10 *Application of the PEER PBEE Methodology to the I-880 Viaduct.* Sashi Kunnath. February 2007.

PEER 2006/09 *Quantifying Economic Losses from Travel Forgone Following a Large Metropolitan Earthquake.* James Moore, Sungbin Cho, Yue Yue Fan, and Stuart Werner. November 2006.

PEER 2006/08 *Vector-Valued Ground Motion Intensity Measures for Probabilistic Seismic Demand Analysis.* Jack W. Baker and C. Allin Cornell. October 2006.

PEER 2006/07 *Analytical Modeling of Reinforced Concrete Walls for Predicting Flexural and Coupled–Shear-Flexural Responses.* Kutay Orakcal, Leonardo M. Massone, and John W. Wallace. October 2006.

PEER 2006/06 *Nonlinear Analysis of a Soil-Drilled Pier System under Static and Dynamic Axial Loading.* Gang Wang and Nicholas Sitar. November 2006.

PEER 2006/05 *Advanced Seismic Assessment Guidelines.* Paolo Bazzurro, C. Allin Cornell, Charles Menun, Maziar Motahari, and Nicolas Luco. September 2006.

PEER 2006/04 *Probabilistic Seismic Evaluation of Reinforced Concrete Structural Components and Systems.* Tae Hyung Lee and Khalid M. Mosalam. August 2006.

PEER 2006/03 *Performance of Lifelines Subjected to Lateral Spreading.* Scott A. Ashford and Teerawut Juirnarongrit. July 2006.

PEER 2006/02 *Pacific Earthquake Engineering Research Center Highway Demonstration Project.* Anne Kiremidjian, James Moore, Yue Yue Fan, Nesrin Basoz, Ozgur Yazali, and Meredith Williams. April 2006.

PEER 2006/01 *Bracing Berkeley. A Guide to Seismic Safety on the UC Berkeley Campus.* Mary C. Comerio, Stephen Tobriner, and Ariane Fehrenkamp. January 2006.

PEER 2005/16 *Seismic Response and Reliability of Electrical Substation Equipment and Systems.* Junho Song, Armen Der Kiureghian, and Jerome L. Sackman. April 2006.

PEER 2005/15 *CPT-Based Probabilistic Assessment of Seismic Soil Liquefaction Initiation.* R. E. S. Moss, R. B. Seed, R. E. Kayen, J. P. Stewart, and A. Der Kiureghian. April 2006.

PEER 2005/14 *Workshop on Modeling of Nonlinear Cyclic Load-Deformation Behavior of Shallow Foundations.* Bruce L. Kutter, Geoffrey Martin, Tara Hutchinson, Chad Harden, Sivapalan Gajan, and Justin Phalen. March 2006.

PEER 2005/13 *Stochastic Characterization and Decision Bases under Time-Dependent Aftershock Risk in Performance-Based Earthquake Engineering.* Gee Liek Yeo and C. Allin Cornell. July 2005.

PEER 2005/12 *PEER Testbed Study on a Laboratory Building: Exercising Seismic Performance Assessment.* Mary C. Comerio, editor. November 2005.

PEER 2005/11 *Van Nuys Hotel Building Testbed Report: Exercising Seismic Performance Assessment.* Helmut Krawinkler, editor. October 2005.

PEER 2005/10 *First NEES/E-Defense Workshop on Collapse Simulation of Reinforced Concrete Building Structures.* September 2005.

PEER 2005/09 *Test Applications of Advanced Seismic Assessment Guidelines.* Joe Maffei, Karl Telleen, Danya Mohr, William Holmes, and Yuki Nakayama. August 2006.

PEER 2005/08 *Damage Accumulation in Lightly Confined Reinforced Concrete Bridge Columns.* R. Tyler Ranf, Jared M. Nelson, Zach Price, Marc O. Eberhard, and John F. Stanton. April 2006.

PEER 2005/07 *Experimental and Analytical Studies on the Seismic Response of Freestanding and Anchored Laboratory Equipment.* Dimitrios Konstantinidis and Nicos Makris. January 2005.

PEER 2005/06 *Global Collapse of Frame Structures under Seismic Excitations.* Luis F. Ibarra and Helmut Krawinkler. September 2005.

PEER 2005//05 *Performance Characterization of Bench- and Shelf-Mounted Equipment.* Samit Ray Chaudhuri and Tara C. Hutchinson. May 2006.

PEER 2005/04 *Numerical Modeling of the Nonlinear Cyclic Response of Shallow Foundations.* Chad Harden, Tara Hutchinson, Geoffrey R. Martin, and Bruce L. Kutter. August 2005.

PEER 2005/03 *A Taxonomy of Building Components for Performance-Based Earthquake Engineering.* Keith A. Porter. September 2005.

PEER 2005/02 *Fragility Basis for California Highway Overpass Bridge Seismic Decision Making.* Kevin R. Mackie and Božidar Stojadinović. June 2005.

PEER 2005/01 *Empirical Characterization of Site Conditions on Strong Ground Motion.* Jonathan P. Stewart, Yoojoong Choi, and Robert W. Graves. June 2005.

PEER 2004/09 *Electrical Substation Equipment Interaction: Experimental Rigid Conductor Studies.* Christopher Stearns and André Filiatrault. February 2005.

PEER 2004/08 *Seismic Qualification and Fragility Testing of Line Break 550-kV Disconnect Switches.* Shakhzod M. Takhirov, Gregory L. Fenves, and Eric Fujisaki. January 2005.

PEER 2004/07 *Ground Motions for Earthquake Simulator Qualification of Electrical Substation Equipment.* Shakhzod M. Takhirov, Gregory L. Fenves, Eric Fujisaki, and Don Clyde. January 2005.

PEER 2004/06 *Performance-Based Regulation and Regulatory Regimes.* Peter J. May and Chris Koski. September 2004.

PEER 2004/05 *Performance-Based Seismic Design Concepts and Implementation: Proceedings of an International Workshop.* Peter Fajfar and Helmut Krawinkler, editors. September 2004.

PEER 2004/04 *Seismic Performance of an Instrumented Tilt-up Wall Building.* James C. Anderson and Vitelmo V. Bertero. July 2004.

PEER 2004/03 *Evaluation and Application of Concrete Tilt-up Assessment Methodologies.* Timothy Graf and James O. Malley. October 2004.

PEER 2004/02 *Analytical Investigations of New Methods for Reducing Residual Displacements of Reinforced Concrete Bridge Columns.* Junichi Sakai and Stephen A. Mahin. August 2004.

PEER 2004/01 *Seismic Performance of Masonry Buildings and Design Implications.* Kerri Anne Taeko Tokoro, James C. Anderson, and Vitelmo V. Bertero. February 2004.

PEER 2003/18 *Performance Models for Flexural Damage in Reinforced Concrete Columns.* Michael Berry and Marc Eberhard. August 2003.

PEER 2003/17 *Predicting Earthquake Damage in Older Reinforced Concrete Beam-Column Joints.* Catherine Pagni and Laura Lowes. October 2004.

PEER 2003/16 *Seismic Demands for Performance-Based Design of Bridges.* Kevin Mackie and Božidar Stojadinović. August 2003.

PEER 2003/15 *Seismic Demands for Nondeteriorating Frame Structures and Their Dependence on Ground Motions.* Ricardo Antonio Medina and Helmut Krawinkler. May 2004.

PEER 2003/14 *Finite Element Reliability and Sensitivity Methods for Performance-Based Earthquake Engineering.* Terje Haukaas and Armen Der Kiureghian. April 2004.

PEER 2003/13 *Effects of Connection Hysteretic Degradation on the Seismic Behavior of Steel Moment-Resisting Frames.* Janise E. Rodgers and Stephen A. Mahin. March 2004.

PEER 2003/12 *Implementation Manual for the Seismic Protection of Laboratory Contents: Format and Case Studies.* William T. Holmes and Mary C. Comerio. October 2003.

PEER 2003/11 *Fifth U.S.-Japan Workshop on Performance-Based Earthquake Engineering Methodology for Reinforced Concrete Building Structures.* February 2004.

PEER 2003/10 *A Beam-Column Joint Model for Simulating the Earthquake Response of Reinforced Concrete Frames.* Laura N. Lowes, Nilanjan Mitra, and Arash Altoontash. February 2004.

PEER 2003/09 *Sequencing Repairs after an Earthquake: An Economic Approach.* Marco Casari and Simon J. Wilkie. April 2004.

PEER 2003/08 *A Technical Framework for Probability-Based Demand and Capacity Factor Design (DCFD) Seismic Formats.* Fatemeh Jalayer and C. Allin Cornell. November 2003.

PEER 2003/07 *Uncertainty Specification and Propagation for Loss Estimation Using FOSM Methods.* Jack W. Baker and C. Allin Cornell. September 2003.

PEER 2003/06 *Performance of Circular Reinforced Concrete Bridge Columns under Bidirectional Earthquake Loading.* Mahmoud M. Hachem, Stephen A. Mahin, and Jack P. Moehle. February 2003.

PEER 2003/05 *Response Assessment for Building-Specific Loss Estimation.* Eduardo Miranda and Shahram Taghavi. September 2003.

PEER 2003/04 *Experimental Assessment of Columns with Short Lap Splices Subjected to Cyclic Loads*. Murat Melek, John W. Wallace, and Joel Conte. April 2003.

PEER 2003/03 *Probabilistic Response Assessment for Building-Specific Loss Estimation.* Eduardo Miranda and Hesameddin Aslani. September 2003.

PEER 2003/02 *Software Framework for Collaborative Development of Nonlinear Dynamic Analysis Program.* Jun Peng and Kincho H. Law. September 2003.

PEER 2003/01 *Shake Table Tests and Analytical Studies on the Gravity Load Collapse of Reinforced Concrete Frames.* Kenneth John Elwood and Jack P. Moehle. November 2003.

PEER 2002/24 *Performance of Beam to Column Bridge Joints Subjected to a Large Velocity Pulse.* Natalie Gibson, André Filiatrault, and Scott A. Ashford. April 2002.

PEER 2002/23 *Effects of Large Velocity Pulses on Reinforced Concrete Bridge Columns.* Greg L. Orozco and Scott A. Ashford. April 2002.

PEER 2002/22 *Characterization of Large Velocity Pulses for Laboratory Testing.* Kenneth E. Cox and Scott A. Ashford. April 2002.

PEER 2002/21 *Fourth U.S.-Japan Workshop on Performance-Based Earthquake Engineering Methodology for Reinforced Concrete Building Structures.* December 2002.

PEER 2002/20 *Barriers to Adoption and Implementation of PBEE Innovations.* Peter J. May. August 2002.

PEER 2002/19 *Economic-Engineered Integrated Models for Earthquakes: Socioeconomic Impacts.* Peter Gordon, James E. Moore II, and Harry W. Richardson. July 2002.

PEER 2002/18 *Assessment of Reinforced Concrete Building Exterior Joints with Substandard Details.* Chris P. Pantelides, Jon Hansen, Justin Nadauld, and Lawrence D. Reaveley. May 2002.

PEER 2002/17 *Structural Characterization and Seismic Response Analysis of a Highway Overcrossing Equipped with Elastomeric Bearings and Fluid Dampers: A Case Study.* Nicos Makris and Jian Zhang. November 2002.

PEER 2002/16 *Estimation of Uncertainty in Geotechnical Properties for Performance-Based Earthquake Engineering.* Allen L. Jones, Steven L. Kramer, and Pedro Arduino. December 2002.

PEER 2002/15 *Seismic Behavior of Bridge Columns Subjected to Various Loading Patterns.* Asadollah Esmaeily-Gh. and Yan Xiao. December 2002.

PEER 2002/14 *Inelastic Seismic Response of Extended Pile Shaft Supported Bridge Structures.* T.C. Hutchinson, R.W. Boulanger, Y.H. Chai, and I.M. Idriss. December 2002.

PEER 2002/13 *Probabilistic Models and Fragility Estimates for Bridge Components and Systems.* Paolo Gardoni, Armen Der Kiureghian, and Khalid M. Mosalam. June 2002.

PEER 2002/12 *Effects of Fault Dip and Slip Rake on Near-Source Ground Motions: Why Chi-Chi Was a Relatively Mild M7.6 Earthquake.* Brad T. Aagaard, John F. Hall, and Thomas H. Heaton. December 2002.

PEER 2002/11 *Analytical and Experimental Study of Fiber-Reinforced Strip Isolators*. James M. Kelly and Shakhzod M. Takhirov. September 2002.

PEER 2002/10 *Centrifuge Modeling of Settlement and Lateral Spreading with Comparisons to Numerical Analyses***.** Sivapalan Gajan and Bruce L. Kutter. January 2003.

PEER 2002/09 *Documentation and Analysis of Field Case Histories of Seismic Compression during the 1994 Northridge, California, Earthquake.* Jonathan P. Stewart, Patrick M. Smith, Daniel H. Whang, and Jonathan D. Bray. October 2002.

PEER 2002/08 *Component Testing, Stability Analysis and Characterization of Buckling-Restrained Unbonded Braces™.* Cameron Black, Nicos Makris, and Ian Aiken. September 2002.

PEER 2002/07 *Seismic Performance of Pile-Wharf Connections.* Charles W. Roeder, Robert Graff, Jennifer Soderstrom, and Jun Han Yoo. December 2001.

PEER 2002/06 *The Use of Benefit-Cost Analysis for Evaluation of Performance-Based Earthquake Engineering Decisions*. Richard O. Zerbe and Anthony Falit-Baiamonte. September 2001.

PEER 2002/05 *Guidelines, Specifications, and Seismic Performance Characterization of Nonstructural Building Components and Equipment*. André Filiatrault, Constantin Christopoulos, and Christopher Stearns. September 2001.

PEER 2002/04 *Consortium of Organizations for Strong-Motion Observation Systems and the Pacific Earthquake Engineering Research Center Lifelines Program: Invited Workshop on Archiving and Web Dissemination of Geotechnical Data, 4–5 October 2001*. September 2002.

PEER 2002/03 *Investigation of Sensitivity of Building Loss Estimates to Major Uncertain Variables for the Van Nuys Testbed.* Keith A. Porter, James L. Beck, and Rustem V. Shaikhutdinov. August 2002.

PEER 2002/02 *The Third U.S.-Japan Workshop on Performance-Based Earthquake Engineering Methodology for Reinforced Concrete Building Structures*. July 2002.

PEER 2002/01 *Nonstructural Loss Estimation: The UC Berkeley Case Study.* Mary C. Comerio and John C. Stallmeyer. December 2001.

PEER 2001/16 *Statistics of SDF-System Estimate of Roof Displacement for Pushover Analysis of Buildings.* Anil K. Chopra, Rakesh K. Goel, and Chatpan Chintanapakdee. December 2001.

PEER 2001/15 *Damage to Bridges during the 2001 Nisqually Earthquake.* R. Tyler Ranf, Marc O. Eberhard, and Michael P. Berry. November 2001.

PEER 2001/14 *Rocking Response of Equipment Anchored to a Base Foundation.* Nicos Makris and Cameron J. Black. September 2001.

PEER 2001/13 *Modeling Soil Liquefaction Hazards for Performance-Based Earthquake Engineering.* Steven L. Kramer and Ahmed-W. Elgamal. February 2001.

PEER 2001/12 *Development of Geotechnical Capabilities in OpenSees.* Boris Jeremić. September 2001.

PEER 2001/11 *Analytical and Experimental Study of Fiber-Reinforced Elastomeric Isolators*. James M. Kelly and Shakhzod M. Takhirov. September 2001.

PEER 2001/10 *Amplification Factors for Spectral Acceleration in Active Regions.* Jonathan P. Stewart, Andrew H. Liu, Yoojoong Choi, and Mehmet B. Baturay. December 2001.

PEER 2001/09 *Ground Motion Evaluation Procedures for Performance-Based Design.* Jonathan P. Stewart, Shyh-Jeng Chiou, Jonathan D. Bray, Robert W. Graves, Paul G. Somerville, and Norman A. Abrahamson. September 2001.

PEER 2001/08 *Experimental and Computational Evaluation of Reinforced Concrete Bridge Beam-Column Connections for Seismic Performance*. Clay J. Naito, Jack P. Moehle, and Khalid M. Mosalam. November 2001.

PEER 2001/07 *The Rocking Spectrum and the Shortcomings of Design Guidelines.* Nicos Makris and Dimitrios Konstantinidis. August 2001.

PEER 2001/06 *Development of an Electrical Substation Equipment Performance Database for Evaluation of Equipment Fragilities.* Thalia Agnanos. April 1999.

PEER 2001/05 *Stiffness Analysis of Fiber-Reinforced Elastomeric Isolators.* Hsiang-Chuan Tsai and James M. Kelly. May 2001.

PEER 2001/04 *Organizational and Societal Considerations for Performance-Based Earthquake Engineering.* Peter J. May. April 2001.

PEER 2001/03 *A Modal Pushover Analysis Procedure to Estimate Seismic Demands for Buildings: Theory and Preliminary Evaluation.* Anil K. Chopra and Rakesh K. Goel. January 2001.

PEER 2001/02 *Seismic Response Analysis of Highway Overcrossings Including Soil-Structure Interaction.* Jian Zhang and Nicos Makris. March 2001.

PEER 2001/01 *Experimental Study of Large Seismic Steel Beam-to-Column Connections.* Egor P. Popov and Shakhzod M. Takhirov. November 2000.

PEER 2000/10 *The Second U.S.-Japan Workshop on Performance-Based Earthquake Engineering Methodology for Reinforced Concrete Building Structures.* March 2000.

PEER 2000/09 *Structural Engineering Reconnaissance of the August 17, 1999 Earthquake: Kocaeli (Izmit), Turkey.* Halil Sezen, Kenneth J. Elwood, Andrew S. Whittaker, Khalid Mosalam, John J. Wallace, and John F. Stanton. December 2000.

PEER 2000/08 *Behavior of Reinforced Concrete Bridge Columns Having Varying Aspect Ratios and Varying Lengths of Confinement.* Anthony J. Calderone, Dawn E. Lehman, and Jack P. Moehle. January 2001.

PEER 2000/07 *Cover-Plate and Flange-Plate Reinforced Steel Moment-Resisting Connections.* Taejin Kim, Andrew S. Whittaker, Amir S. Gilani, Vitelmo V. Bertero, and Shakhzod M. Takhirov. September 2000.

PEER 2000/06 *Seismic Evaluation and Analysis of 230-kV Disconnect Switches.* Amir S. J. Gilani, Andrew S. Whittaker, Gregory L. Fenves, Chun-Hao Chen, Henry Ho, and Eric Fujisaki. July 2000.

PEER 2000/05 *Performance-Based Evaluation of Exterior Reinforced Concrete Building Joints for Seismic Excitation.* Chandra Clyde, Chris P. Pantelides, and Lawrence D. Reaveley. July 2000.

PEER 2000/04 *An Evaluation of Seismic Energy Demand: An Attenuation Approach.* Chung-Che Chou and Chia-Ming Uang. July 1999.

PEER 2000/03 *Framing Earthquake Retrofitting Decisions: The Case of Hillside Homes in Los Angeles.* Detlof von Winterfeldt, Nels Roselund, and Alicia Kitsuse. March 2000.

PEER 2000/02 *U.S.-Japan Workshop on the Effects of Near-Field Earthquake Shaking.* Andrew Whittaker, ed. July 2000.

PEER 2000/01 *Further Studies on Seismic Interaction in Interconnected Electrical Substation Equipment.* Armen Der Kiureghian, Kee-Jeung Hong, and Jerome L. Sackman. November 1999.

PEER 1999/14 *Seismic Evaluation and Retrofit of 230-kV Porcelain Transformer Bushings.* Amir S. Gilani, Andrew S. Whittaker, Gregory L. Fenves, and Eric Fujisaki. December 1999.

PEER 1999/13 *Building Vulnerability Studies: Modeling and Evaluation of Tilt-up and Steel Reinforced Concrete Buildings.* John W. Wallace, Jonathan P. Stewart, and Andrew S. Whittaker, editors. December 1999.

PEER 1999/12 *Rehabilitation of Nonductile RC Frame Building Using Encasement Plates and Energy-Dissipating Devices.* Mehrdad Sasani, Vitelmo V. Bertero, James C. Anderson. December 1999.

PEER 1999/11 *Performance Evaluation Database for Concrete Bridge Components and Systems under Simulated Seismic Loads.* Yael D. Hose and Frieder Seible. November 1999.

PEER 1999/10 *U.S.-Japan Workshop on Performance-Based Earthquake Engineering Methodology for Reinforced Concrete Building Structures.* December 1999.

PEER 1999/09 *Performance Improvement of Long Period Building Structures Subjected to Severe Pulse-Type Ground Motions*. James C. Anderson, Vitelmo V. Bertero, and Raul Bertero. October 1999.

PEER 1999/08 *Envelopes for Seismic Response Vectors.* Charles Menun and Armen Der Kiureghian. July 1999.

PEER 1999/07 *Documentation of Strengths and Weaknesses of Current Computer Analysis Methods for Seismic Performance of Reinforced Concrete Members.* William F. Cofer. November 1999.

PEER 1999/06 *Rocking Response and Overturning of Anchored Equipment under Seismic Excitations.* Nicos Makris and Jian Zhang. November 1999.

PEER 1999/05 *Seismic Evaluation of 550 kV Porcelain Transformer Bushings.* Amir S. Gilani, Andrew S. Whittaker, Gregory L. Fenves, and Eric Fujisaki. October 1999.

PEER 1999/04 *Adoption and Enforcement of Earthquake Risk-Reduction Measures.* Peter J. May, Raymond J. Burby, T. Jens Feeley, and Robert Wood.

PEER 1999/03 *Task 3 Characterization of Site Response General Site Categories*. Adrian Rodriguez-Marek, Jonathan D. Bray, and Norman Abrahamson. February 1999.

PEER 1999/02 *Capacity-Demand-Diagram Methods for Estimating Seismic Deformation of Inelastic Structures: SDF Systems*. Anil K. Chopra and Rakesh Goel. April 1999.

PEER 1999/01 *Interaction in Interconnected Electrical Substation Equipment Subjected to Earthquake Ground Motions.* Armen Der Kiureghian, Jerome L. Sackman, and Kee-Jeung Hong. February 1999.

PEER 1998/08 *Behavior and Failure Analysis of a Multiple-Frame Highway Bridge in the 1994 Northridge Earthquake.* Gregory L. Fenves and Michael Ellery. December 1998.

PEER 1998/07 *Empirical Evaluation of Inertial Soil-Structure Interaction Effects.* Jonathan P. Stewart, Raymond B. Seed, and Gregory L. Fenves. November 1998.

PEER 1998/06 *Effect of Damping Mechanisms on the Response of Seismic Isolated Structures.* Nicos Makris and Shih-Po Chang. November 1998.

PEER 1998/05 *Rocking Response and Overturning of Equipment under Horizontal Pulse-Type Motions.* Nicos Makris and Yiannis Roussos. October 1998.

PEER 1998/04 *Pacific Earthquake Engineering Research Invitational Workshop Proceedings, May 14–15, 1998: Defining the Links between Planning, Policy Analysis, Economics and Earthquake Engineering.* Mary Comerio and Peter Gordon. September 1998.

PEER 1998/03 *Repair/Upgrade Procedures for Welded Beam to Column Connections.* James C. Anderson and Xiaojing Duan. May 1998.

PEER 1998/02 *Seismic Evaluation of 196 kV Porcelain Transformer Bushings.* Amir S. Gilani, Juan W. Chavez, Gregory L. Fenves, and Andrew S. Whittaker. May 1998.

PEER 1998/01 *Seismic Performance of Well-Confined Concrete Bridge Columns*. Dawn E. Lehman and Jack P. Moehle. December 2000.

ONLINE PEER REPORTS

The following PEER reports are available by Internet only at http://peer.berkeley.edu/publications/peer_reports_complete.html.

PEER 2012/103 *Performance-Based Seismic Demand Assessment of Concentrically Braced Steel Frame Buildings.* Chui-Hsin Chen and Stephen A. Mahin. December 2012.

PEER 2012/102 *Procedure to Restart an Interrupted Hybrid Simulation: Addendum to PEER Report 2010/103.* Vesna Terzic and Bozidar Stojadinovic. October 2012.

PEER 2012/101 *Mechanics of Fiber Reinforced Bearings.* James M. Kelly and Andrea Calabrese. February 2012.

PEER 2011/107 *Nonlinear Site Response and Seismic Compression at Vertical Array Strongly Shaken by 2007 Niigata-ken Chuetsu-oki Earthquake.* Eric Yee, Jonathan P. Stewart, and Kohji Tokimatsu. December 2011.

PEER 2011/106 *Self Compacting Hybrid Fiber Reinforced Concrete Composites for Bridge Columns.* Pardeep Kumar, Gabriel Jen, William Trono, Marios Panagiotou, and Claudia Ostertag. September 2011.

PEER 2011/105 *Stochastic Dynamic Analysis of Bridges Subjected to Spacially Varying Ground Motions.* Katerina Konakli and Armen Der Kiureghian. August 2011.

PEER 2011/104 *Design and Instrumentation of the 2010 E-Defense Four-Story Reinforced Concrete and Post-Tensioned Concrete Buildings.* Takuya Nagae, Kenichi Tahara, Taizo Matsumori, Hitoshi Shiohara, Toshimi Kabeyasawa, Susumu Kono, Minehiro Nishiyama (Japanese Research Team) and John Wallace, Wassim Ghannoum, Jack Moehle, Richard Sause, Wesley Keller, Zeynep Tuna (U.S. Research Team). June 2011.

PEER 2011/103 *In-Situ Monitoring of the Force Output of Fluid Dampers: Experimental Investigation.* Dimitrios Konstantinidis, James M. Kelly, and Nicos Makris. April 2011.

PEER 2011/102 *Ground-motion prediction equations 1964 - 2010.* John Douglas. April 2011.

PEER 2011/101 *Report of the Eighth Planning Meeting of NEES/E-Defense Collaborative Research on Earthquake Engineering.* Convened by the Hyogo Earthquake Engineering Research Center (NIED), NEES Consortium, Inc. February 2011.

PEER 2010/111 *Modeling and Acceptance Criteria for Seismic Design and Analysis of Tall Buildings.* Task 7 Report for the Tall Buildings Initiative - Published jointly by the Applied Technology Council. October 2010.

PEER 2010/110 *Seismic Performance Assessment and Probabilistic Repair Cost Analysis of Precast Concrete Cladding Systems for Multistory Buildlings.* Jeffrey P. Hunt and Božidar Stojadinovic. November 2010.

PEER 2010/109 *Report of the Seventh Joint Planning Meeting of NEES/E-Defense Collaboration on Earthquake Engineering. Held at the E-Defense, Miki, and Shin-Kobe, Japan, September 18–19, 2009.* August 2010.

PEER 2010/108 *Probabilistic Tsunami Hazard in California.* Hong Kie Thio, Paul Somerville, and Jascha Polet, preparers. October 2010.

PEER 2010/107 *Performance and Reliability of Exposed Column Base Plate Connections for Steel Moment-Resisting Frames.* Ady Aviram, Božidar Stojadinovic, and Armen Der Kiureghian. August 2010.

PEER 2010/106 *Verification of Probabilistic Seismic Hazard Analysis Computer Programs.* Patricia Thomas, Ivan Wong, and Norman Abrahamson. May 2010.

PEER 2010/105 *Structural Engineering Reconnaissance of the April 6, 2009, Abruzzo, Italy, Earthquake, and Lessons Learned.* M. Selim Günay and Khalid M. Mosalam. April 2010.

PEER 2010/104 *Simulating the Inelastic Seismic Behavior of Steel Braced Frames, Including the Effects of Low-Cycle Fatigue.* Yuli Huang and Stephen A. Mahin. April 2010.

PEER 2010/103 *Post-Earthquake Traffic Capacity of Modern Bridges in California.* Vesna Terzic and Božidar Stojadinović. March 2010.

PEER 2010/102 *Analysis of Cumulative Absolute Velocity (CAV) and JMA Instrumental Seismic Intensity (I_{JMA}) Using the PEER–NGA Strong Motion Database.* Kenneth W. Campbell and Yousef Bozorgnia. February 2010.

PEER 2010/101 *Rocking Response of Bridges on Shallow Foundations.* Jose A. Ugalde, Bruce L. Kutter, and Boris Jeremic. April 2010.

PEER 2009/109 *Simulation and Performance-Based Earthquake Engineering Assessment of Self-Centering Post-Tensioned Concrete Bridge Systems.* Won K. Lee and Sarah L. Billington. December 2009.

PEER 2009/108 *PEER Lifelines Geotechnical Virtual Data Center.* J. Carl Stepp, Daniel J. Ponti, Loren L. Turner, Jennifer N. Swift, Sean Devlin, Yang Zhu, Jean Benoit, and John Bobbitt. September 2009.

PEER 2009/107 *Experimental and Computational Evaluation of Current and Innovative In-Span Hinge Details in Reinforced Concrete Box-Girder Bridges: Part 2: Post-Test Analysis and Design Recommendations.* Matias A. Hube and Khalid M. Mosalam. December 2009.

PEER 2009/106 *Shear Strength Models of Exterior Beam-Column Joints without Transverse Reinforcement.* Sangjoon Park and Khalid M. Mosalam. November 2009.

PEER 2009/105 *Reduced Uncertainty of Ground Motion Prediction Equations through Bayesian Variance Analysis.* Robb Eric S. Moss. November 2009.

PEER 2009/104 *Advanced Implementation of Hybrid Simulation.* Andreas H. Schellenberg, Stephen A. Mahin, Gregory L. Fenves. November 2009.

PEER 2009/103 *Performance Evaluation of Innovative Steel Braced Frames.* T. Y. Yang, Jack P. Moehle, and Božidar Stojadinovic. August 2009.

PEER 2009/102 *Reinvestigation of Liquefaction and Nonliquefaction Case Histories from the 1976 Tangshan Earthquake.* Robb Eric Moss, Robert E. Kayen, Liyuan Tong, Songyu Liu, Guojun Cai, and Jiaer Wu. August 2009.

PEER 2009/101 *Report of the First Joint Planning Meeting for the Second Phase of NEES/E-Defense Collaborative Research on Earthquake Engineering.* Stephen A. Mahin et al. July 2009.

PEER 2008/104 *Experimental and Analytical Study of the Seismic Performance of Retaining Structures.* Linda Al Atik and Nicholas Sitar. January 2009.

PEER 2008/103 *Experimental and Computational Evaluation of Current and Innovative In-Span Hinge Details in Reinforced Concrete Box-Girder Bridges. Part 1: Experimental Findings and Pre-Test Analysis.* Matias A. Hube and Khalid M. Mosalam. January 2009.

PEER 2008/102 *Modeling of Unreinforced Masonry Infill Walls Considering In-Plane and Out-of-Plane Interaction.* Stephen Kadysiewski and Khalid M. Mosalam. January 2009.

PEER 2008/101 *Seismic Performance Objectives for Tall Buildings.* William T. Holmes, Charles Kircher, William Petak, and Nabih Youssef. August 2008.

PEER 2007/101 *Generalized Hybrid Simulation Framework for Structural Systems Subjected to Seismic Loading.* Tarek Elkhoraibi and Khalid M. Mosalam. July 2007.

PEER 2007/100 *Seismic Evaluation of Reinforced Concrete Buildings Including Effects of Masonry Infill Walls.* Alidad Hashemi and Khalid M. Mosalam. July 2007.

The Pacific Earthquake Engineering Research Center (PEER) is a multi-institutional research and education center with headquarters at the University of California, Berkeley. Investigators from over 20 universities, several consulting companies, and researchers at various state and federal government agencies contribute to research programs focused on performance-based earthquake engineering.

These research programs aim to identify and reduce the risks from major earthquakes to life safety and to the economy by including research in a wide variety of disciplines including structural and geotechnical engineering, geology/seismology, lifelines, transportation, architecture, economics, risk management, and public policy.

PEER is supported by federal, state, local, and regional agencies, together with industry partners.

PEER Core Institutions:
University of California, Berkeley (Lead Institution)
California Institute of Technology
Oregon State University
Stanford University
University of California, Davis
University of California, Irvine
University of California, Los Angeles
University of California, San Diego
University of Southern California
University of Washington

PEER reports can be ordered at http://peer.berkeley.edu/publications/peer_reports.html or by contacting

Pacific Earthquake Engineering Research Center
University of California, Berkeley
325 Davis Hall, mail code 1792
Berkeley, CA 94720-1792
Tel: 510-642-3437
Fax: 510-642-1655
Email: peer_editor@berkeley.edu

ISSN 1547-0587X